DEVELOPMENT OF A RECTENNA WITH A SIW CAVITY BACKED SLOT ANTENNA AND A FABRY-PÊROT ANTENNA

A THESIS SUBMITTED TO
THE GRADUATE SCHOOL OF NATURAL AND APPLIED SCIENCES
OF
MIDDLE EAST TECHNICAL UNIVERSITY

BY

EFECAN BOZULU

IN PARTIAL FULFILLMENT OF THE REQUIREMENTS
FOR
THE DEGREE OF MASTER OF SCIENCE
IN
ELECTRICAL AND ELECTRONICS ENGINEERING

JULY 2015

Approval of the thesis:

DEVELOPMENT OF A RECTENNA WITH A SIW CAVITY BACKED SLOT ANTENNA AND A FABRY-PÊROT ANTENNA

submitted by **EFECAN BOZULU** in partial fulfillment of the requirements for the degree of **Master of Science in Electrical and Electronics Engineering Department, Middle East Technical University** by,

Prof. Dr. Gülbin Dural Ünver _____
Dean, Graduate School of **Natural and Applied Sciences**

Prof. Dr. Gönül Turhan Sayan _____
Head of Department, **Electrical and Electronics Engineering**

Prof. Dr. Özlem Aydın Çivi _____
Supervisor, **Electrical and Electronics Eng. Dept., METU**

Examining Committee Members:

Prof. Dr. Nilgün Günalp
Electrical and Electronics Engineering Dept., METU _____

Prof. Dr. Özlem Aydın Çivi
Electrical and Electronics Engineering Dept., METU _____

Prof. Dr. Gülbin Dural Ünver
Electrical and Electronics Engineering Dept., METU _____

Prof. Dr. Birsen Saka
Electrical and Electronics Eng. Dept., Hacettepe Uni. _____

Assoc. Prof. Dr. Lale Alatan
Electrical and Electronics Engineering Dept., METU _____

Date: _____

I hereby declare that all information in this document has been obtained and presented in accordance with academic rules and ethical conduct. I also declare that, as required by these rules and conduct, I have fully cited and referenced all material and results that are not original to this work.

Name, Last Name: EFECAN BOZULU

Signature :

ABSTRACT

DEVELOPMENT OF A RECTENNA WITH A SIW CAVITY BACKED SLOT ANTENNA AND A FABRY-PÊROT ANTENNA

Bozulu, Efecan

M.S., Department of Electrical and Electronics Engineering

Supervisor : Prof. Dr. Özlem Aydın Çivi

July 2015, 100 pages

A rectenna is a term that is used for an antenna that is integrated with a microwave rectifier for the purpose of capturing microwave power and converting it to DC power. Rectennas are mostly employed for wireless power transmission via microwaves. In this thesis work a substrate integrated waveguide cavity backed (SIWCB) slot antenna and a Fabry-Pérot antenna is designed, manufactured and tested to be used as the receiving antenna of a rectenna system along with a microwave rectifier to be used as the rectifying part of this system. All system is designed to operate at 2.45 GHz. Microwave rectifier is designed to have a 56% RF to DC conversion efficiency. Microwave rectifier is realized by distributed elements and a microwave diode with using harmonic balance simulation. SIWCB slot antenna is selected in this design for its low profile, easy integration with microwave elements, low cost, ease of fabrication and high efficiency. Designed SIWCB slot antenna has microstrip to grounded coplanar waveguide transformation for its feeding. Designed antenna has a gain of 2.9 dBi and 10 dB bandwidth of 20 MHz. Fabry-Perot antenna is designed using a two layered frequency selective structure (FSS) of subwavelength units. This designed FSS is used for the formation of the Fabry-Pérot cavity. In this thesis work Fabry-Perot antenna is preferred for its high gain, low cost and ease of fabrication. A simple patch antenna is used as the primary radiating element. Designed Fabry-Pérot antenna exhibits a gain of 10.5 dBi with 10 dB bandwidth of 26 MHz. These developed elements are used for formation of a rectenna system whose power trans-

mission efficiency is also measured in the laboratory environment. All simulation results are in good agreement with measured values for microwave rectifier, SIWCB slot antenna, FSS Fabry-Pérot antenna and rectenna system.

Keywords: Microwave Rectifier, Fabry-Pérot Antenna, SIWCB Antenna, Wireless Power Transmission, Rectenna

ÖZ

SIW OYUKLA ARKALANDIRILMIŞ ANTEN VE FABRY-PÊROT ANTEN İLE DOĞRULTUCU ANTENLERİN GELİŞTİRİLMESİ

Bozulu, Efecan
Yüksek Lisans, Elektrik ve Elektronik Mühendisliği Bölümü
Tez Yöneticisi : Prof. Dr. Özlem Aydın Çivi

Temmuz 2015 , 100 sayfa

Doğrultucu anten, mikrodalga enerjiyi doğru akıma çevirmek amacı ile bir araya getirilmiş bir anten ve mikrodalga doğrultucuyu tanımlamak için kullanılan bir terimdir. Doğrultucu antenler genel olarak mikrodalgalar aracılığı ile kablosuz enerji iletiminde kullanılmaktadır. Bu tez çalışmasında bir dalga klavuzlu mikrodalga oyuk ile arkalandırılmış yarık anten ve bir Fabry-Pérot anten doğrultucu antenin alma antenleri olarak tasarlanmıştır. Bir mikrodalga doğrultucu ise doğrultucu antenin doğrultma görevini üstlenmesi için tasarlanmıştır. Bütün sistem 2.45 GHz frekansında çalışması için tasarlanmıştır. Mikrodalga doğrultucu % 56 RF'den Doğru akıma çevirme yeteneğine sahiptir. Tasarlanmış olan doğrultucu dağıtık elementler ve bir mikrodalga diyot kullanılarak, harmonik dengeleme metodu ile geliştirilmiştir. Tasarlanan dalga klavuzlu mikrodalga oyuk ile arkalandırılmış yarık anten düşük profili, mikrodalga elemanlar ile kolay entegrasyonu ve üretim kolaylığı sebebi ile seçilmiştir.Tasarlanan dalga klavuzlu mikrodalga oyuk ile arkalandırılmış yarık anten mikroşeritten, GCPW a geçiş içeren bir yöntem ile beslenmektedir. Bu anten 2.9 dBi kazanç göstermiş ve 10 dB bant genişliği 26 MHz olarak ölçülmüştür. Fabry-Perot anten iki katlı bir frekans seçimli yüzey aracılığı ile tasarlanmıştır. Tasarlanan frekans seçimli yüzey dalga boyu altı ünitelerden oluşmaktadır. Bu tasarlanmış olan yüzey Fabry-Pérot oyuğun oluşturulmasında kullanılmıştır. Fabry-Pérot antenin beslenmesi için basit bir yama anten kullanılmıştır. Bu Fabry-Pérot anten 10.5 dBi kazanç ve 26 MHz, 10 dB bant ge-

nişliği göstermiştir. Bu tasarlanan elemanlar bir doğrultucu antenin oluşturulmasında kullanılmış ve bu oluşturulan doğrultucu anten sistemi laboratuvar ortamında ölçülmüştür. Bütün ölçüm sonuçları tasarlanan bütün elementler için simülasyon sonuçları ile uyumlu çıkmıştır.

Anahtar Kelimeler: Mikrodalga doğrultucu, Fabry-Pérot Anten, SIWCB Anten, Kablosuz enerji iletimi, doğrultucu anten

ACKNOWLEDGMENTS

TABLE OF CONTENTS

APPENDICES

LIST OF TABLES

TABLES

LIST OF FIGURES

FIGURES

LIST OF ABBREVIATIONS

FTBT	Front-to-Back Ratio
WPT	Wireless Power Transmission
HB	Harmonic Balance
BPF	Band Pass Filter
TRL	Through Reflect Line
SOLT	Short Open Load Through
SMA	Subminiature A
GCPW	Grounded Coplanar Waveguide
SIW	Substrate Integrated Waveguide
SPS	Solar Power Satellite
FSS	Frequency Selective Structure

CHAPTER 1

INTRODUCTION OF RECTENNA CONCEPT AND WIRELESS POWER TRANSFER

Acquaintance of mankind with wireless power transmission as an idea can be traced back to introduction of industrial electric distribution. Tesla was first to be ignited with the idea, going as far as building a giant tower of what we call today a Tesla coil. After many unsuccessful attempts, he was more than convinced about his own ideas [1] and abandoned the project for a long time. Although the adventure of wireless power transmission may seem to end abruptly at the beginning, concept had thrived over years and re-emerged in a science fiction short story by renowned writer Isaac Asimov, "Reason" in 1941. Where the wireless power transmission system is depicted as a huge solar panel system that is outside of atmosphere, delivering its power to earth via microwave transmission. This staging of a wireless power system is a far more realistic one. So realistic that, after a couple of decades, with the advancement in the technology that is allowing the construction of such a system, "Department of Energy" (DoE) and NASA of United States of America actually investigated the possibility of building such a system with the budget of 50 million $ [2].

This innovative step by the US government has paved the road for many studies been shaped the wireless energy transfer today. Many important experiments had conducted under that movement. A noteworthy of them is the experiment that is conducted by JPL (Jet Propulsion Laboratories) and Raytheon company in 1975 [3]. This experiment was performed with transmitting 30kW microwave power at 2.45GHz from a 26.8m^2 source dish antenna to a receiver antenna array that consists of dipole-type antennas located 1.6 km away from the source [6]. Result of this experiment is a

radiated RF power to DC power conversion efficiency of 84% and a DC-DC efficiency of 54%. Even though being old, this experiment still holds the record for distance and efficiency. Studies in this era has continued with the public demonstrations of helicopters that are powered wirelessly [5]. However, this investigation, that has opened the path for such studies, have come to an end with the conclusion of impossibility of building an out-of-earth solar station to transmit power to earth in 1980.

Nevertheless, it is not all lost. Wireless power transmission is still a hot topic in engineering. NASA is still working on Space Solar Power projects started in 1999 and JAXA(Japan Aerospace Exploration Agency) at its tail [4]. Ambitions of technology power houses would convince the world that science fiction is not that much of a fiction after all.

"Wireless power transmission", as a term, can be interpreted as transmission of power without any mechanical contact between source and destination points. What is intended to imply with "mechanical" description is that the source and destination points lack a direct contact between them allowing transmission of power. In the case of electric energy, aside from other means and mediums which are also require a physical contact, this transmission mediums are structures that can carry current.

To achieve such a task, electromagnetic waves stand as a powerful candidate with more than one method and principle to exploit them. Electromagnetic waves can be used in different methods for transmission of power. It is possible to group electromagnetic solutions for wireless power transmission problem under two categories; near-field and far-field. The definition of near-field and far-field transmission can be associated with the classical region definitions of antennas [45]. Near-field transmission and far-field transmission can be distinguished from each other in terms of their range. As their names imply near-field transmission has a very short range compared to far-field transmission.

In near-field transmission, inductive and capacitive couplings are implemented with pairs of metal electrodes or coil wires. In figure 1.1 an inductive coupling wireless device block diagram is presented [7]. In figure 1.1, charging equipment is shown with target device which is required to be charged. With tightly placed coil wires of target device and charger, a strong mutual coupling is introduced resulting in a flow

of flux from charger to target. Most important constrain on this mode of operation is tight closing of coil wires, since mutual coupling is directly related to distance between the coils and their relative alignment.

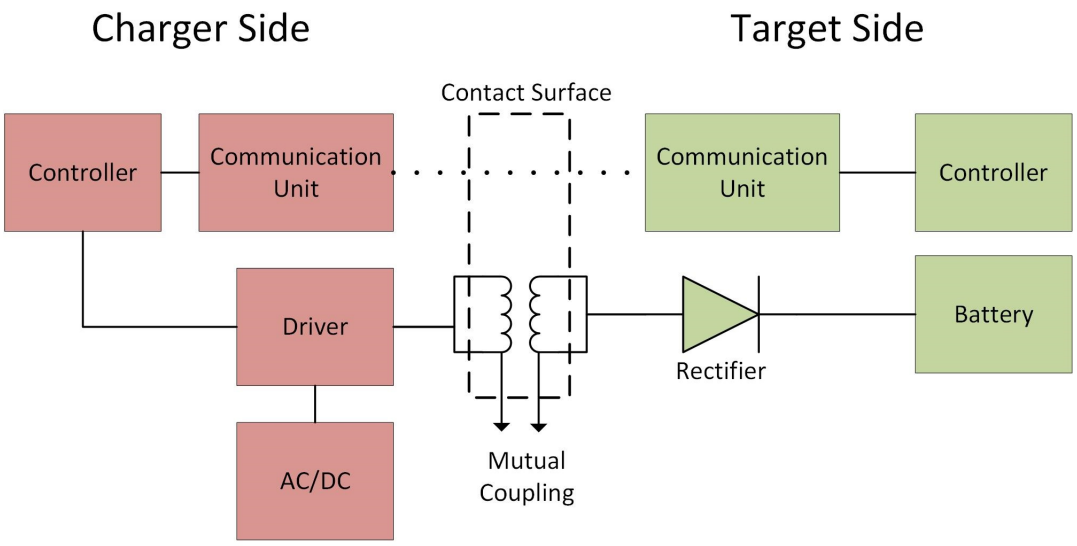

Figure 1.1: Block diagram of a simple near-field power transmission system.

Aside from basic inductive and capacitive coupling, a newly emerging, more promising method is introduced by researchers at MIT [8]. This new method, named as "Resonance Inductive Coupling" achieves a 40% efficiency in 2.5 meters.

Near-field transmission is the most widely used and commercially available type of wireless power transmission. With the proliferation of mobile devices and a suppression from the market persuaded many hardware developers to offer wireless charging devices [7].

The second category for wireless power transmission is far-field transmission. Far-field radiation employs the propagative nature of the time varying magnetic and electric fields. This radiative power is different in its nature compared to near-field radiation, since it is radiative, transmitted power is radiated whether there is a receiver on the other side of the system or not. This radiative nature of the transmission is related to the far-field definition of the radiating antenna element itself. In other words, receiver part of the system is unable to affect the transmitter part. Most distinctive feature of this type of transmission is that the power that is not intercepted by the

receiving antenna of the system is lost.

This type of transmission can be compared to a data link, where the power transmission still occurs, however only a meaningful part of the power is enough to be useful. This manner of a communication system is expressed in terms of SNR. What is fundamentally different in a power transmission application is amount of power that should be received by the receiving part of the system to be useful.

A simple visualization of a far-field power transmission is presented in figure 1.2. In figure 1.2 transmitting and receiving sides are physically separated. This separation depends on the application. In an SPS (Solar Powered Satellite) application this distance may cover hundreds of kilometers or just some meters in a sensor node powering application. Transmitting side of the system is responsible from the generation of electromagnetic waves that are required to be captured by receiving side of the system. Transmitting antenna is spatially configured to deliver its maximum energy in to the direction of the receiving antenna which is also configured to receive the maximum power from the transmitting antenna. On the receiving side, after the receiving antenna, an RF to DC energy converter is connected to the system, which is feeding the load.

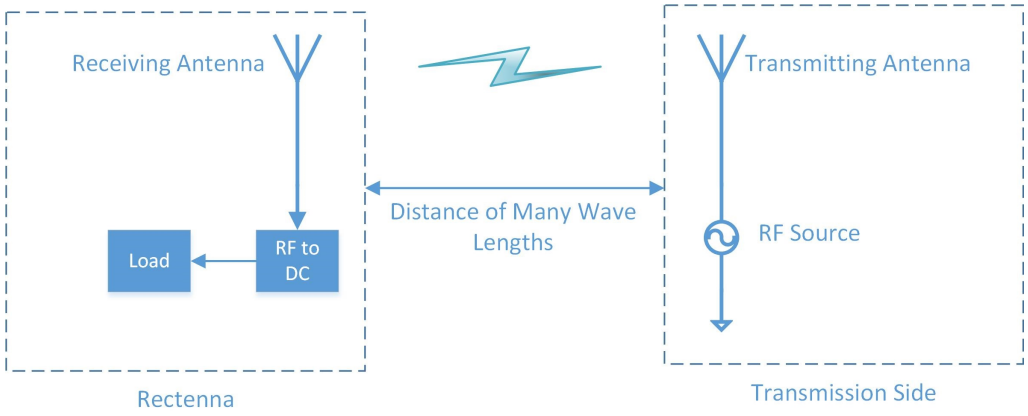

Figure 1.2: Block diagram of a simple far field power transmission system.

In the case of far-field power transmission, directive nature of antennas plays an important role. This aspect of antennas are obvious in Friis transmission equation 1.1

[45].

$$P_r = P_t \frac{G_t G_r \lambda^2}{(4\pi R)^2} \tag{1.1}$$

In Friis transmission equation, received (P_r) and transmitted (P_t) powers are related with the distance (R), wavelength (λ) and gains (G_r and G_t) of receiving and transmitting antennas. Assuming unity antenna gains ($G_r G_t = 1$) and 2.45 GHz frequency of operation, power ratio between transmitted and received power turns out to be 40 dB in 1 meter range. This figure indicates that to transfer 20 dBm of power as 10 dBm to receiving antenna, at least a 30 dB of total antenna gain is required.

This simple calculation demonstrates the effect of antenna design on the possible performance of the system. Conversion efficiency of RF to DC power is also another parameter that affects the performance of the system.

These explained wireless power transmission techniques have different application areas, regarding their properties and abilities as tabulated in table 1.1. Near-field power transmission techniques are generally used in environments where usage of a cable is not applicable or not preferred. Inductive coupling is used in charging of toothbrushes or electric shaving machines. This usage is preferred since the environment this devices are used is not suitable for usage of connectors to charge. Usage of connector may cause short circuits or even electric shocks to user. Resonance inductive coupling however, is a more promising technique for high power applications. Mobile device charging is considered as a main application area for this technology, since it offers a little bit more flexibility in range compared to inductive and capacitive charging.

In the applications requiring long range transmission, far-field techniques are used. A catchy application is powering up of a UAV (Unmanned Aerial Vehicle) [9] with wireless power transmission. With wireless power ability, powered drone is not required to stop by a base for recharges or refills. This gives drone an unprecedented capability of reconnaissance. In the case of SPS(Solar Power Satellite), far-field transmission is considered as a very powerful candidate for transmission of power [1], [2] [3], [4]. SPS applications are still considered as very expensive projects, however with the ad-

vancements in space applications and therefore lowering of cost for per metric tone load, such projects will be investible in three to four decades.

To simplify the concept in far-field power transmission as a unified element, rectenna concept is introduced to the literature by W.C. Brown [10]. Rectenna is a term comprising the antenna element and rectifier, rectifying antenna in other words. This unified structure stands for the unit structure for far-field wireless power transmission. This unit typically includes an antenna and a rectifier that is connected to it. Even though designs differ, it is possible to propose a general structure for a rectenna. In figure 1.3, a general block diagram for a rectenna is given.

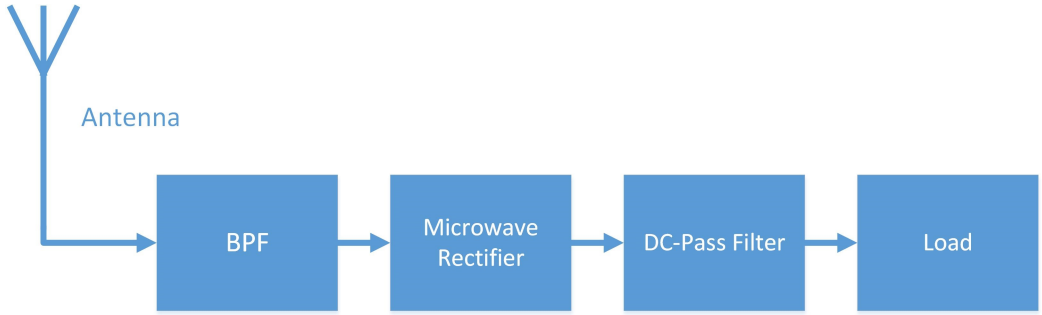

Figure 1.3: General block diagram of rectenna.

In a rectenna, an antenna plays an important role in capturing of the power that is transmitted. Captured power depends on the antenna effective area and power density of the field that is captured. After the antenna, a low pass filter is generally used for keeping generated harmonics from reradiation out of the antenna. After the filter, a microwave rectifier is used for conversion of RF power to DC power. Efficiency of microwave rectifier has a direct effect on the total efficiency of the whole transmission system. In the case of a whole system performance, an overall Figure of Merit (FoM) for the system can be proposed as follows,

$$FoM = e_L e_R \tag{1.2}$$

where e_L represents the link efficiency of the antenna, which can be defined as the ratio between available power at the ports of the receiving antenna and the transmitted power by the transmitting antenna. e_L depends on the antenna parameters and space orientation of the receiving and transmitting antenna. e_R represents the conver-

sion efficiency of microwave rectifier and is a function of frequency and input power depending on the design.

After microwave rectifier, a DC-Pass filter is employed in designs to separate microwave power from DC power. The DC-Pass filter also provides a shielding for the RF circuit from voltage measurement probes. Other functions may also be assigned to DC-Pass filter depending on the design.

During the design of a rectenna, it is proper to evaluate the microwave rectifier and antenna part separately for efficiency calculations. This is due to the fact that power that is captured by the rectifier antenna depends on the power density of the transmitting antenna at the distance where the receiving antenna is positioned. Thus, most of the literature work concentrate mainly on microwave rectifier efficiency with a given power density for the capturing antenna. However, as it has been explained, antenna and its parameters play a crucial role in the efficiency and success of the system.

In literature many noteworthy rectenna designs are presented with novelties. Some of the reported rectennas are different in operation and design compared to dominant design trends in the literature. An interesting approach is presented in [14], where the power transmission system is regarded as an N-port network and maximum power transfer eigenvalues are presented as weighting elements to input antenna array. A similar study about the elements of rectenna array, is performed in [11], in which the two different power transmission regimes are tested. One of the approach is building an antenna array and then connecting the microwave rectifier to its output, other approach is to connect a microwave rectifier to all elements and then combining their outputs in DC domain. A very novel rectenna design is presented in [15]. Presented design is a differential mode rectenna, which employs the diode on the feeding of the antenna and exploits the out of phase voltages that are induced on the system. This design is further improved with parallel and series stackable configurations [16]. Other literature studies that present monolithic structures as rectenna elements are notable as well [19], [12].

To investigate the concept of rectenna systems, high gain single element antennas with a microwave rectifier circuit has been developed and evaluated in this thesis work to act as a rectenna system. Rectenna system has been selected to operate at 2.45 GHz

ISM band for the abundance of literature research and ease of design.

Objectives of this thesis work can be summed up in few titles:

1. To develop and build a fully functional rectenna system for demonstration of this concept.
2. To investigate the concept of microwave rectifier, development tools, different topologies, design procedures and finally construction of a microwave rectifier.
3. Design, fabrication and measurement of a SIW cavity backed slot antenna.
4. Design, fabrication and measurement of a Fabry-Pérot cavity backed antenna.

In the direction of the listed objectives of this thesis work, a microwave rectifier is designed and manufactured. Design procedure, modelling and manufacturing steps of this element of rectenna system are presented in Chapter 2.

For the investigation antenna element directivity, two antennas are designed and manufactured. These two antennas are a substrate integrated waveguide cavity backed slot antenna and a frequency selective superstrate, Fabry-Pérot cavity backed antenna. Development processes and working principles of these antennas are explained into minute detail in chapters 3 and 4 respectively. Finally, these designed elements are integrated to form a rectenna system. Integrated system is used for measurement purposes and obtained measurement values are presented in chapter 5. Discussion of the results and future work are presented in final chapter of this thesis work.

Table 1.1: Different near-field and far-field power transfer technologies with range, frequency and application areas, possible and current

Type	Technology	Range	Directivity	Frequency	Applications
Near-Field	Inductive Coupling	Short	Low	Hz-MHz	Inductive forging, battery charging
	Capacitive Coupling	Short	Low	MHz-GHz	Battery charging
	Resonant Inductive Coupling	Mid	Low	Hz-MHz	Mobile device charging, RFID, vehicle charging
Far-Field	Microwaves	Long	High	GHz	SPS, remote drone powering
	Microwaves	Long	High	GHz	SPS, Space power network

CHAPTER 2

MODELING, DESIGN, MANUFACTURING AND TESTING OF MICROWAVE RECTIFIER

2.1 General Principal and Modeling of Microwave Rectifiers with Harmonic Balance Simulation

A microwave rectifier is simply a rectifier that operates in microwave region of electromagnetic spectrum. Identical in operation to their lower frequency counterparts, they serve the purpose of rectification of sinusoidal input waves. Most prominent application of rectifier circuits in electronics engineering is AC to DC conversion of input voltage and currents. Inevitably, in a system that is designed for conversion of input microwave energy to DC power, rectifiers are employed as crucial elements in rectenna designs. In microwave engineering, aside from their usage as simply power converters, rectifiers are used as detectors in controlled environments for detection of microwave power, either as part of a measurement system or in a microwave module.

Microwave rectifier circuit is the most important part of a rectenna system in terms of its efficiency, since it directly effects the figure of merit (FoM) of the system. Figure 2.1 presents a general block diagram of a microwave rectifier. Block diagram in figure 2.1 refers to a typical microwave rectifier used in WPT(Wireless Power Transmission) or energy harvesting applications, some of the blocks can be omitted in designs if the sole purpose of the design is just the detection of microwave power rather than increasing the efficiency of the circuit, as it is desired in DC conversion applications.

In figure 2.1 first block, band pass filter, serves the purpose of keeping the input power

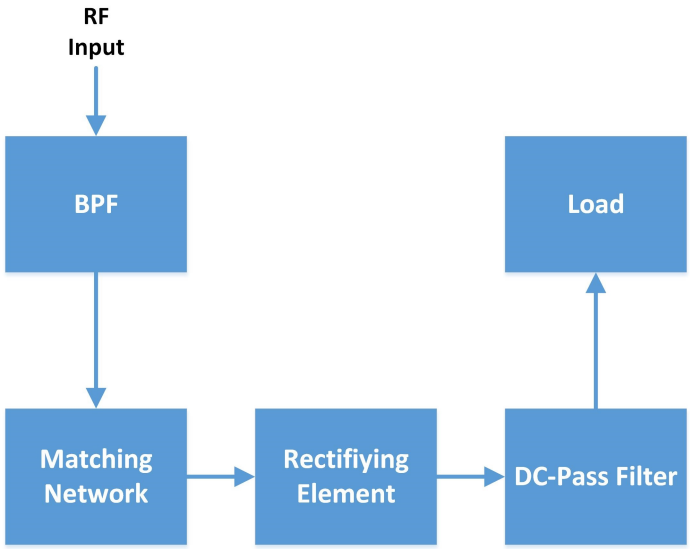

Figure 2.1: Block Diagram of a microwave rectifier.

confined inside of the circuit by reflecting back the reflected power from the rest of the circuit. This effect of the BPF is the circuit by reflecting back the reflected power from the rest of the circuit. This effect of the BPF is be discussed in the subsequent sections. Another purpose of BPF in microwave rectifiers, especially in rectenna applications where the outside environment is not controlled by direct feeding, is keeping the non-linear rectifying element from interference that is caused by other sources. This interference can generate undesired DC components inside of the circuit, which may cause the wandering off of other desired DC components and eventually may lead to deterioration of conversion efficiency, since the circuit is fine tuned for operating under a certain input power and frequency.

Second block of the microwave rectifier circuit is a matching network, whose objective is tuning of input impedance of the circuit to feeding impedance in order to minimize the reflected power. This block can be minimized to increase the efficiency of the microwave rectifier by using non-standard input impedances, if the circuit is desired to operate with an integrated antenna in a monolithic structure, further discussion will be presented on this topic in the final chapter of this thesis work. Third element is the rectifying element itself, which is responsible for desired non-linear behaviour. Final stage is a DC-Pass filter, which is used for isolation of DC and RF parts from each other. This block can be used as only a band pass filter for measurement purposes or can be used as an auxiliary element in the design itself, this topic is

also discussed in subsection 2.2.3 of this chapter.

Most important figure for the evaluation of rectifiers is RF-to-DC conversion efficiency. This efficiency can be expressed as 2.1.

$$\varepsilon = \frac{dc\ output\ power}{RF\ input\ power} \tag{2.1}$$

Equation 2.1 however stands for overall efficiency of a rectifier, for a correct conversion efficiency expression, RF input power should be replaced with RF accepted power. Main distinctive, numerical property of microwave rectifiers is their efficiency. Given equation 2.1 is the main definition for all efficiency numbers that are given.

In literature, different topologies for microwave rectifiers are presented based on different applications. Even though classification of them could not be an accurate approach, since topologies differ from each other in many aspects, It is possible to classify them in two main categories.

First one of the categories can be characterized with their employment of rectifying elements in a charge pump topology. This class of topology utilizes rectifying elements with capacitors and other elements. In literature, designs [11] ,[12] , [13] , [14] and [17] fall in to this class. This class encompasses classic rectifiers like Greinacher rectifiers and multi-stage Dickinson charge pumps. Second class, recognizes rectifying element as a single diode and relies on reflections from load point of the circuit, which is the last block in figure 2.1. This category mostly, not all of them, employs the reflected waves from DC-Pass filter of the circuit and uses them for improving efficiency. In literature, designs that are presented in [18] , [19] and [20] fall into this category. Both have advantages and disadvantages with respect to each other in different points of views.

First category employs more discreet elements, such as capacitors. Usage of capacitors inserts some parasitic behaviour of course, since they are packaged and parasitic content of them presents an unknown element in to the circuit. This uncertain parasitic effect, makes the conducted simulation more prone to discrepancies between the realized circuit. When stages of rectification are added, more parasitic elements are included in the design, which further degrades the reliability of conducted simula-

tions. However, they can realize better efficiencies with quite simple topologies. For example, with a simple two stage rectification as shown in figure 2.2, without working much on filters, they can present 70% to 80% percent conversion efficiencies in designs. In table 2.1 efficiencies of different designs that fall into first category are presented.

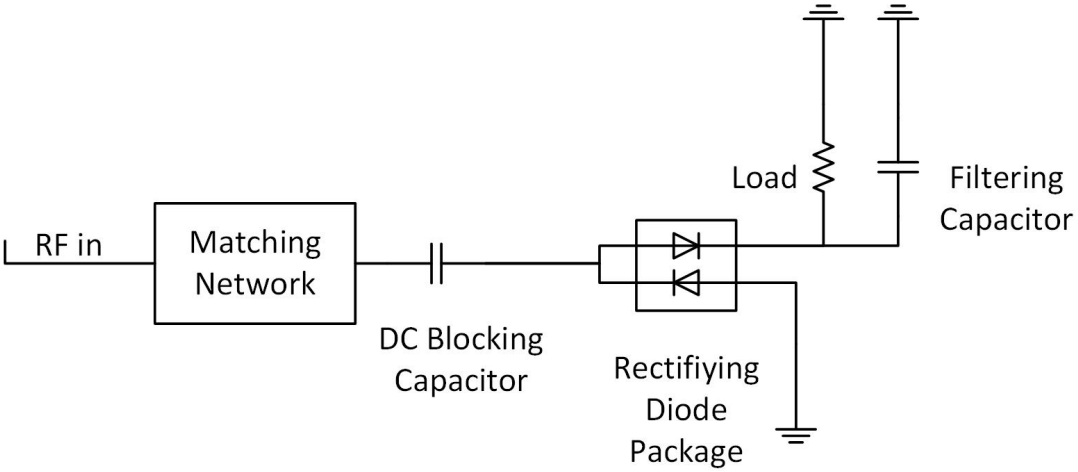

Figure 2.2: Typical topology of a class one rectifier with two stage rectification.

Table 2.1: Comparison of efficiencies for class one topologies in literature.

Reference	Efficiency	Power
[11]	70 %	0.1585 mW
[12]	60 %	0.3162 mW
[13]	70 %	3.1623 mW
[14]	41 %	10 mW
[17]	82.3 %	158 mW

A typical topology of class two rectifiers is given in figure 2.5. Second class of rectifiers have the advantage of using only distributed elements for rectifying circuit, except from load and diode itself. Since all of the components are realized from distributed elements, designer is not limited to design according to predefined lumped values and can invent better approaches. This property of class two rectifiers also enhances the relationship between the simulation and realization, since no lumped element is used, no parasitic is introduced into the circuit. This approach eliminates

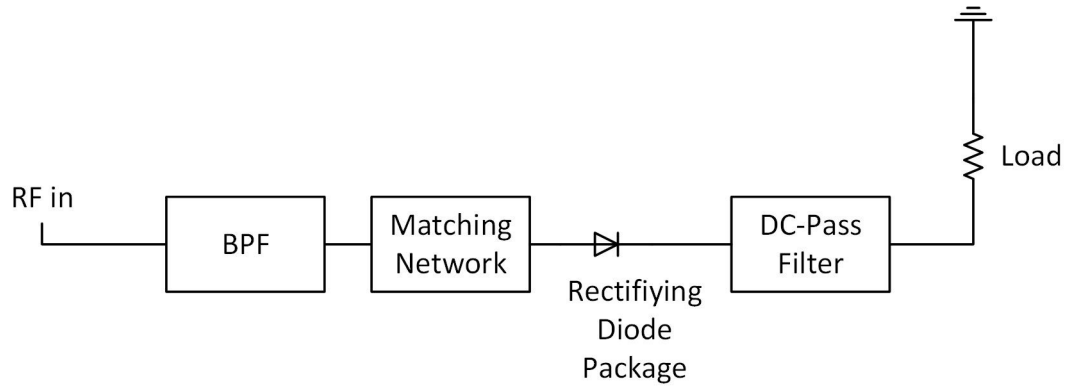

Figure 2.3: Typical topology of a class two rectifier.

the need for measurement of parasitic values of packaged lumped elements, especially for higher frequency applications. For comparison purposes, efficiencies that are achieved by this class of rectifiers in literature are given in table 2.2. Detailed information about the working principles of microwave rectifiers is presented in 2.1.1.

Table 2.2: Comparison of efficiencies for class two topologies in literature.

Reference	Efficiency	Power
[18]	85 %	1200 mW
[19]	68 %	100 mW
[20]	70 %	1.5849 mW

In this thesis work, a type two microwave rectifier is developed, designed and manufactured for the purpose of building a rectenna system. In this design HSMS2820 diode is used as a rectifying element and circuit implementation material is selected as FR4.

In the following sections of this chapter; design, development, manufacturing and testing results of a microwave rectifier that is studied in this thesis work will be discussed and presented up to minute details. By this presentation, development tools and methods will be justified and further conceptual designs and simulated developments will be presented. This presentation will proceed with the modeling of rectifying diode, design, manufacturing and testing of auxiliary circuit elements and final

design and manufacturing of the aforementioned microwave rectifier circuit.

2.1.1 General Principle of Microwave Rectifiers

Explanation of general working principles of microwave rectifiers can also be divided into two in accordance with the previous section. For the sake of brevity, working principles of class one rectifiers will be explained shortly, however class two rectifiers are studied in more detail, since the rectifier that is designed in this thesis work is a class two rectifier.

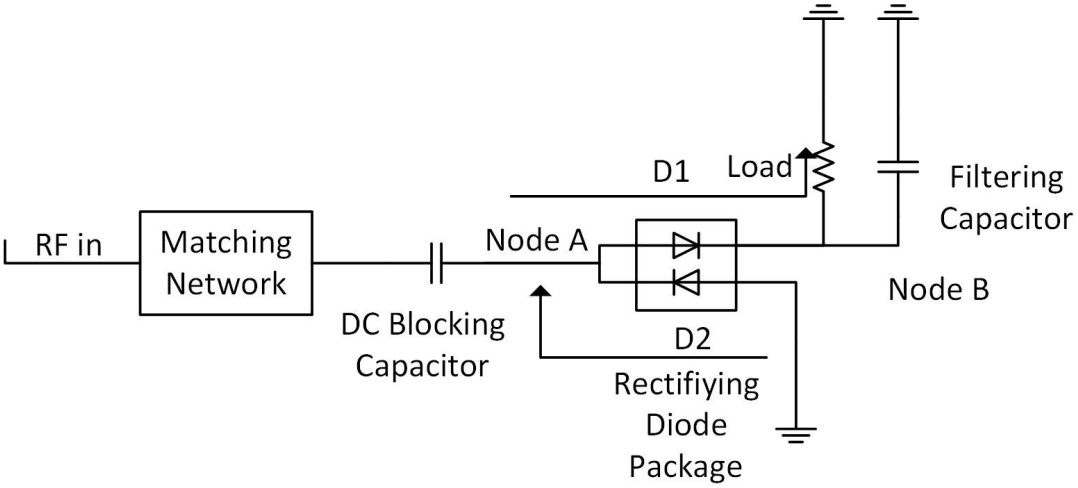

Figure 2.4: Working Mechanism of a class one rectifier.

Class one rectifiers are generally explained in time domain. When the input waveform increases, it can get through DC blocking capacitor as indicated in figure 2.4, since it is a high frequency waveform. Then it gets rectified by diode D1 and its residual high frequency components are grounded by filtering capacitor. On the negative cycle of the input continuous wave, diode D2 rectifies the negative part. Generated DC component of the negative cycle cannot run through to input port since input port is blocked by a DC blocking capacitance, however any residual high frequency component propagates through the circuit. With voltage potential build up on the capacitor, diode D2 shuts down and charge that is accumulated on DC blocking capacitance runs through diode D1 and finally through load. In steady state, this continuous behaviour induces a constant voltage on the load.

For class two rectifiers, whole device can be considered as a cavity where fundamental frequency and its harmonic are reflected back and forth inside the circuit. This class of rectifiers can be considered as a single diode mixer, where fundamental frequency is being mixed with itself over and over again. This is actually the explanation for the requirement of a DC-Pass filter structure where fundamental frequency is reflected back to the reflecting diode itself. In this mode of operation, DC-Pass filter is used for storage of unused cycle of the continuous wave form where the diode is in off state.

Derivation of a loss mechanism and operating principle of microwave rectifiers are based on references [18] ,[30], [31] and [32]. To not overflow the concept with design procedure, only results of this derivations are used in subsection 2.2.5.

2.2 Development of Rectifying Circuit

Microwave rectifier developed in this work is a class two rectifier whose general topology can be seen in figure 2.5. Flow chart of design of a rectifier is given in figure 2.6.

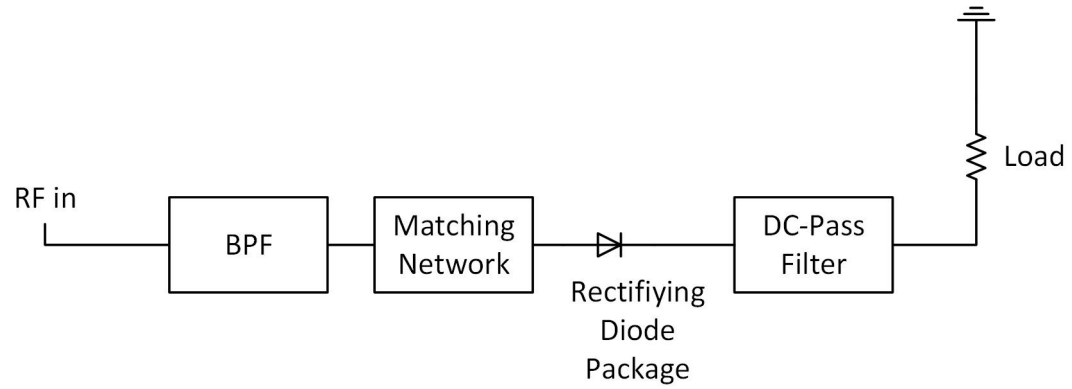

Figure 2.5: Typical topology of a class two rectifier.

Design process starts with declaration of requirements. Requirement of the design is selected as at least 60% RF to DC conversion efficiency, 2.45 GHz operation for ease of design and abundance of literature material for comparison. 10 dBm is selected as the typical input power level for the rectifier. This power level and frequency specifications are main inputs for selection of diode rectifying element.

In the second step of proposed development process, class two rectifiers are preferred since they require minimal usage of distributed elements. Since no packaged components are used in the design, all other linear elements can be implemented with distributed circuit parts. This feature of class two rectifiers are specifically important in higher frequency designs, since packaged lumped elements introduce further parasitic elements to the circuit. This introduced parasitic elements are likely to create a disagreement between simulation and comparison in designs.

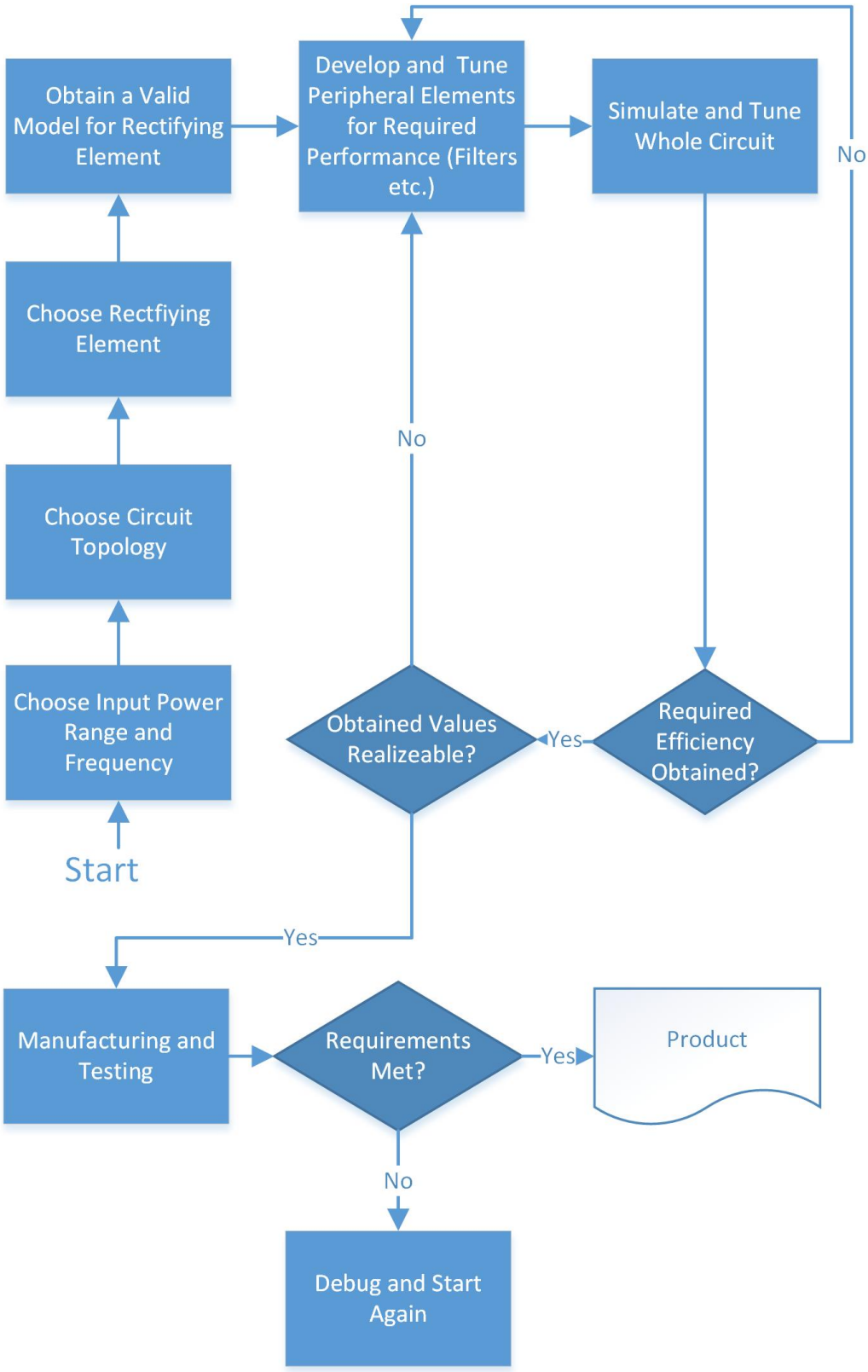

Figure 2.6: Flow chart of development process of rectifier.

As explained before choosing a rectifying element is crucial since it effects the whole design. Most important parameters of the diode are saturation current, I_s and junction capacitance C_j. These two parameters directly effects the performance of the diode at selected frequencies and power levels. Another important parameter of the diode is the break down voltage. Break down voltage is an important factor for high input levels. HSMS282x series diodes are selected for operation in 2.45GHz and 10 dBm input power level as it is suggested by the manufacturer in [26]. Saturation current of the diode is very important in zero bias detection applications, since I_b, bias current, is not applicable due to the nature of the application. As I_s, saturation current, gets lower, non-linear characteristic behaviour of diode is becomes more evident, which is a desired characteristic for zero bias rectifier applications. However there is a trade-off between I_s and C_j, junction capacitance that is inherent to the silicon design of Schottky diode. Increase in C_j degrades the rectification characteristic of the diode. This can simply explained from model of the diode. An increase in the parallel C_j capacitance leads to a lower impedance, especially in high frequencies. This low impedance leads to a lower current through R_j and aggravates the non-linear characteristics of rectifier through equation 2.3.

Fourth step in design process requires the extraction of valid models for rectifying element. However, rectifying diode in time domain exhibits a non-linear behaviour that prevents the modelling of device with simple linear parameters such as S-parameters. In the case of a non-linear device, which is the rectifying diode in this case, S-parameters cannot define the behaviour of non-linear device alone. Input power must also be taken into account for a complete definition. Another point the classical S-parameters cannot recognize in the non-linear behaviour is generation of different frequencies from input power. In non-linear device modelling, S-parameters are extended to include other harmonics that are generated by the device, which are defined as large signal S-parameters. They are explained in literature in, [21] and [22].

For the sake of brevity, large signal S-parameters are not explained in this thesis, since they are not used directly. This explained non-linear effects are included via a Harmonic Balance simulation. Large signal S-parameters are introduced briefly to reader in the purpose of introducing non-linearity concept with harmonic generation. In S-parameters measurement of the device, linear S-Parameters are used in a predefined

power level, which is the design requirement in this work and selected as 10 dBm. This power level and S-parameters, after the measurement, are used for mimicking the measurement environment of the non-linear device under test in simulations.

In simulation of microwave rectifiers, "Harmonic Balance" (HB) method is used which is a general method of simulation for non-linear circuits such as, mixers, power amplifiers and oscillators. HB is the choice of method for the simulation of non-linear devices among microwave engineers due to its speed and accuracy. Many HB solvers are available mostly as a part of a more complex simulation software package like AWR/MWO® and ADS® by Agilent®.

In analysis, HB method starts from writing Kirchoff's equations in frequency domain and divides circuit in two parts, a linear part which is already defined by nodal equations and a non-linear part, whose definition comes from both linear part and self defined non-linear equations. In the case of a diode, diode itself is defined by the SPICE equations, I-V relations, however this equations are defined in time domain. What harmonic balance method does is that it calculates response of the circuit for current, for time domain voltages then checks for nodal equations for currents in frequency domain. This simulation method continues in an iterative manner. What satisfied is the Kirchoff's equations in frequency domain. Algorithm in simulation corrects the initial condition to reduce the error and then conducts the simulation again. This iterative process continues until Kirchoff's equations are satisfied with a predefined error rate.

2.2.1 Rectifying Diode

Rectifying diode, that is used in the development of microwave rectifier circuit has been measured and remodelled to guarantee an agreeing performance between the simulation and realization. For measurement of diode package instead of TRL calibration, only a SOTL calibration is conducted on the measurement reference plane of the measurement device. This method of measurement requires modelling and design of other parts of the circuit that is used in the measurement of diode package, this part is actually the Coax-to-Planar translation itself. After modelling of the coax-to-planar connector, diode package itself is measured and its parasitic elements are extracted to

realize the measurement. modelling of Coax-to-Planar part of the circuit is explained in Appendix A.

The diode that is being selected for measurement, HSMS2820 diode, comes in a SOT-23 package. Parameters of diode for non-linear operation is being provided by the manufacturer [26] in data sheet of the diode. However parasitic elements of the package are questionable and to be extracted even though some information is provided by the manufacturer in application notes [27].

Before going any deeper into the subject it would be appropriate to discuss the non-linear model of diode itself. A Schottky diode can be modelled as a resistance that is in serial connection with capacitor and junction resistance pair as depicted in figure 2.7. This model is quite simple compared to other models. In literature more complex models are used such as [28] and [29].

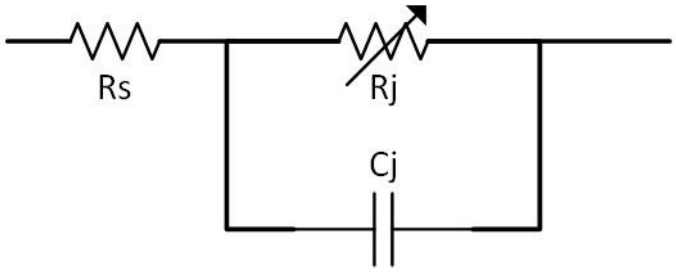

Figure 2.7: Simplified model for Schottky diode.

In Figure 2.7, R_s represents an ohmic contact resistance that is caused by the touching metal of the Schottky diode to p^+ substrate. R_j is the junction resistance that is causing the non-linear behaviour, which relates the voltage drop on the device with the current as in equation 2.2.

$$R_j = \frac{8.33 \times 10^{-5} \times n \times T}{I_b + I_s} \tag{2.2}$$

Where n is ideality factor, T is the temperature in Kelvins, I_b the base biasing current that is applied to the diode and I_s is the saturation current. Those parameters are SPICE parameters of the diode. SPICE parameters for the device are listed in 2.3. In the design of a microwave rectifier for power transfer applications, I_b is not present.

Current through a Schottky diode is related to its voltage as given in equation 2.3.

$$I = I_s\left[e^{\frac{V_b}{V_{nt}}} - 1\right] \tag{2.3}$$

Table 2.3: Given spice parameters for measured diode

Parameter	Units	HSMS-282x
B_V	V	15
C_{j0}	pF	0.7
E_G	eV	0.69
I_{BV}	A	1×10^{-4}
I_S	A	2.2×10^{-8}
N	-	1.08
R_S	Ω	6
P_B	V	0.64
P_T	-	2
M	-	0.5

In the application of an energy harvester, a DC bias is, of course, unavailable, thus in the development of circuits, I_b is disregarded.

For the extraction of the parasitic components, diode is placed in a test circuit. Realization of the circuit is presented in figure 2.8.

SOT-23 package model is primarily used for tuning of the real parasitic values of the package. SOT-23 package model that is supplied by the manufacturer can be viewed in figure 2.9. SOT-23 package is a three legged package and used for different diode configurations. It may include 2 diodes, however in case of HSMS 2820 it includes an only one diode. For different configurations, for example, HSMH2822, HSMH2823 and HSMH2824 same package is used and other diode is placed in the package configuration that is shown with dashed lines in figure 2.9.

In harmonic balance simulation, circuit that is proposed in figure 2.9 is constructed and simulated, later on, parasitic values are extracted for a realistic representation. Parasitic values that are given by the manufacturer can be seen in table 2.4.

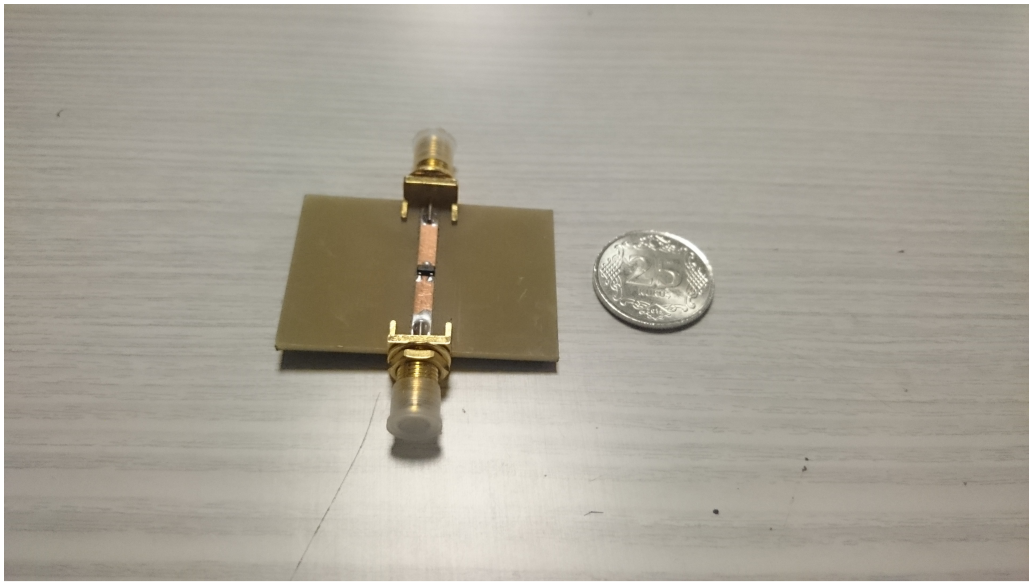

Figure 2.8: Realized test circuit for HSMS2820 diode.

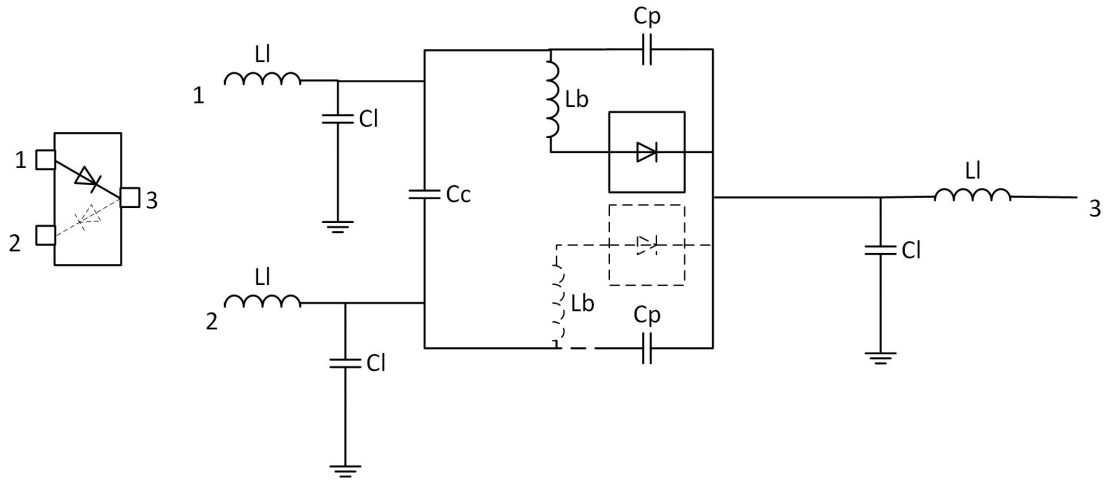

Figure 2.9: Circuit model of SOT-23 Package.

However this values are not in good agreement with measurements and extracted for matching

In figure 2.10, measurement and simulation results are given with different parasitic values. Gray dashed line shows a harmonic balance (HB) simulation with given parameters at table 2.4. Brown line is the real measurement of the test circuit and blue line is the simulation of circuit with extracted values. As can be seen from the Smith Chart at figure 2.10, extracted parameters agree with the measurements up to 4 GHz, however parasitic parameters are extracted to agree with the simulation at 2.45 GHz as it is marked in the chart. Red line is included in the chart for comparison of the

characteristic of the diode itself alone without any parasitic components that is added to the circuit by package.

It should also be noted that all measurements are taken with 10 dBm input power and all simulations are measurement of s-parameters, input impedances are extracted from this data. The measurement device is an Agilent Technologies PNA Network Analyzer, which has DC coupling.

Table 2.4: Parasitic package values that are given and extracted

	Element	L_L	C_L	C_P	C_C	L_B
	Description	Leadframe	Leadframe	Package	Coupling	Bondwire
		Inductance	Capacitance	Capacitance	Capacitance	Inductance
	Units	nH	pF	pF	pF	nH
SOT-23 (Given)	To 3 GHz	0.5	0	0.08	0.06	1.0
SOT-23 (Extarected)	To 3 GHz	0.5	0.03	0.04	0.03	0.5

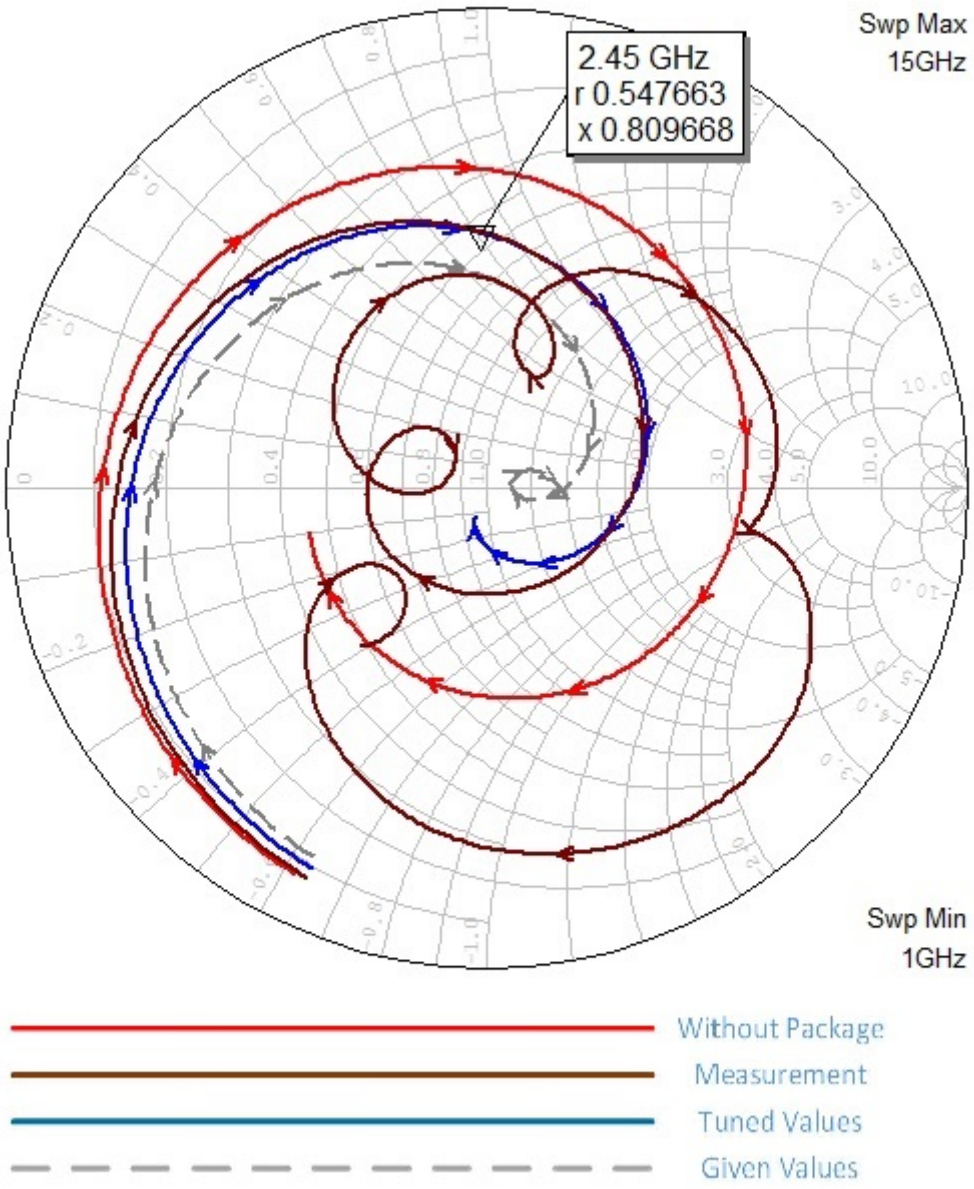

Figure 2.10: Input impedances for given (Gray-dashed), measured(Brown) and extracted(Blue) diode package parameters with the impedance of diode alone without package(red) from 1GHz to 15 GHz.

It is evident in figure 2.10 that parasitic components are taking over the impedance characteristic of the SOT-23 packaged HSMS2820 diode and proposed parasitic model for the device is insufficient. For broadband modeling of the package, more complex and frequency dependent models should be proposed. However for development in center frequency, which is 2.45 GHz, proposed extracted model is adequate.

This parasitic component extraction is mainly conducted to obtain a good agreement between simulation and measurement results. This parasitic model is used in simulation environment.

In the fifth step, matching circuit and filters are designed. These filters are namely DC-Pass filter and bandpass filter.Designs of DC-Pass filter and BPF are presented in sections 2.2.3 and 2.2.2 respectively.

Simulation and Tuning step includes conducted harmonic balance simulations of the whole rectifier circuit and tuning of other elements such as, DC load and matching sections. In the development and refinement of such elements an iterative process is used. Where the lengths and impedances of distributed parts of the circuit are first found in the optimizer of the development environment, which is AWR-MWO® in our case, and then are simulated in full wave simulations for better accuracy. Full wave simulators used in this phase of development are Sonnet® and ANSYS-HFSS®. Details of the rectifying circuit simulations are given in section 2.2.5.

Development cycle given in figure 2.6 is repeated till the required efficiency level is reached. In each iteration step, distributed parts are tuned again or redesigned and included in harmonic balance simulation.

2.2.2 Design of Band Pass Filter

Non-linear rectifying elements inevitably introduce harmonics to rectifying circuit. In the case of high input power, power of these harmonics can be used for further improvement of efficiencies of rectifiers. Rejection of other frequency bands is another assignment to band pass filter. Since introduction of other frequencies may disrupt the operation of rectifying diode by inducing other DC voltages and currents inside of the circuit.

During the evaluation of harmonic balance simulation results, it is observed that a band pass filter likely to present more line and dielectric losses to circuit than its contribution to efficiency. This high losses are due to the selected high loss substrate FR4. Thus in this design a band pass filter is not presented. However for a low loss substrate, usage of a band pass filter is likely to increase the conversion efficiency in the design.

2.2.3 Design of DC-Pass Filter

DC-Pass filter is used for isolation between RF and DC parts of the circuit while reflecting back the fundamental frequency and its harmonic components to rectifying element.

In the design of DC-Pass filter a bias-tee like characteristic is selected except that, different from a bias-tee element, which is a circuit element used for isolation of RF and DC parts, RF input of the circuit is not forwarded to another port, instead reflected back to input port.

Idea behind the design of this structure is reflecting back the RF power by abrupt changes in characteristic impedance, as it is in a stepped impedance low pass filter. Another idea is to introduce as many possible open circuit conditions to the circuit with $\lambda/4$ transmission lines to obtain a good return in S_{11} but leaving a short circuit path for DC to complete its circuit on DC load.

The design uses a whole λ length transmission line starting from an open circuit then transforming into a short circuit and finally an open circuit again. A layout of the final DC-Pass filter is presented in figure 2.13.

As with the rest of the circuit, DC-Pass filter is also placed on 1.6 mm, $(\epsilon = 4.66)$ FR4 substrate. Dimensions of DC-Pass filter are presented in figure 2.12 with exact dimensions in table 2.5.

Input of the circuit is port 1 and output is port 2. Circuit uses 6 open circuit conditions to enhance S_{11} return at 2.45 GHz and first harmonic 4.9 GHz. First the circuit with one open circuit is designed. Then circuits with 2, 4 and 6 open circuits are examined.

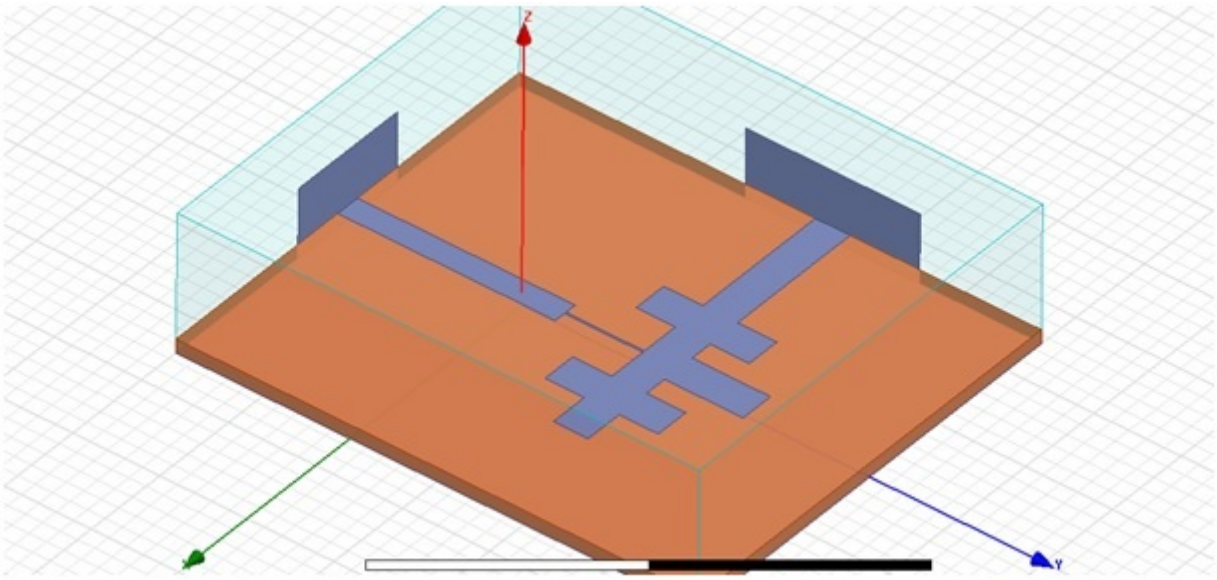

Figure 2.11: Physical layout of the 6 open circuit DC-Pass filter in HFSS simulation environment.

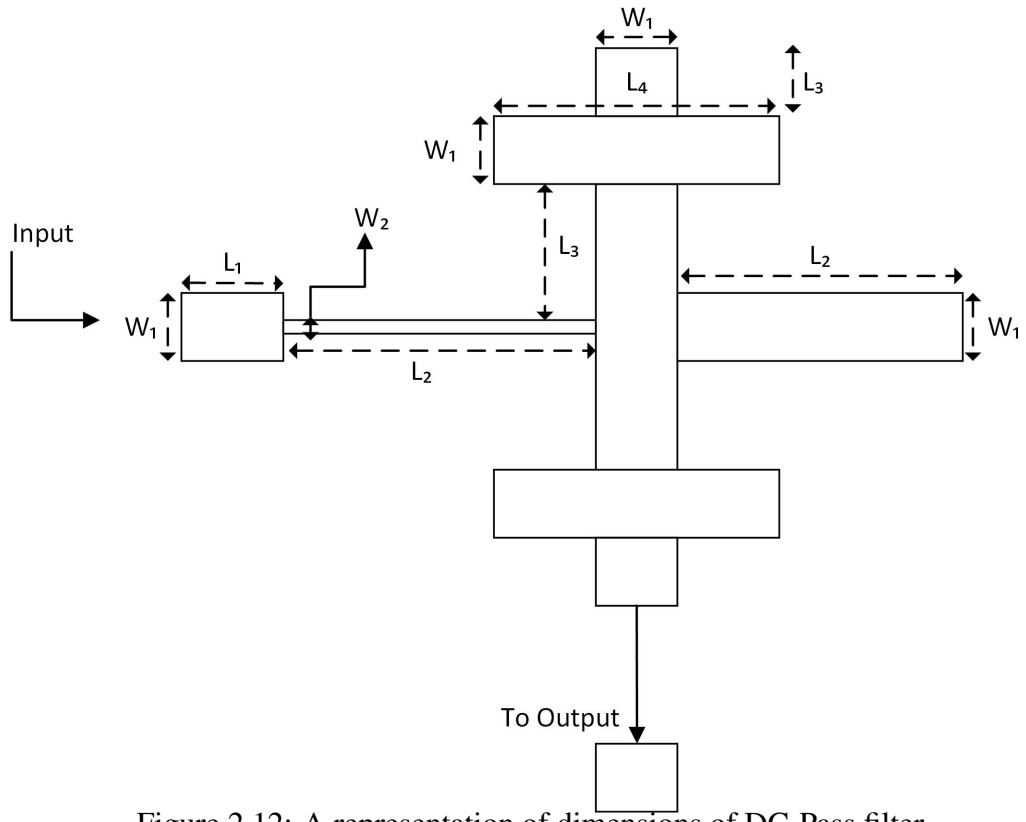

Figure 2.12: A representation of dimensions of DC-Pass filter.

For comparison purposes S_{11} values are plotted for all these cases in figure 2.14, frequency sweep is from 0.1GHz to 15 GHz for the investigation of fundamental

Table 2.5: Exact dimensions of DC-Pass filter

Dimension	Length
W_1	4 mm
W_2	0.25 mm
L_1	2.893mm
L_2	9 mm
L_3	4.5 mm
L_4	13 mm

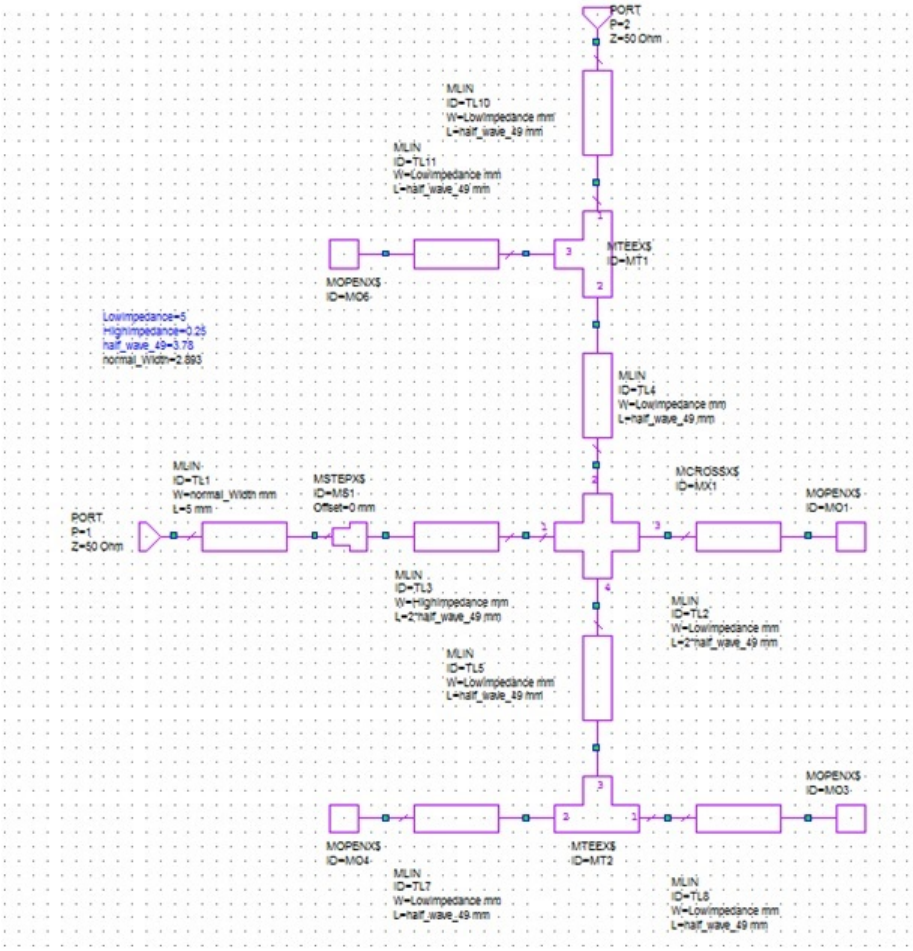

Figure 2.13: Layout of final DC-Pass filter.

frequency to higher order harmonics.

Figure 2.14 is obtained from a linear simulation in AWR-MWO®. As can be expected a linear solver is not very powerful in the simulation of distributed structures such as

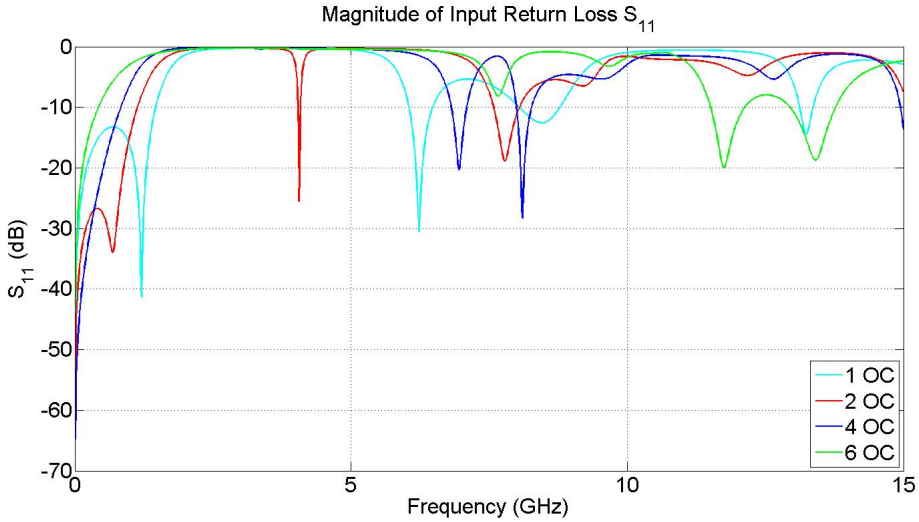

Figure 2.14: Comparison of DC-Pass filters with 1, 2 , 4 and 6 open circuit conditions.

this design. Thus simulations in ANSYS-HFSS® and Sonnet® are also conducted for 6 OC circuit. Figure 2.15 presents this results. Physical layout of the 6 open circuit DC-Pass filter in HFSS simulation environment is presented in figure 2.11.

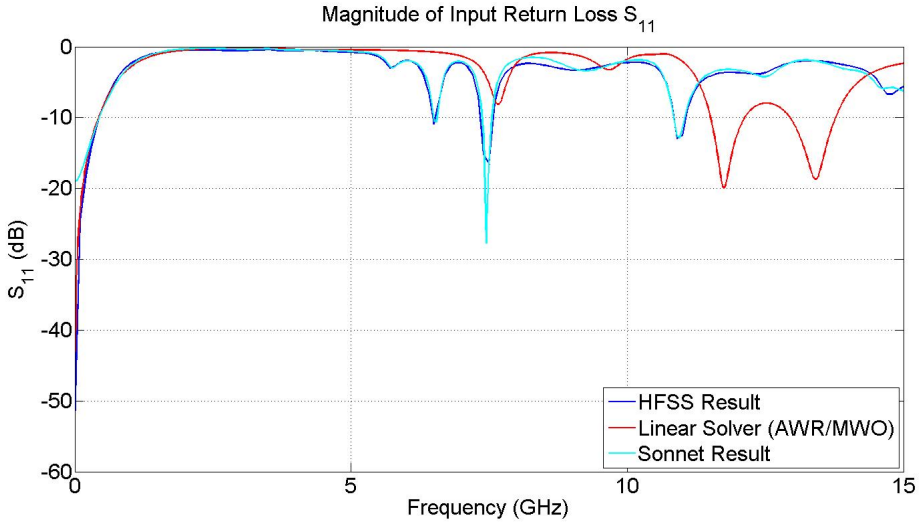

Figure 2.15: Comparison of ANSYS-HFSS® and Sonnet® simulations of 6-OC circuit.

As indicated in figure 2.15, simulations of Sonnet® and ANSYS-HFSS® is in very good agreement, the reason behind the discrepancy in DC is due to the fact that sonnet approximates a low frequency as DC, such as 13kHz. Another comparison is presented in figure 2.15 between linear solver AWR-MWO® and full wave solvers

ANSYS-HFSS® and Sonnet®. This Results indicate that solutions of linear solver and full-wave simulators are not in very good agreement. This behaviour of linear extracted models are well known for complex structures. Since the structures are closely placed, linear modelling of the structures require consideration of inter-element couplings, which are not realized in linear models.

Simulation results indicate a very good return of -0.25 dB around fundamental frequency, 2.45 GHz and -0.45 dB around 4.9 Ghz, first harmonic.

2.2.4 Tuning and Optimization of Microwave Rectifier

After the design of DC-Pass filter, whole circuit is shown figure 2.16 which is simulated in harmonic balance simulation. In this simulation, matching parameters and other distributed network elements are optimized with optimization engine of AWR-MWO®. Used optimization methods are "Pointer-Robust Optimizer", "Pointer Gradient Optimizer", "Simplex Optimizer" and "Genetic (Gaussian Distribution) Optimizer". Usage of optimization tools will not be discussed in any further detail in this thesis work. However, results of this process, which is matching network will be presented. Optimization parameters are dimensions of matching network stubs. Different optimizers are used for the purpose of saving them from local optimization points. Among this optimizers, "Genetic Optimizer" is found to be very successful for finding global optimum point.

Layout of the optimized matching network is shown in figure 2.17. Dimensions of matching network is represented on figure 2.17. Real values for shown dimensions are given in table 2.6. Width of transmission lines in figure 2.17 is 2.94 mm.

In the optimization of circuit, an embedded sonnet solver from AWR-MWO® environment is used. In the lower left corner a shorted via can be seen. This shorted via is placed for the completion of DC path inside of the circuit, since RF port does not necessarily present DC coupling.

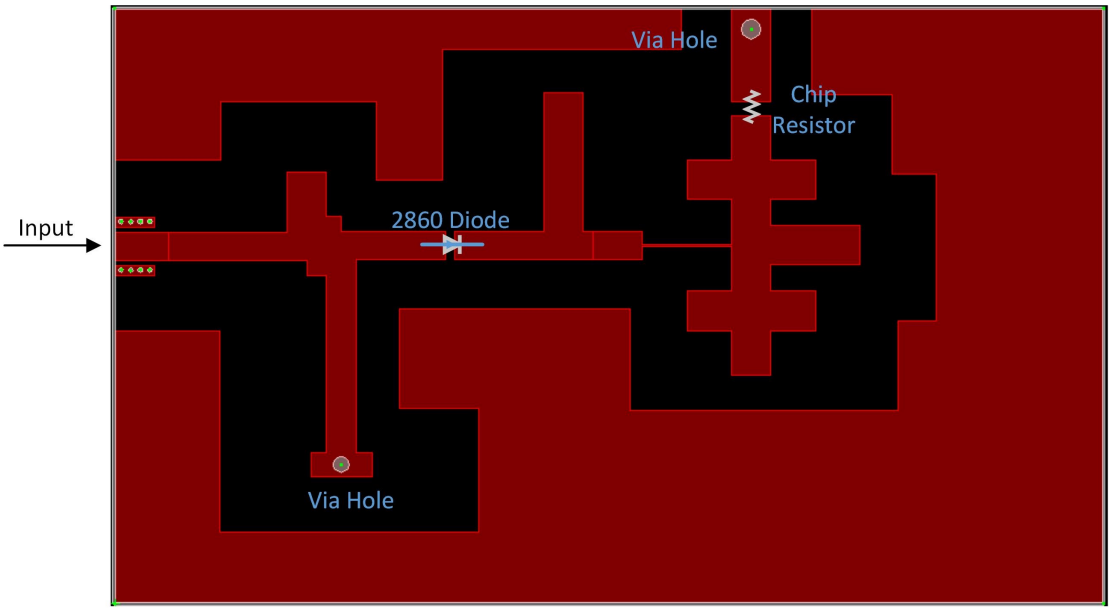

Figure 2.16: Layout of microwave rectifier as a whole, red parts represent unpeeled copper conductor, other discreet elements, DC load and diode, are also presented.

Table 2.6: Exact dimensions of Matching network

Dimension	Length
W_1	4 mm
W_2	6.2 mm
W_3	4 mm
L_1	12 mm
L_2	6.1 mm
L_3	17.9 mm
L_4	14 mm
L_5	5.5 mm
L_6	11 mm
L_7	5 mm
L_8	4 mm

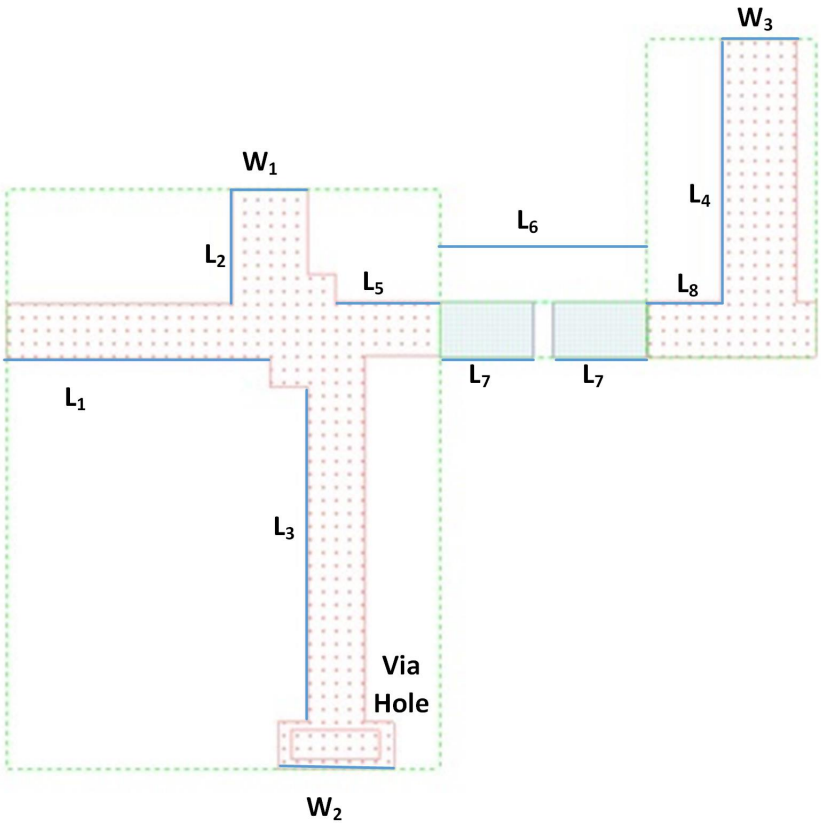

Figure 2.17: Matching network layout with the place that is left open for the placement of diode.

2.2.5 Performance of Microwave Rectifier

In this section, information about the performance of rectifier will be discussed.

Picture of developed microwave rectifier is displayed in figure 2.18.

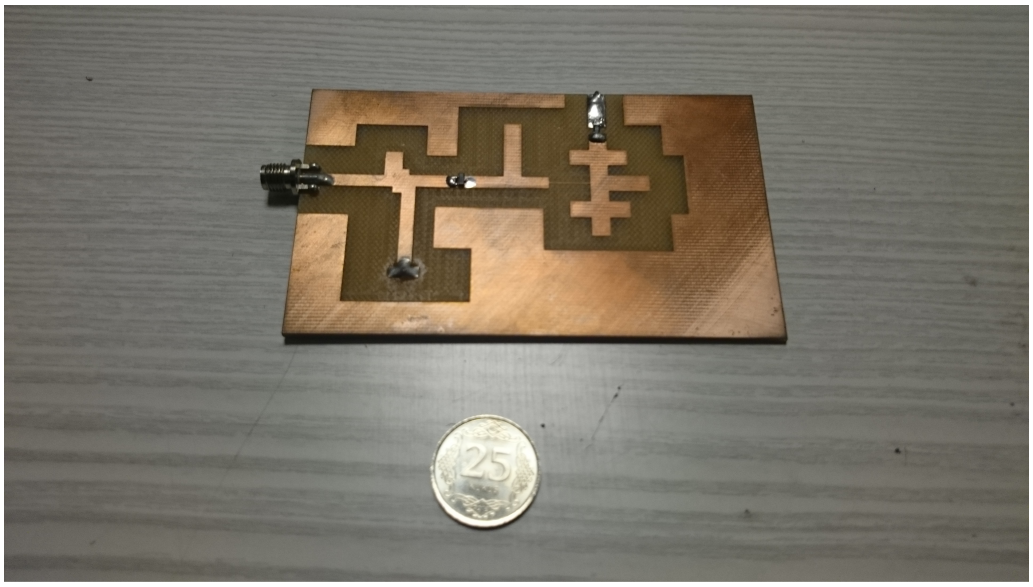

Figure 2.18: Picture of developed microwave rectifier.

Simulated microwave rectifier shows an efficiency of 59.3%. This efficiency may be found relatively low compared to references from literature, however considering the high loss substrate in this design this efficiency can be increased by simply using a lower loss substrate. With replacement of substrate losses from FR4 substrate, whose tangent loss is 0.016, with a lower loss material, such as Rogers 5880, simulation yields an efficiency of 60.81%. This efficiency is observed after further tuning of the circuit when Rogers 5880 is used.

This efficiency could be further enhanced by a more proper diode and topology selection. For this purpose, a different simulation is conducted, with 2862 diodes, which is a diode pair and same proposed DC-Pass structure. This example simulation yields an 80.56% efficiency with a high loss FR4 for circuit, with a low loss material this simulation yields a 84.84% efficiency. It should be noted that in this demonstration simulation, a capacitor is used for charge pump, which is not characterized and may lead to a loss due to its parasitic series resistance that is present in its model. Very high efficiency of this demonstration design can be attributed to hybrid nature of its

topology, which is created with the usage of a proper DC-Pass filter. This design, however, is not going to be explained in here, since it has not been implemented. Nevertheless, real implemented circuit in this design, is a proof of the concept and the development method for microwave rectifiers, which also validates the other simulated circuits. Starting from this point, further development of microwave rectifiers, as it is proposed, with higher efficiencies are possible.

Conversion efficiency is calculated based on the formulation derived in [18], [30], [31] and [32] and it is found as 49.788%. Compared to value obtained by simulations 59.3%, it is seen that there is a difference of 10%. The reasons for this behaviour lies in the assumptions that are made for derivation of the expressions. However, theoretical equations still stand a good approximation and can be taken as a basis for further design selections and evaluations.

Power harmonic contents of simulated measurement point is presented in figure 2.19. Only 4 harmonics are included for this simulation with DC and centre frequency itself.

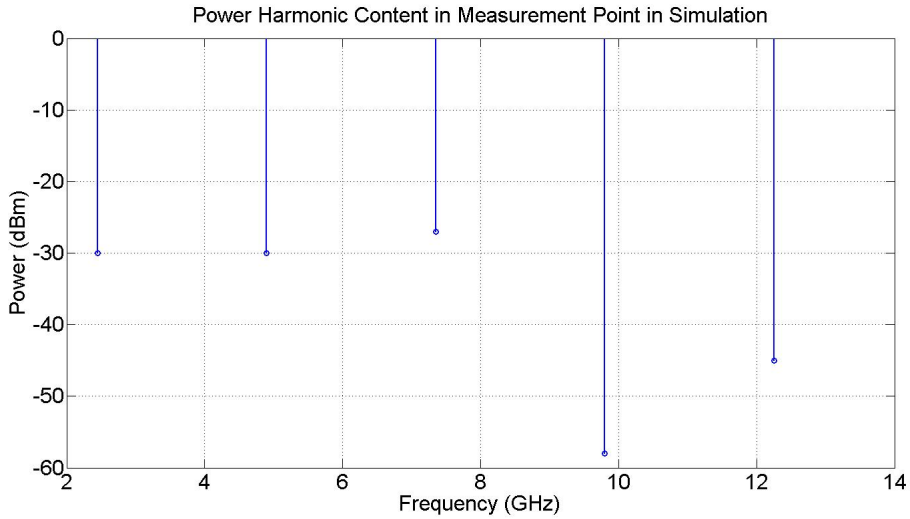

Figure 2.19: Harmonic content of measurement point in simulation.

Power bandwidth and frequency bandwidth of the circuit also measured in the scope of this work. Simulated and measured power bandwidth is displayed in figure 2.20.

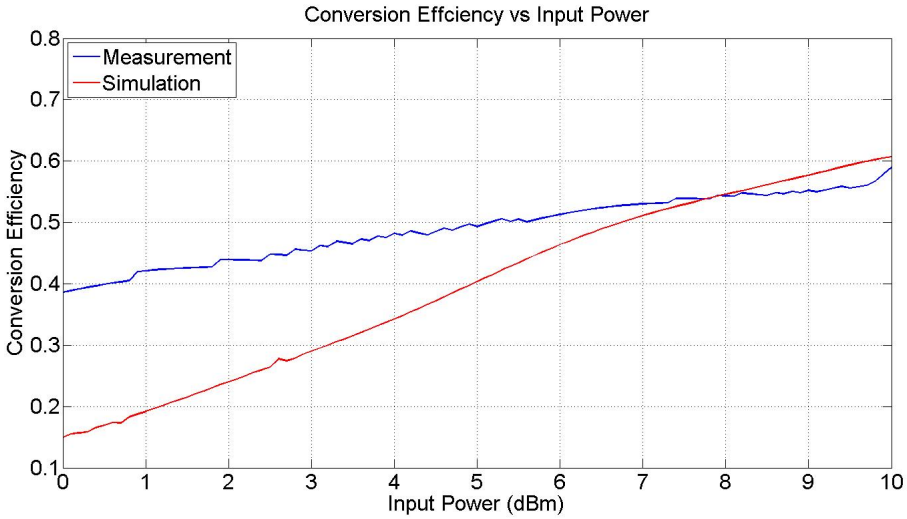

Figure 2.20: Comparison of simulated and measured conversion efficiencies of manufactured microwave rectifier with changing input power level.

The discrepancies around 0 dBm input power is due to the characterization process. Since characterization of the diode is performed at a certain power level, which is 10 dBm, and tuning of diode parameters are also performed in this power level. Thus the simulation and measurement results are disagreeing except for 10 dBm input power level.

Frequency bandwidth of the structure is presented in figure 2.21. As indicated in figure 2.21, simulated and measured conversion efficiencies are in good agreement. Tendency of drop at the end of graph can be attributed to loss frequency characteristic of used connector in the circuit. Even though loss mechanism is included in the simulation frequency, which is 2.45 GHz, its frequency dependent characteristic is not used in the simulation. As can be seen from measured loss characteristic of SMA connector from figure A.6, insertion loss of the connector increases with frequency.

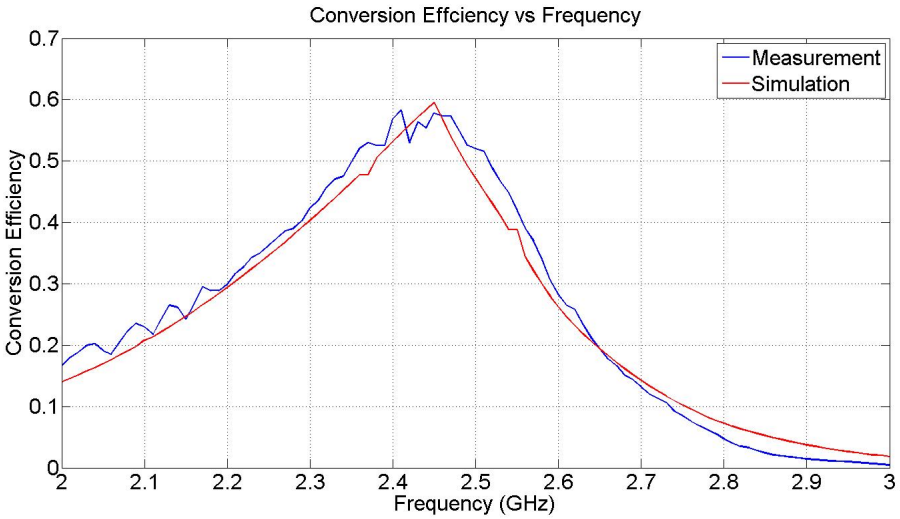

Figure 2.21: Comparison of simulated and measured conversion efficiencies of rectifier circuit with changing input frequency.

Further efficiency enhancements can be obtained in usage of rectifiers in rectenna applications. Instead of matching the whole circuit to a 50Ω feed, complex impedances that are presented by antennas can be used. This method requires determination of optimized input impedance which eliminates the necessity for a matching network, thus eliminating the dielectric and transmission line losses that are introduced by matching network. However this method requires a realizable input impedance that can be generated in the antenna.

2.3 Conclusion

In this chapter , development cycle of a microwave rectifier is introduced and used for design of a microwave rectifier which will be used in this thesis work. Simulation and measurement values for power and frequency bandwidth values for designed rectifier are presented in figures 2.20 and 2.21 respectively. This developed microwave rectifier satisfies the proposed design requirements with a measured RF to DC conversion efficiency of 56%. This value is comparable to the simulation value of 59%. This value can be found lower than some literature references. However, with the selection of a lower loss material this value can be improved easily.

Figure 2.21 is very good agreement with the values of simulation results. However,

for figure 2.20 simulation and measurement values differ from each other as the power level decreases. This behaviour is due to the selected modeling input power level of the diode. Since 10 dBm is selected for the target power range, this power level is used in the modelling and extraction of parasitic parameters. Thus, simulation and measurements agree on this power level, 10 dBm.

With the development of a microwave rectifier, one of the objectives of this thesis work is completed.

CHAPTER 3

DESIGN, MANUFACTURING AND TESTING OF A SUBSTRATE INTEGRATED WAVEGUIDE CAVITY BACKED SLOT ANTENNA

In the last decade, many applications for civilian usage that require tremendous amounts of bandwidth are introduced to literature [36], [37], [34], [35]. These applications are seeing 58-66 GHz unlicensed bandwidth as a potential application area [38]. However, classical printed microwave transmission mediums are not appropriate for this applications, due to their losses at high frequencies and radiation prone natures. In such cases SIW technology is presented as a successful candidate for applications targeting higher frequency market. SIW's low cost for mass production and possibility of integrating them with packaged components further popularizes the medium as a choice. With requirement of building SoP(System on Package) components, other microwave elements are also required to be compatible with this new technology.

SIW is formed by embedding two parallel rows of cylindrical copper plated vias in a substrate that is cladded with conductors on both sides. These vias act as conducting walls and this structure acts as a waveguide. Even though side walls are not solid conductor, it acts exactly as a waveguide under some certain conditions, regarding the geometry and frequency of operation [33].

With the development of SIW technology, integration of SIW elements with antennas is an unavoidable requirement. For this requirement, different SIW antennas are developed in literature such as, SIW cavity backed slot antennas [39], [40], SIW cavity backed patch antennas [42], SIW opening horn antennas [43] and SIW slot arrays

[44].

Cavity backed antennas are mostly preferred for their higher gains and low back-to-front ratios. However, their thick geometry hinder their utilization in applications where the space left for antenna is limited in height. SIW cavity backing shows a great reduction in large profiles of cavity backed antennas. In this thesis work, a SIW cavity backed slot antenna has been designed, manufactured and tested for being used as the power capturing antenna of the rectenna system. This antenna is designed to operate at 2.45 GHz frequency.

SIW cavity designed in this work is practically less than $\lambda_0/150$ in height, compared to classical cavity backed antennas which are generally $\lambda_0/4$ in profile [48], this design shows a great reduction in thickness. Operation principles are same as any other slot antenna, where an electric field is created on the slot by out of phase voltages on the opposite longer sides of slot. This electric field distribution, that is created on the slot gives rise to the radiation in the form of an equivalent magnetic current. With classical theory, the radiation pattern of this slot can be determined by using two fundamental principles [45]. Electric field that is present on the surface of the slot is turned into electric and magnetic currents and with the replacement of the slot surface with a perfect electric conductor, classical $\vec{M}_s = -2\hat{n} \times \vec{E}$ slot formula is obtained.

3.1 Design of SIW Cavity Backed Antenna

Rogers 5880 of 0.788 mm thickness is used as a substrate. Both sides of the substrate are cladded by a coper of 35μm thick. A SIW cavity is formed by installing electroplated vias into this substrate. This structure can be seen in figure 3.1 in layout form, where both of its sides are shown. Dimensions that are presented in figure 3.1 are listed in table 3.1. For dimetric 3D rendered visual image of designed antenna in simulation environment please refer to figure 3.2.

Feeding structure of the antenna consists of a microstrip line that is connected to a grounded coplanar waveguide (GCPW) which ends with a short circuit. Characteristic impedances of GCPW and microstrip line are both calculated to be 50 Ω. The width of the inner conductor of GCPW is same as the microstrip line. Impedance of the microstrip line is calculated to be 50 Ω by simply setting the width of the conducting line, since substrate height and permittivity are predetermined with the selection of substrate. This line width is also applicable to GCPW, thus only parameter left for tuning of its impedance to 50 Ω is the gap between the centre conductor and ground plane. For this particular design, as it has been listed in the table 3.1, width of the microstrip line is 2.4 mm, which is also the width of the centre conductor for the GCPW. Gap between the centre line and ground plane is 1.8 mm in GCPW. This particular feeding mechanism is fixed in structure and cannot be varied for further investigation, aside from the length of GCPW extending into the cavity, which is a crucial parameter in matching of the antenna structure to 50 Ω .

Radiating slot in this design is backed by the SIW cavity. This cavity is responsible for the formation of out of phase voltage that is giving rise to the radiation on the surface of the slot. The resonance frequency of this structure can be easily determined with classical rectangular cavity models, such as by equation 3.1, that can be found in general literature and text books [46], in conjunction with equivalence transformation equations that are used for transforming SIW walls in to linear conductor walls as suggested in [33].

$$(f_r)_{mnp} = \frac{1}{2\pi\sqrt{\mu\epsilon}}\sqrt{\left(\frac{m\pi}{a}\right)^2 + \left(\frac{n\pi}{b}\right)^2 + \left(\frac{p\pi}{c}\right)^2} \tag{3.1}$$

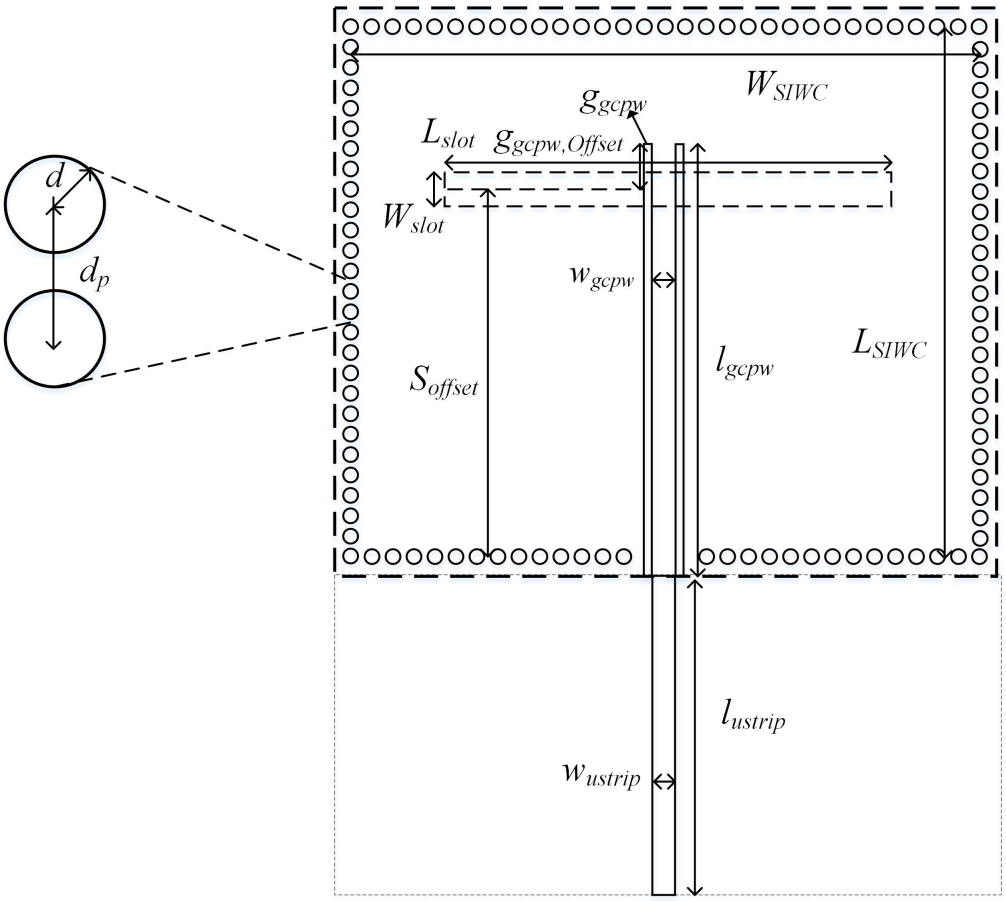

Figure 3.1: Layout of designed antenna with both of its sides. Drawing is not to scale.

$$L_{Effective} = L - 1.08\frac{d^2}{d_p} + 0.1\frac{d^2}{L} \tag{3.2}$$

In the equation 3.2, d_p represents the distance between the centre of two consecutive vias and d represents the via diameter. For SIW to be acting as a guiding medium, relationship between d_p, d and λ must satisfy equations 3.3.

$$d/d_p \geq 0.5 \tag{3.3a}$$

$$d/\lambda_0 < 0.1 \tag{3.3b}$$

Values selected for this SIW structure are 2 mm for via diameter (d) and 3 mm for via distance (d_p). These values satisfy the conditions of equation 3.3 at 2.45 GHz frequency.

Table 3.1: Listing of Real dimensions that are shown in figure 3.1

Dimension	Value
W_{slot}	5 mm
L_{slot}	45 mm
W_{SIWC}	72 mm
L_{SIWC}	72 mm
l_{gcpw}	50.3 mm
w_{gcpw}	2.4 mm
g_{gcpw}	1.8 mm
l_{ustrip}	30 mm
w_{ustrip}	2.4 mm
S_{offset}	32.5 mm
$g_{gcpw,Offset}$	13.8 mm
d_p	3 mm
d	2 mm

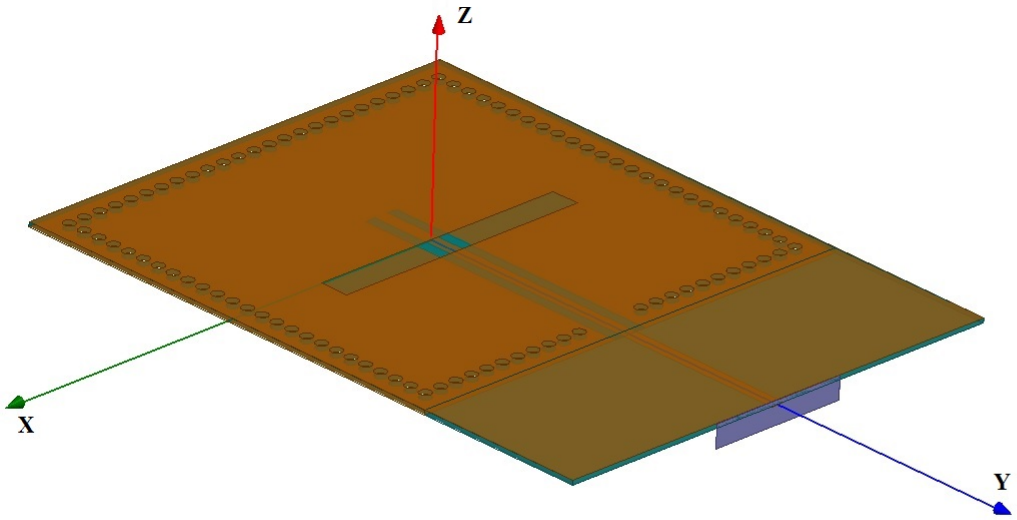

Figure 3.2: 3D rendered image of designed antenna in simulation environment Ansoft HFSS® in dimetric perspective.

However, existence of slot and feed line disturb the cavity modes. Therefore equations 3.1 and 3.2 can not be used for calculation of resonant frequencies of the structure directly. Analysis of this antenna can be modelled in a full-wave solver environment. Resonant frequencies can be found by solving the eigen frequencies of the structure. For this purpose, as with the rest of this thesis work, Ansoft HFSS® is used as the full-wave solver. Results of this eigenvalue calculations are used for determination of the radiation frequencies of the structure.

For the design of SIW cavity backed (SIWCB) antenna, the paper [39] is taken as a reference for design. In [39] a SIWCB antenna operating at 10 GHz with 140MHz bandwidth is designed. This reference work is extended to the desired frequency of 2.45GHz with proper feeding and radiation efficiency.

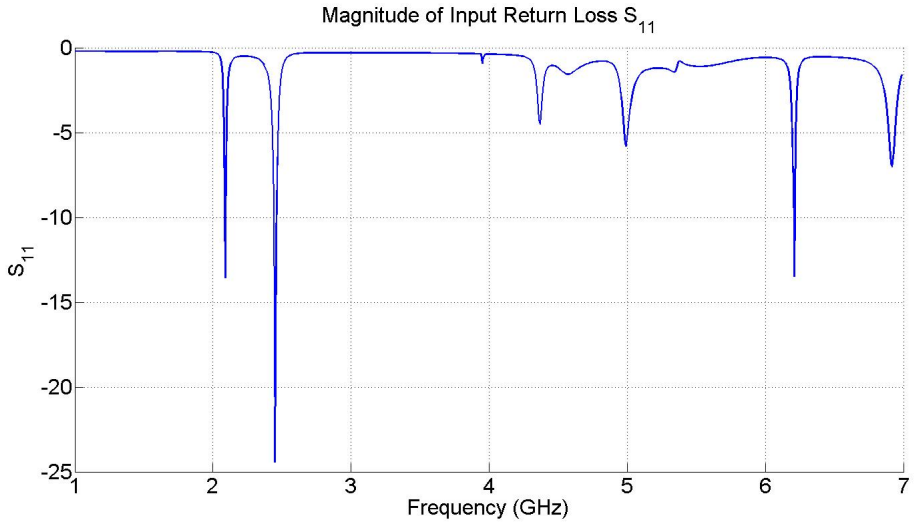

Figure 3.3: S_{11} simulation results for designed SIWCB Slot Antenna.

S_{11} simulation results for designed antenna are presented in figure 3.3 where the radiation frequencies can be interpreted. As indicated, designed antenna presents radiations in different frequencies. These frequencies are related to excited modes inside of the SIW cavity. Aside from 2.45 GHz desired radiation frequency, antenna shows other radiation frequencies. First of this radiation frequencies, 2.09 GHz, is related to TM_{110} mode of the cavity. Magnitude of complex electric field for this radiation is plotted in figure 3.4. As expected from the first mode of the cavity, only one maximum for magnitude of electric field exists around the cavity. This excited first mode also creates a radiation from the slot of the antenna, however, its radiation efficiency

is comparably low compared to desired radiation frequency of the antenna, 2.45 GHz. Magnitude of complex electric field is plotted in figure 3.5. Even though not recognizable at first glance, excited mode for radiation at 2.45 is TM_{120}. The radiation of TM_{120} is more efficient than TM_{110}. This situation is due to the fact that TM_{110} mode cannot create out of phase voltages on the sides of the slot efficiently. In the case of TM_{120} mode, voltages that are induced on the longer opposite sides of the slot are out of phase. Radiation efficiencies for these two modes are 72% and 52% respectively. Other radiation frequencies in this antenna design are due to higher order modes of cavity.

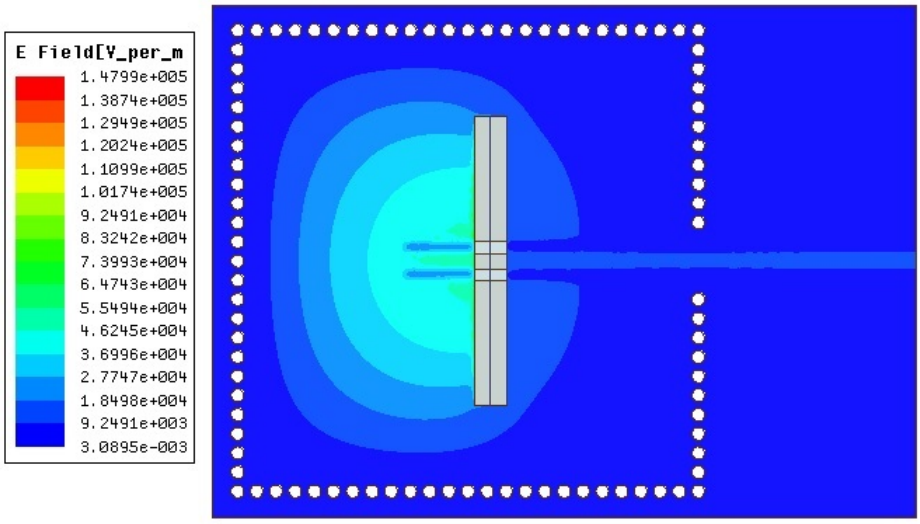

Figure 3.4: Magnitude of Complex electric field at 2.09 GHz.

Slot length is selected to be in resonant with the radiation frequency in this design to maximize radiation efficiency. Resonant slot length is half of the guided wavelength. In literature [45] it is shown that this half wavelength is used in slot antennas to give maximum directivity and radiation efficiency. This half wavelength behaviour can further be explained with voltages that are present on the slot. Since the short sides of the slot are shorted out, no voltage difference exists between the two opposing sides of the slot at the edges of the slot, this is the boundary condition, however maximum

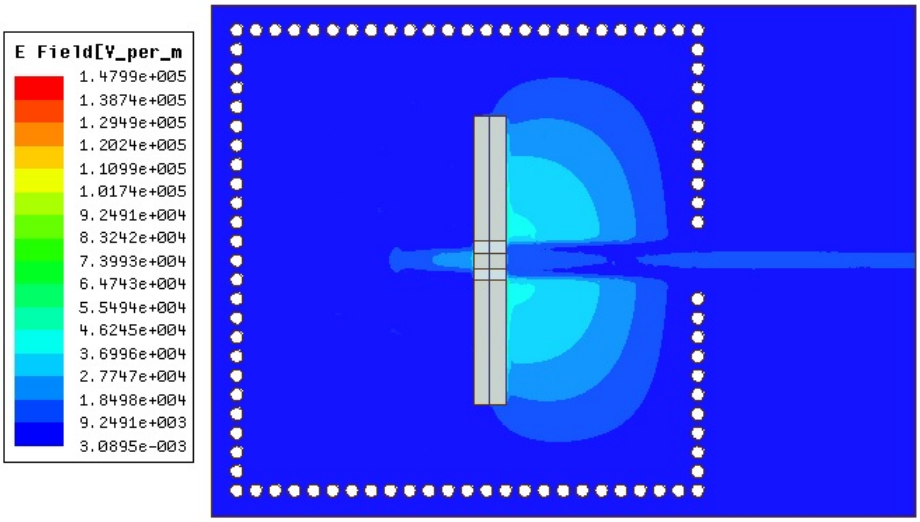

Figure 3.5: Magnitude of Complex electric field at 2.45 GHz.

voltage difference is created in the middle of the slot, giving rise to maximum electric field. Antenna radiates with adding up of these voltage differences in phase. For lengths larger than half wavelength, voltage distribution on the slot will be larger than half wavelength, in which the out of phase parts will be cancelling each other leaving the slot with a less strong voltage distribution, thus with a lesser directivity and efficiency. For slot lengths that are shorter than half wavelength, voltages that are adding up in phase are not as strong as in the case of half wavelength, thus again a lesser efficiency and directivity is obtained. Finally, as a result, half wavelength for the slot is the optimum length for maximum efficiency and directivity. It should be noted that currents around this slot are in opposite direction and does not radiate.

Before going any further into the effects of geometrical dimensions on antenna performance, it would be suitable to discuss the simulation result. Simulation result for S parameters around centre frequency are visible in figure 3.6. -10dB and -5dB bandwidths of the antenna are around 20 MHz and 50 MHz respectively. As expected, it is a narrow band antenna since it employs the cavity modes for radiation.

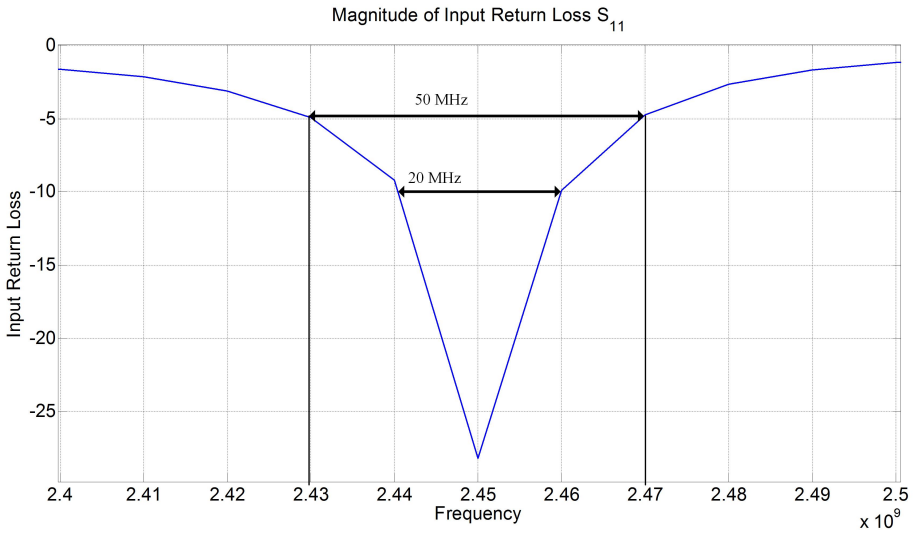

Figure 3.6: Simulation result for magnitude of input return loss of designed SIWCB antenna.

Simulated radiation patterns in E and H planes of the antenna are also presented in figure 3.7. In figure 3.7, E-plane has a half power beam width of 88°. This value is 108° for H-plane. HPBWs (Half Power Beam Width) of designed SIW antenna is slightly more than a straight patch antenna designed on same substrate with the same thickness. In a same frequency patch antenna, HPBWs are 60° and 80° in E and H planes respectively.

As explained, efficiency of the designed antenna is 72%. This radiation efficiency is below some SIWCB designs such as one reported in [39] as 84 %.

For further investigation, parametric study is performed. The investigated parameters are length and width of the slot, relative position of slot to the centre of the cavity, substrate height and the length of grounded coplanar waveguide line that is extending into the SIW cavity. Radiation efficiency, maximum directivity and input return loss are examined to observe the effect of these parameters.

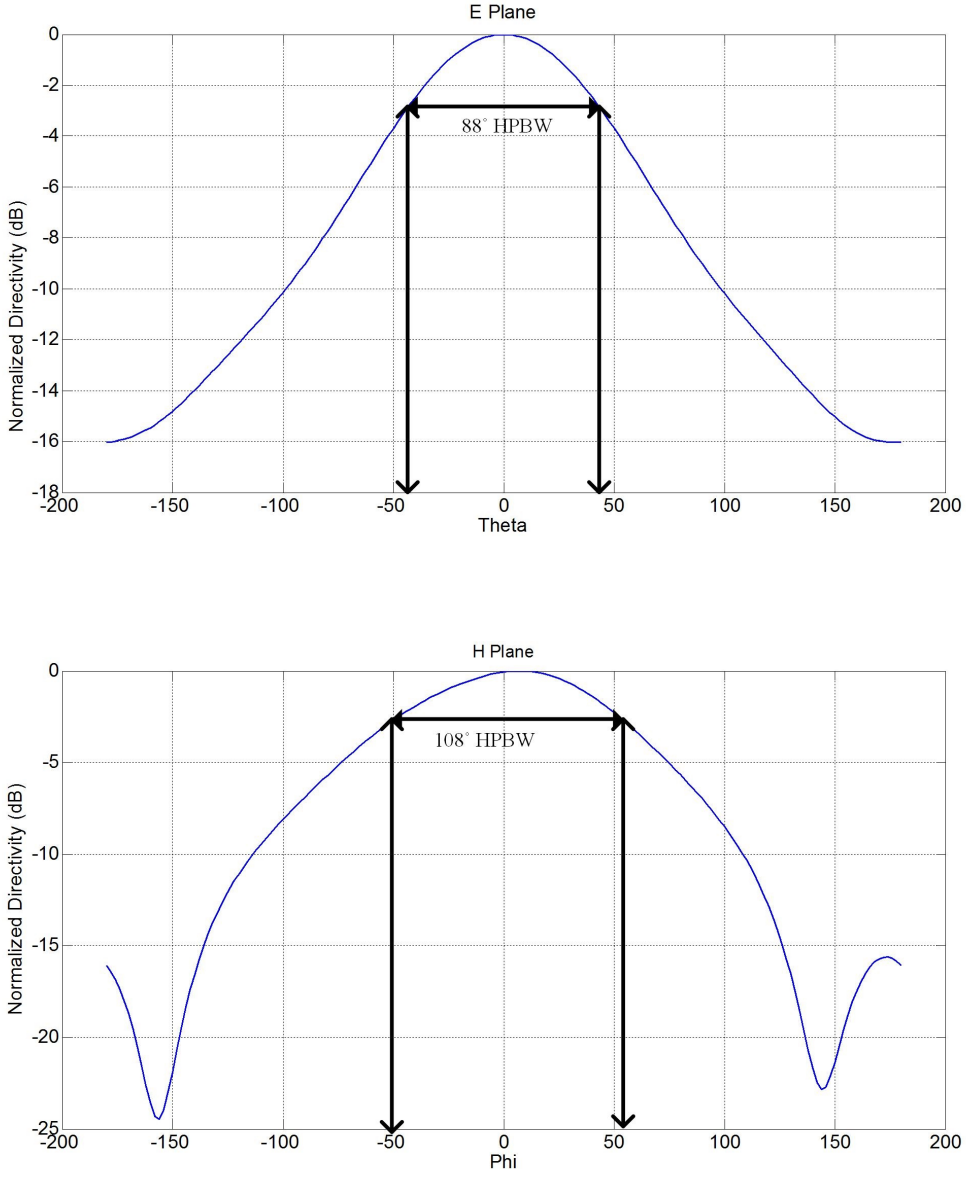

Figure 3.7: Simulation result for E and H field radiation pattern, measurement is for normalized directivity.

3.1.1 Effect of cavity length and width on parameters of the SIWCB slot antenna

Substrate integrated waveguide cavity of the slot antenna is varied in length and width by changing the distance between the centre of cavity vias. Via distances are varied between 2.7 mm and 3.3 mm with 0.1 mm steps. This variation of via distances does not violate the conditions presented in equation 3.3.

First cavity length is varied from 64.8 and 79.2 by changing the via distances. Results of cavity length variation in terms of S parameters are plotted in figure 3.8.

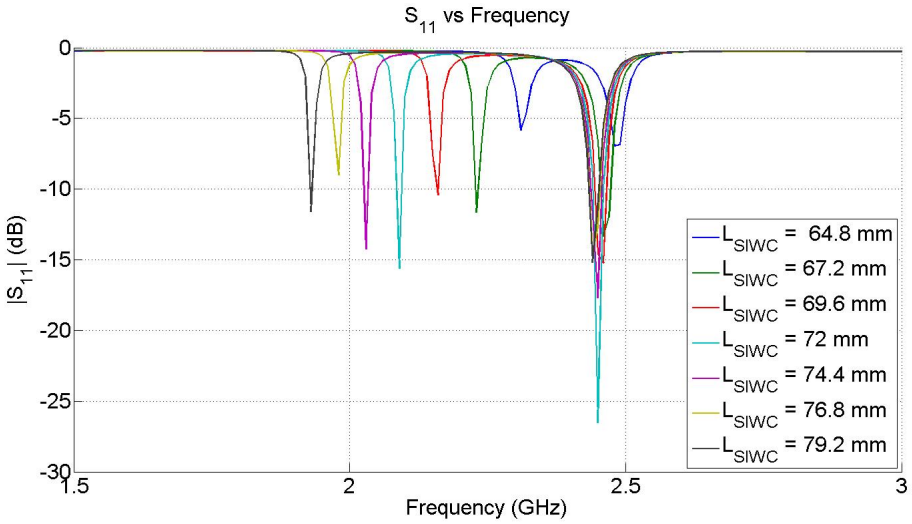

Figure 3.8: Simulation result for variation of cavity length around centre frequency of 2.45GHz, cavity length is varied from 64.8 mm to 79.2 mm.

As can be observed from figure 3.8, first resonance frequency of the antenna changes its frequency with change of cavity width, while second radiation frequency mainly stays around 2.45 GHz. Since the fields that are giving rise to radiation in first frequency are mainly located in the upper half of the SIW cavity, cavity region between the slot and short end of the cavity, first radiation frequency is effected in this variation. Likewise the fields that are creating the second radiation frequency are mainly located in the lower half of the cavity, thus they are slightly effected by the cavity length.

Cavity size is also varied in width from 64.8 mm 79.2 mm. Results of this variation are presented in figure 3.9.

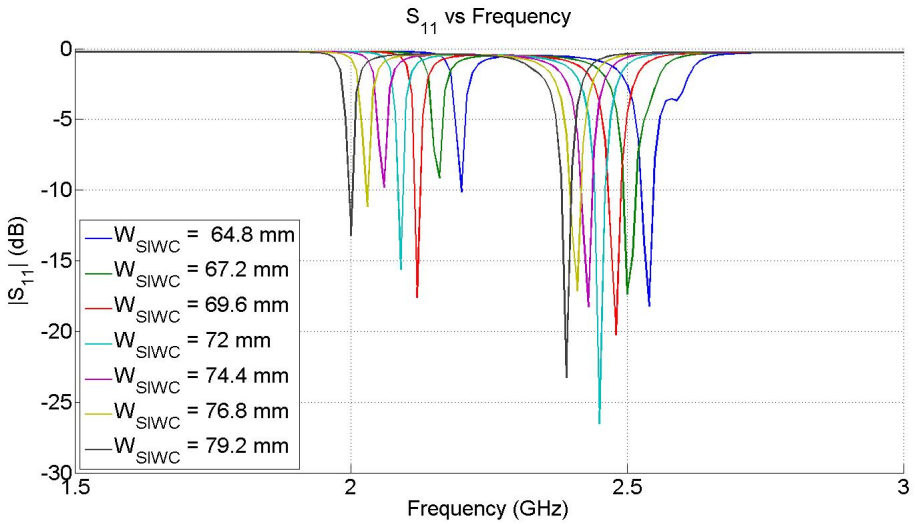

Figure 3.9: Simulation result for variation of cavity width around centre frequency of 2.45GHz, cavity length is varied from 64.8 mm to 79.2 mm.

As expected, cavity width effects the both radiation frequencies. Since both upper and lower parts of the cavity are effected by the change cavity width, both radiation frequencies change. Obvious from from both figures 3.8 and 3.9, as the cavity dimension increases, radiation frequency decreases.

3.1.2 Effect of sloth length and width on parameters of the SIWCB slot antenna

Slot length and width are varied to develop further insight about their effect on impedance and radiation efficiency of the antenna.

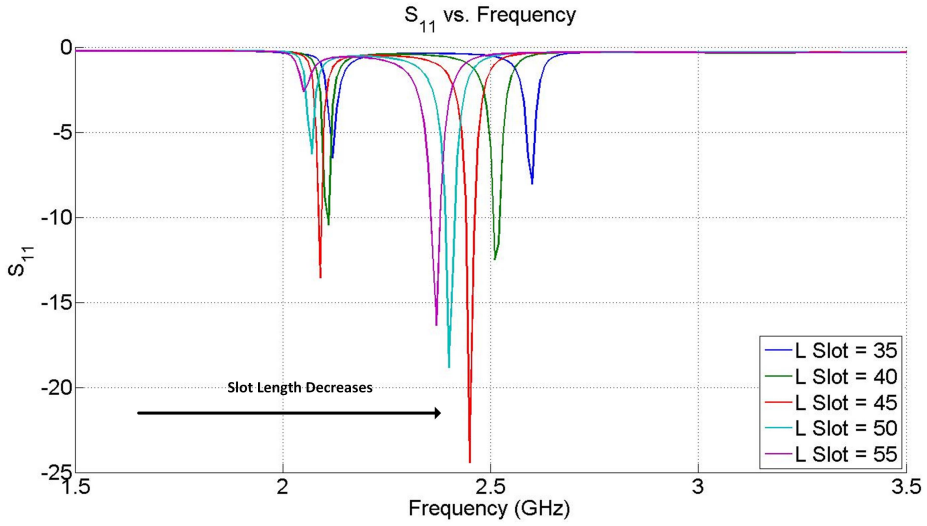

Figure 3.10: Simulation result for variation of slot length around centre frequency of 2.45GHz, slot length is varied from 55 mm to 35 mm with 5 mm steps.

Slot length is varied between 55 mm to 35 mm in steps of 5 mm where as all other dimensions are kept as given in table 3.1. Resultant S_{11} parameters of antenna can be seen in figure 3.10. In figure 3.10, resonance frequency changes as the length of the slot is changed. Increase in the length of the slot causes a decrease in the resonance frequency of slot. In figure 3.10 different S parameters can be observed for different resonant frequencies, issue of impedance mismatch of different resonant frequencies can be eliminated by simply tuning the stub length of GCPW feeding line.

In figure 3.11, relationship between radiation efficiency and frequency is presented for different slot lengths. As can be observed, maximum radiation efficiencies are observed at resonant frequencies of each slot. As presented earlier, TM_{110} radiation is in lover efficiency in all slot lengths.

Another variation that would effect the antenna performance is the slot width as indicated in the figure 3.1 with W_{slot}. In this variation, as it has been done for slot length, relationship between slot width, S_{11} and radiation efficiency are studied. In figure 3.12 sloth width is varied from 1 mm to 9 mm with 2 mm steps. In figure

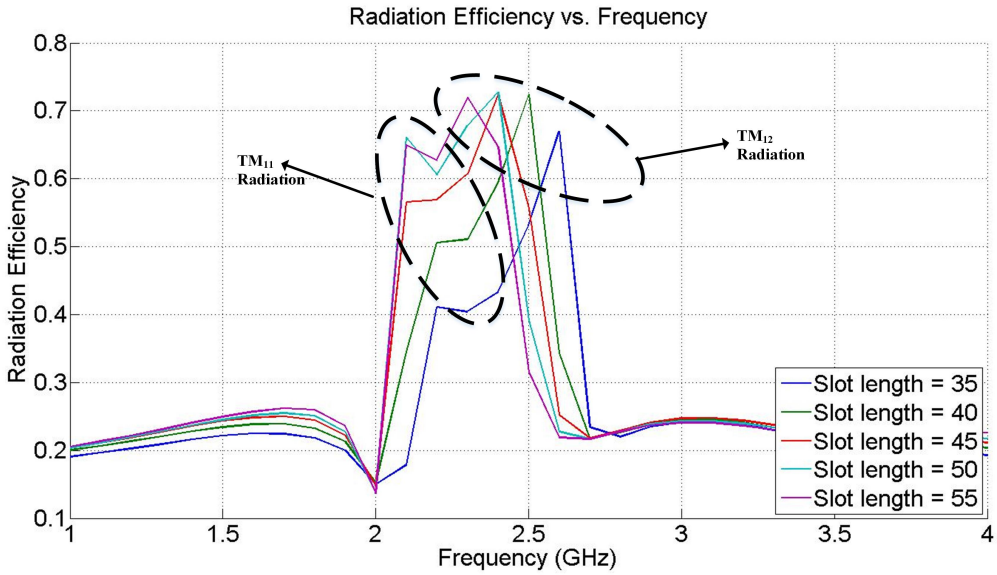

Figure 3.11: Radiation efficiency of designed antenna with variation of slot length, which is varied from 55 mm to 35 mm with 5 mm steps.

3.12, resonant frequency decreases with the increasing slot width. This relationship shows a dependency of radiation frequency to slot width, as it was also the case for slot length. Bandwidth of the antenna is not effected in this variation as can be seen in figure 3.12.

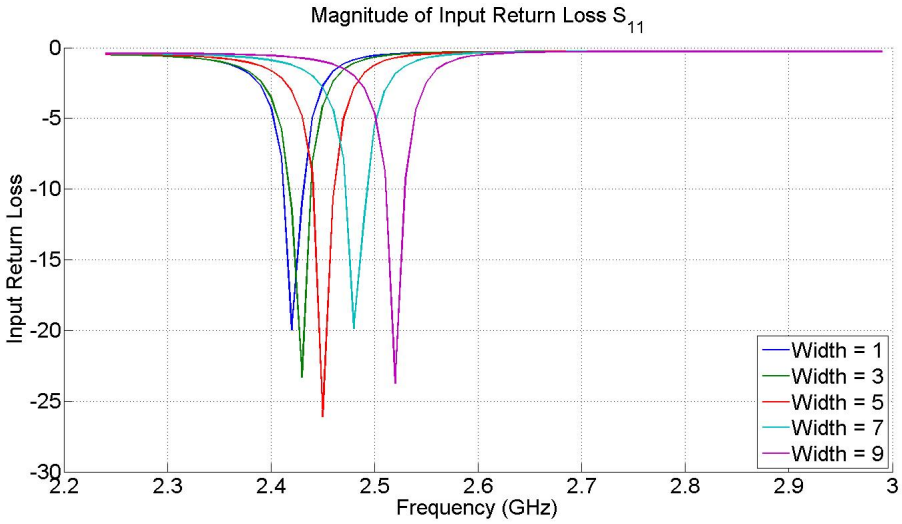

Figure 3.12: Simulation result for variation of slot width around centre frequency of 2.45GHz, slot width is varied from 1 mm to 9 mm with 2 mm steps.

Antenna radiation efficiency is also investigated for different sloth widths. Figure

3.13 presents this relationship. Radiation efficiency indicates a medium variation around 62% and 73%. This behaviour suggests that antenna radiation efficiency is slightly effected by the width of the slot in this design. With this behaviour in mind it can be concluded that for the design of the antenna, aside from its effect on radiation frequency, slot width can be left as a last tuning element for this design for efficiency of the antenna.

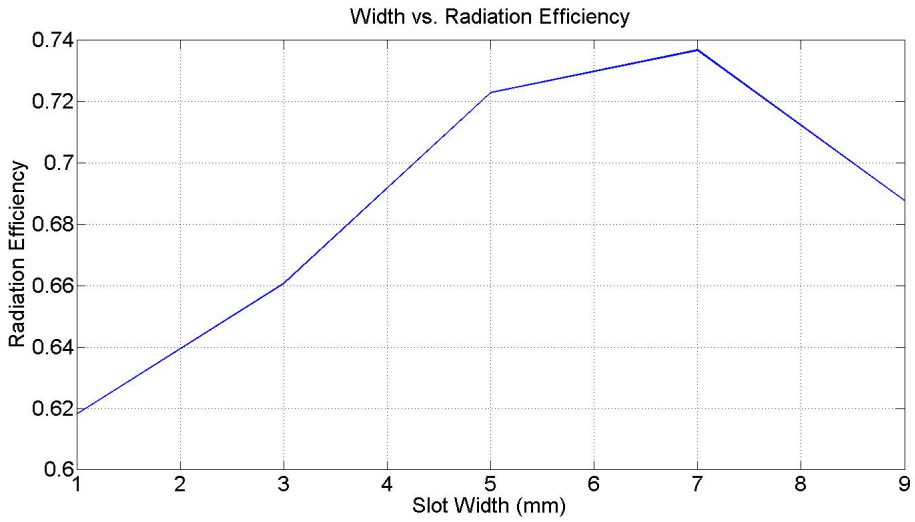

Figure 3.13: Radiation efficiency of designed antenna with variation of slot width, which is varied from 1 mm to 9 mm with 2 mm steps.

In this antenna design, slot length and width play an important role in frequency of radiation. This variations do not show a bandwidth enhancement or degradation. In conclusion, radiation frequency of the sloth is not only effected by the supporting SIW cavity structure but also by the dimensions of the slot. As can be concluded from the previous discussions about the dimensions of the slot and its effect on radiation frequency, sloth length is more dominant compared to slot width. As previously mentioned, change of slot dimensions are of course expected to change the impedance of slot and thus radiation frequency of the structure.

3.1.3 Effect of substrate thickness on parameters of the SIWCB slot antenna

Further investigation about the geometry of the antenna is being conducted on the substrate thickness. Substrate thickness is being varied between 0.5 mm to 2 mm in

0.5 mm steps for this study.

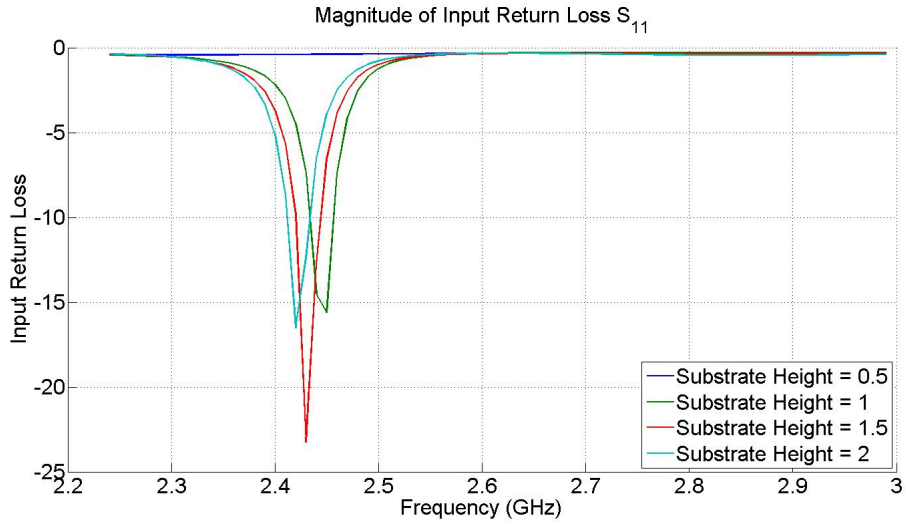

Figure 3.14: Simulation result for variation of substrate height around centre frequency of 2.45GHz, substrate height is varied from 0.5 mm to 2 mm with 0.5 mm steps.

Relationship between substrate height and radiation frequency is shown in 3.14. As can be interpreted from figure 3.14, substrate height effects the radiation frequency in the smallest manner, where a doubling and tripling of the substrate height, effects the radiation frequency in only 10 MHz steps. Under the effect of substrate height, 0.5 mm does not produce a radiation characteristic, this is due to the close placement of conductor plates of the substrate. At first glance it can be thought that change of substrate height mainly effects the characteristic impedances of both microstrip line and GCPW along with SIW. However, a closer inspection shows that this change of characteristic frequencies for all counted propagation mediums are effected in the same manner, in other words their characteristics change towards the same direction. For example a change of 0.788 mm of substrate height, which is nominal design, to 0.5 mm changes characteristic impedance from 49.763 Ω to 36.1 Ω and GCPW impedance changes from 49.68 Ω to 36.22 Ω. This manner of impedance transformation happens in all propagation mediums. Thus effect of substrate height on characteristic impedances of these propagation mediums is unrelated in context. It should be noted that this simulation results were obtained by feeding the structure in driven model solver of the simulator, thus driving port of the structure is directly matched to wave port of the structure. However in the implementation of the device,

of course, a 50 Ω is used for feeding the structure with conventional coaxial cables and SMA connectors.

Relationship between substrate thickness and radiation efficiency is presented in figure 3.15. As indicated in the figure 3.15, radiation efficiency of the antenna increases with substrate height. This effect of the substrate thickness can be explained with the radiation mechanism of the antenna. Since the radiation occurs with the electric fields that are created on the slot, it is inevitable that some of the electric fields are coupled to ground, instead of the opposite end of the slot especially in low substrate thicknesses. As the substrate thickness increases, more electric field is coupled to other side of the slot, thus a higher electric field value is obtained.

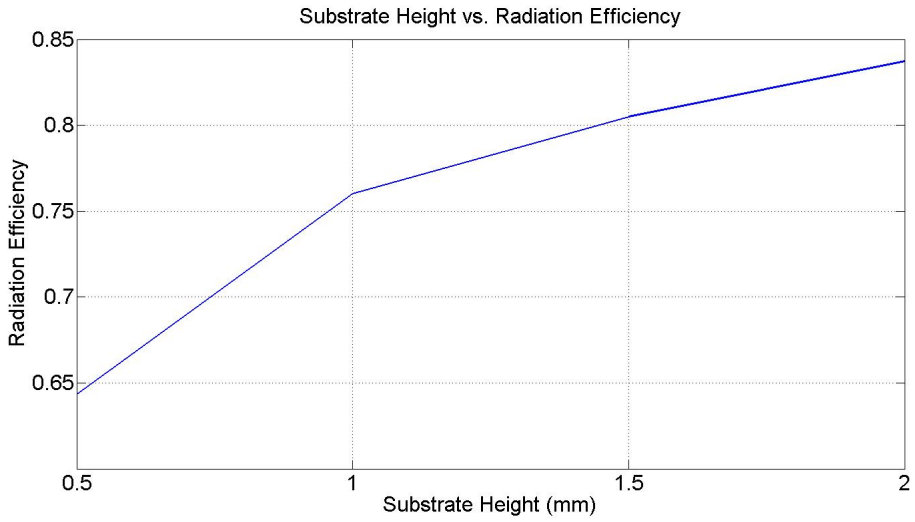

Figure 3.15: Radiation efficiency of designed antenna with variation of substrate height, which is varied from 0.5 mm to 2 mm with 0.5 mm steps.

Bandwidth of the antenna increases with the substrate thickness. For 1, 1.5 and 2 mm substrate thicknesses, bandwidth of the antenna is found to be 50, 55 and 60 MHz respectively. This phenomena is shared among all cavity backed antennas. The increase in cavity depth increases the bandwidth of the structure [39].

3.1.4 Effect of sloth and feeding line position on parameters of the SIWCB slot antenna

Position of the radiating slot on the SIW cavity is another critical dimension for design of the SIWCB antenna. By using the name, slot position, position of the slot along the feeding line is implied. Slot position is defined with respect to the centre of the SIW cavity. 0 mm means that the slot is in the centre of the cavity, while 8 mm means position of the slot is shifted towards the feeding point of the SIW, -8 mm means that slot is shifted towards the short circuited end of the SIW. Figure 3.16 shows the effect of the slot position on the radiation frequency, by exhibiting S parameters. As expected, change of slot position directly effects the radiation frequency, since, as explained previously, change of slot position changes the lengths of SIW sections that are lying between the radiating slot and short circuit endings of the cavity, thus giving a different frequency for the solution of the resonant frequency of the structure.

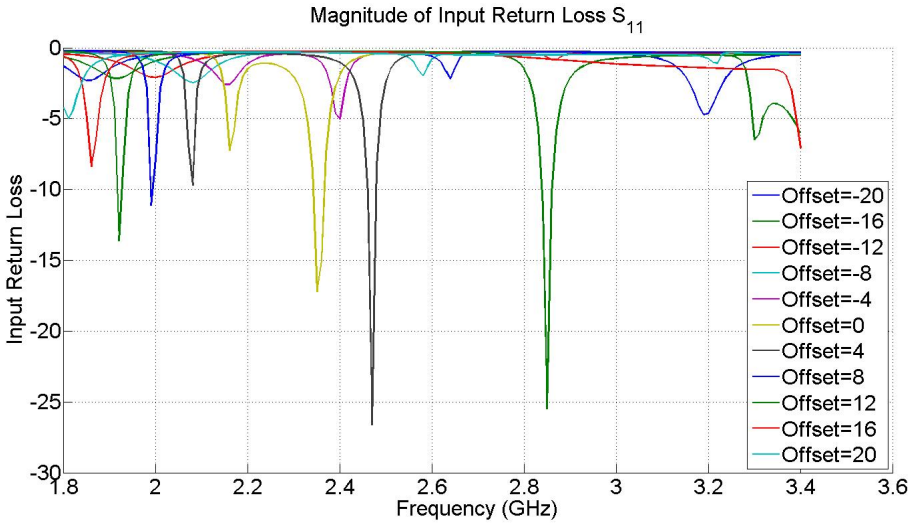

Figure 3.16: Simulation result for variation of slot position around centre frequency of 2.45 GHz, slot position is varied from -20 mm to 20 mm with 4 mm steps.

Figure 3.16 shows the S parameters of the structure between 1.8 GHz and 3.4 GHz. In figure 3.16, it can be observed that as the absolute value of the slot position gets closer to zero, radiation frequencies gets closer to each other. For the special case of 0 mm slot position shift, it can be considered for a symmetry point, however, due to the longitudinal asymmetry of the structure, caused by the feeding GCPW, this slot position also produces two different frequencies. This behaviour of the structure

suggest higher bandwidths are possible for the structure, by concatenating this two radiation frequencies [41].

Figure 3.17 presents the resultant S_{11} characteristics versus frequency for different GCPW lengths. As can be observed from figure 3.17, length of GCPW affects the matching of the antenna. Radiation frequency of the structure is also effected by GCPW length, since GCPW structure disturbs the impedances of both slot and SIW cavity.

After the design of SIW cavity and slot, GCPW length is used as a final tuning element for the antenna.

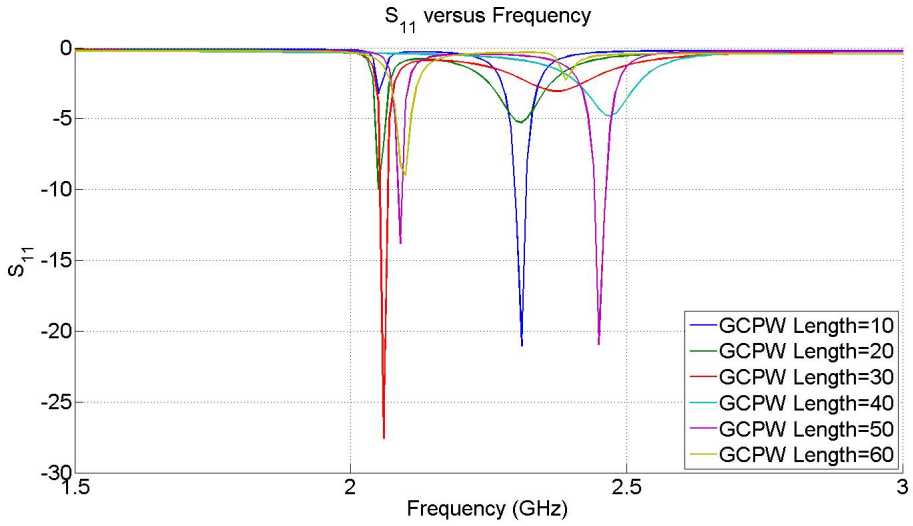

Figure 3.17: Effect of GCPW length on the radiation frequency.

SIW Cavity backed slot antenna has been developed under the discussions and conclusions that have been presented and an antenna that will be used for the rectenna system is designed. This antenna structure is implemented with the dimensions given in table 3.1.

3.2 Manufacturing and Testing of SIW Cavity Backed Antenna

Designed SIW cavity backed antenna is manufactured at the Electrical and Electronics Engineering Department of METU with fast prototyping PCB machine. SIW vias are electroplated with copper. Some imperfections are inspected by a microscope and presented in figure 3.18. In figure 3.18 poor coating can be identified with the appearance of the substrate, which is black. Photograph of the manufactured antenna can be seen in figure 3.19.

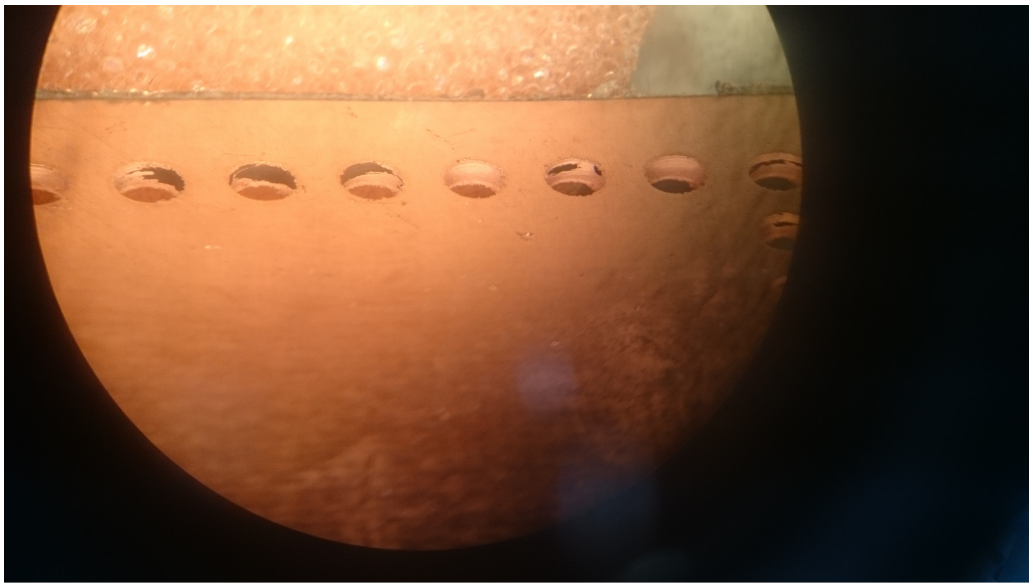

Figure 3.18: A close up photo of the copper coating of vias through microscope.

Input return loss is measured and compared with simulations as shown in 3.20.

As observed, measurements of the antenna, agree well with the simulations. Approximately 20 MHz deviation at the resonant frequencies are observed

Radiation patterns are measured in the Anechroic chamber. E and H plane radiation pattern measurements are compared with simulated pattern in 3.21 and 3.22 respectively.

E and H plane radiation patter measurements and simulated patterns are also in agreement, however, there are some discrepancies at back radiation. Simulated directivity of the structure is 4.36 dB and efficiency of the antenna is measured to be 71.5 %.

Gain of the manufactured antenna is found to be 2.9 dBi, which is in good agreement

Figure 3.19: Photo of the both sides of the SIWCB antenna.

with simulated value of 2.95 dBi. These differences in gain and efficiency of the antenna are due to the loss that is introduced to the antenna during the electroplating of the cavity forming vias. As presented in figure 3.18, electroplating process used in manufacturing of this antenna is not very successful and leads to further unexpected losses in the system.

Designed structure is implemented on a single substrate with its feeding system. This property gives antenna an ease of integration with both microstrip and GCPW structures, which are used extensively in implementing microwave structures, especially GCPW. Designed antenna has a 10 dB bandwidth of 20 MHz. Its planar structure gives the advantage low profile while presenting high radiation efficiencies. Its cavity backing results in a good front-to-back ratio (FTBR) of 17.9513 dB. Low cost of

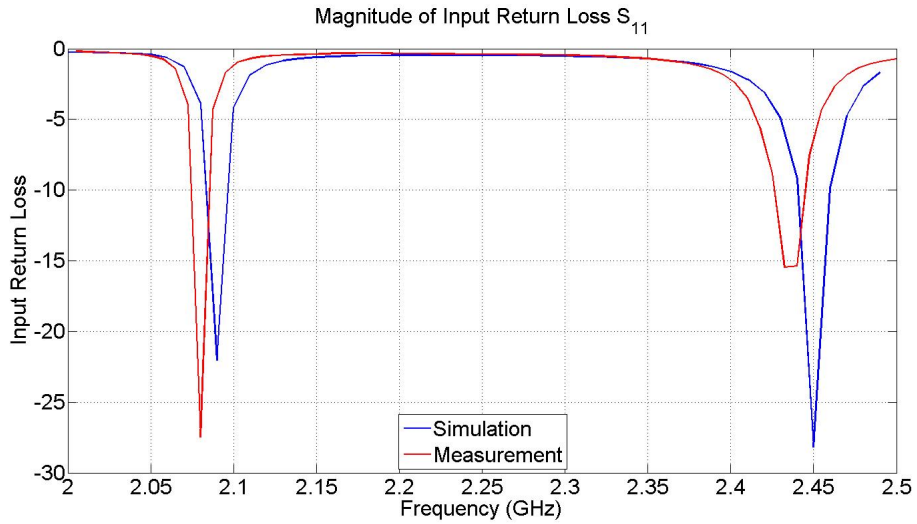

Figure 3.20: Simulation and measurement comparison of input return loss of the designed SIWCB antenna.

the antenna and easy fabrication can be listed as further advantages of the designed antenna.

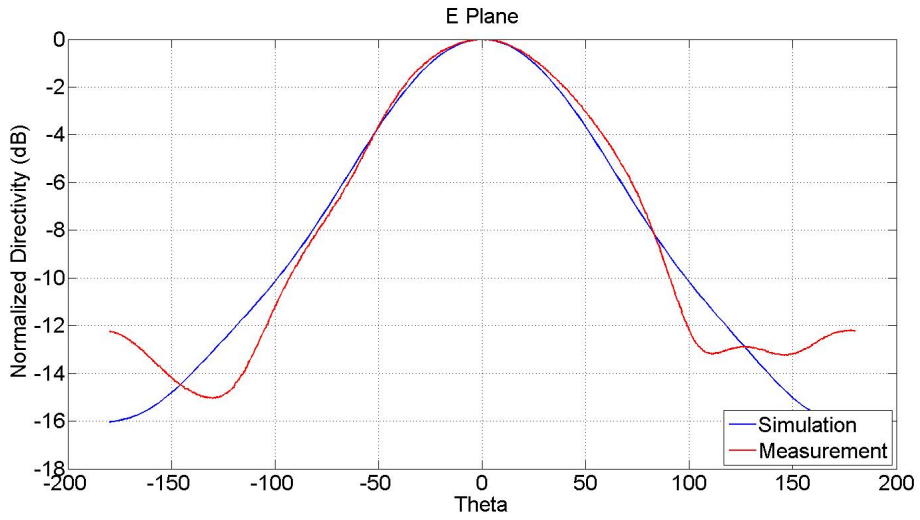

Figure 3.21: Simulation and measurement comparison of E plane radiation characteristic of the designed SIWCB antenna.

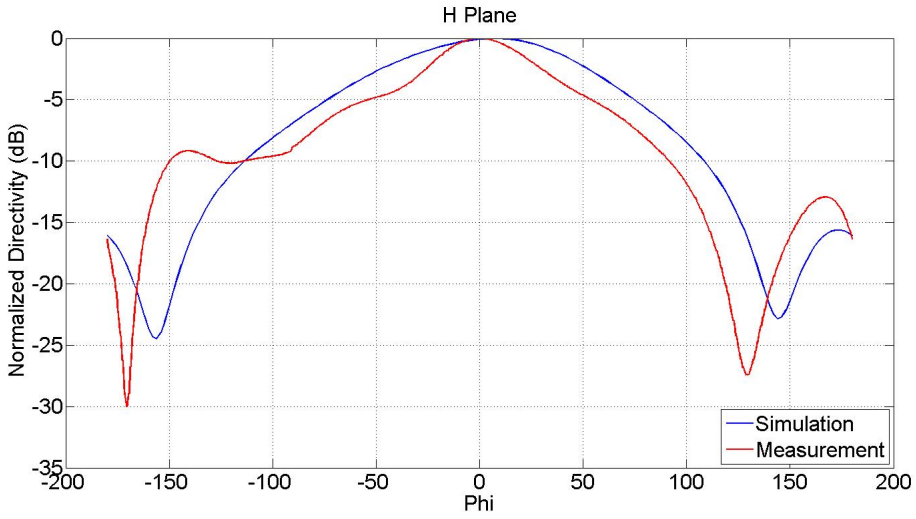

Figure 3.22: Simulation and measurement comparison of H plane radiation characteristic of the designed SIWCB antenna.

CHAPTER 4

DESIGN, MANUFACTURING AND TESTING OF A FREQUENCY SELECTIVE SURFACE SUPERSTRATE FABRY-PEROT CAVITY BACKED ANTENNA

Fabry-Perot cavity backed antennas that employ frequency selective structures(FSS) for their enhancement of directivity are widely used, and lots of examples can be found in literature such as [49], [50] and [51].

General structure of an FSS Fabry-Pérot antenna consists of a radiating element, which is the primary source of radiation in structure, an FSS which is placed above the primary source at a certain height and a ground plane beneath the primary source.

Fabry-Perot cavity backed antennas offer a great improvement in directivity of single elements. This directivity enhancement mostly comes from the employment of superstates to form an oscillating cavity structure, which is referred as Fabry-Pérot cavity here. FSS structures are designed so that their reflective characteristic at design frequencies are used for formation of a semi-permeable cavity along with the ground plane. Since the primary source is radiating into cavity, waves that are populating the cavity add up in constructive phases on each other on the surface of FSSS structure. These added up waves create an equivalent current distribution on the FSS structure and finally these currents radiate in to free space.

The major trade off of this structures is about the size of the antenna. Higher directivity is achieved with the sacrifice of the antenna dimension. Nevertheless, this trade off may be reasonable depending on the application. For example, a planar structure that is restricted in horizontal dimensions, usage of an FSS could help the designer, if no

vertical limitation exists. These kind of structures can be used in applications where a radome is already present. In this case radome itself may be used in the advantage of better directivity with employment of itself as an FSS.

In the case of this study, Fabry-Pérot cavity structures are selected for their offer of high directivity. Higher directivity values are obtainable, without going through design of an array with Fabry-Pérot structures. Design of a Fabry-Pérot structure involves the design of an FSS geometry and design of whole radiating structure with the primary radiating element. In this study a Fabry-Pérot cavity antenna is designed with a patch antenna as its radiating element. Design that is presented in this study differs from the literature at the point of its employment of FSS. In literature most of the study is conducted with the employment of FSS structures which are as large as many wavelengths, however, in this study an FSS is used whose dimension is in one to one wavelength of the operation frequency. Another different part of this study is the employment of FSS structure in 2.45 GHz ISM band, while most of the study in literature is done at frequencies higher than 8 GHz due to the wavelength limitations of the structures. This is because lower frequencies require bulkier and bigger structures.

Fabry-Pérot cavity antenna consists of an FSS structure and a primary source for the feeding of the structure. Geometry of such a structure can be seen in figure 4.1. In figure 4.1 primary radiating element can be considered as a simple patch antenna, or in most general case a hertzian dipole. Even though not explicitly explained in many sources, formation of radiating structure, obviously, requires a ground plane to exist beneath the structure. This ground plane is represented in the analysis with a perfect reflection surface ($\Gamma_{GND} = -1, \phi_{GND} = -\pi$). FSS at the top of the structure is the part that is responsible for the high directivity. FSS structure acts as an impedance layer and shows reflection coefficient (Γ_{FSS}, ϕ_{FSS}) depending on its design.

Before going into any more detail of the design, it would be appropriate to introduce an approach for the analysis of this kind of antennas and their design.

This type of structures can be analysed with a ray-trace approach [49], where the rays that are radiated by the primary source are reflecting back and forth between the FSS and ground plane.

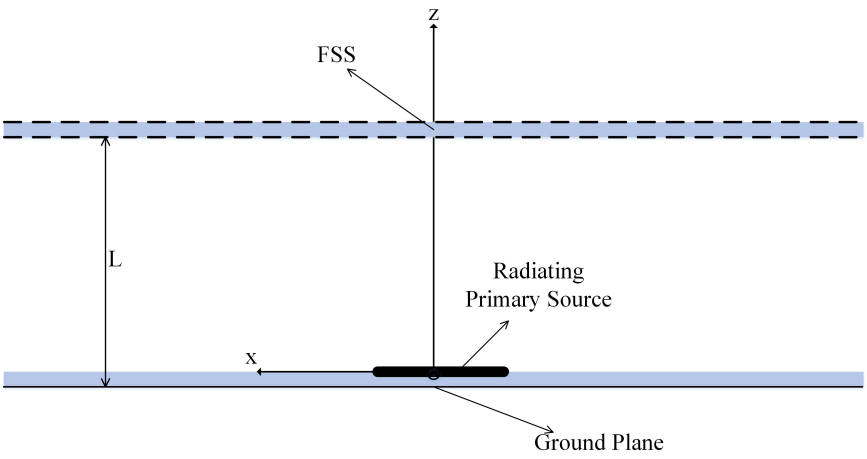

Figure 4.1: Representation of a simple Fabty-Pérot structure.

As reported in [49], power pattern that is the result of leaked waves through the FSS can be expressed as,

$$P(\theta) = \frac{\left[1 - \Gamma_{FSS}^2(\theta)\right]}{1 + \Gamma_{FSS}^2(\theta) - 2\Gamma_{FSS} cos\Big[\phi_{FSS}(\theta) - \pi - 4\pi L/\lambda_0\Big]} F^2(\theta) \tag{4.1}$$

Where in equation 4.1 L represents the distance between the FSS and ground plane, λ_0 is the free space wavelength and $F(\theta)$ represents the radiation pattern of the primary source. In this stage it should be noted that reflection coefficient for the FSS structure has two radial dependencies. In other words, reflection of FSS depends on the direction of impinging field in both spherical angles Θ and Φ. However for the sake simplicity angular dependencies is dropped in the expression. Dependency on direction also clues about the field orientation characteristic of the FSS structure, which may yield different reflection coefficients for TE and TM oriented waves.

For the calculation of resonant frequency of the formed cavity phase calculation of the travelling waves can be explicitly written.

$$\phi(\theta) - \pi - \frac{4\pi L}{\lambda_0} = 2N\pi \tag{4.2}$$

Equation 4.2 can be explained in accordance with figure 4.2 as follows, starting with a 0 radian phase at the ground plane level, wave travels a distance L in z direction, which changes its phase by the multiple of wave number times length ($\beta = 2\pi/\lambda$),

($\delta\phi = \beta L$). After this phase shift, wave reflects from the FSS structure, in this case wave experiences a phase shift that is $\Gamma_{FSS}(\theta)$ in accordance with its incident angle, which is θ. Afterwards wave again travels the distance L, which is equal to the first experienced phase difference and finally reflects back from the ground with introduction of $-\pi$ phase shift. This change of phase, results in a multiple of a full wave cycle for resonance and arrival of wave at the same phase on FSS. This result is indicated in equation 4.2.

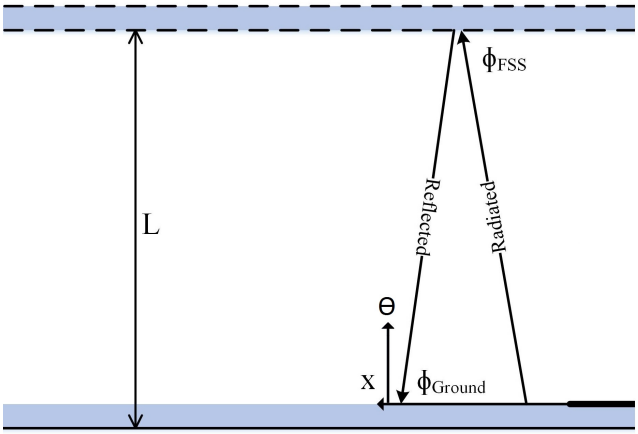

Figure 4.2: Waves inside of Fabry-Pérot cavity.

Equation 4.2 is obtained under the assumption of infinite FSS and ground plane. However this result can be attributed to a perfectly same phase radiation of the structure. In inhomogeneous phase radiations, this issue becomes complicated and from different incident angles, different phase differences for reflection must be introduced. For the structure given in figure 4.2, the thickness of the substrate that is supporting the primary radiation structure introduces another phase difference for waves, however this additional phase difference is only significant with much thicker substrate lengths. For thick substrate cases a modified wave number is calculated by including substrate permittivity. Determination of radiated fields of a source embedded inside impedance layers requires more complicated derivations. In this case, transverse equivalent network (TEN) models can be used [56], [57]. These studies consider more general cases such as multiple impedance layers that are operating as FSSs or partially reflective surfaces (PRS).

Since broadside radiation is the point of interest in this investigation, θ value can be replaced with zero in equation 4.1. Which yields in terms of gain G in linear scale as,

$$G = \frac{1+R}{1-R} \tag{4.3}$$

Where R is the reflection coefficient of the FSS in linear scale at broadside direction.

4.1 Design and modelling of FSS structure

FSS are used extensively for different purposes, from electromagnetic absorbers to shielding, waveguide filters and in Cassegrainian subreflectors in parabolic-dish antennas [58]. FSS structure that has been designed and modelled in this study consists of two parallel patch arrays. These two arrays are identical in geometry however, their orientation in the structure is out of phase by 180 degrees. Geometry of a single unit cell of the structure is shown in figure 4.3, and the dimensions are given in table 4.1. Orientation and alignment of the elements are given in figure 4.4. In figure 4.4, dashed patch lines are under the supporting substrate and solid lines are on the other surface of the substrate. These two arrays are symmetrical with mentioned phase shift.

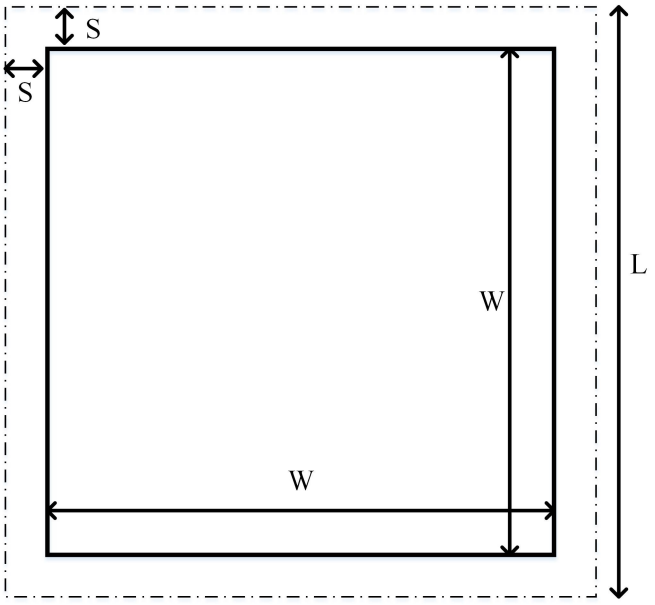

Figure 4.3: Unit Cell of designed FSS structure.

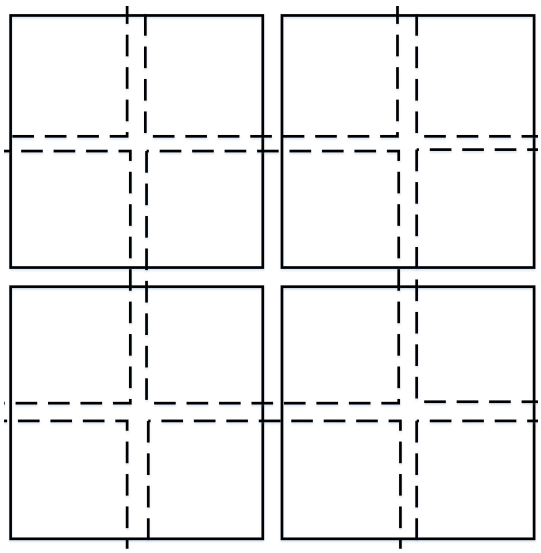

Figure 4.4: Orientation of patch arrays that are forming the FFS.

Table 4.1: Dimensions of FFS structure

Name	Dimension
S	0.1 mm
W	9.8 mm
L	10 mm

Unit cell of designed FSS structure in simulation environment is depicted in 4.5. Designed FSS structure consists of 13 x 13 of unit elements.

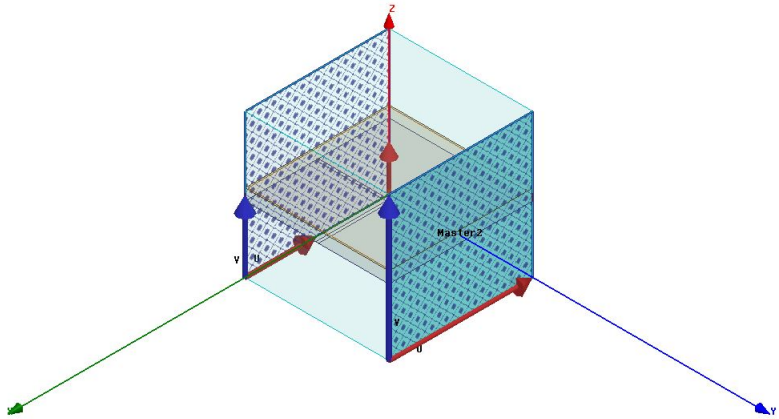

Figure 4.5: Single element of FSS in simulation environment.

FSS unit cells are selected to be sub-wavelength elements with $\lambda/12$ in dimension in one edge. Total dimension of selected structure is nearly λ in one dimension. For the design of the FSS unit cell, W value in table 4.1 is varied. Reflection coefficient

versus this design parameter is plotted in figure 4.6.

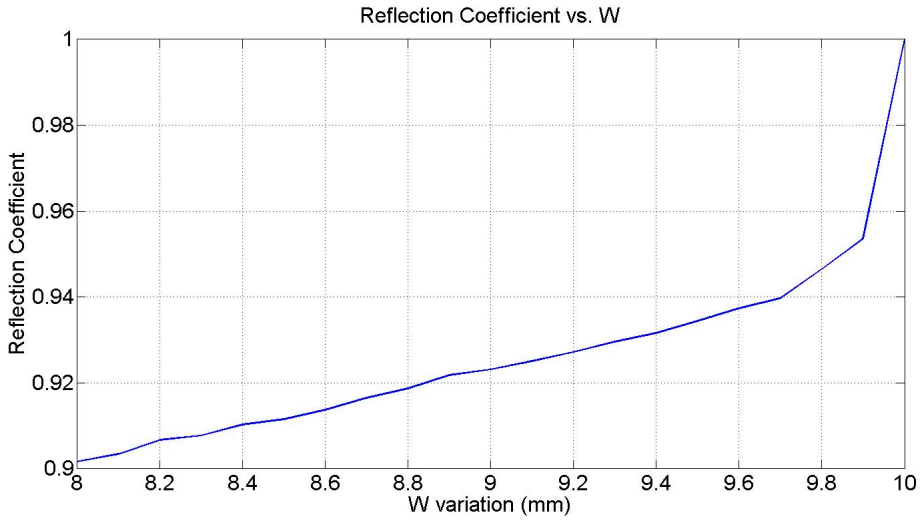

Figure 4.6: Reflection coefficient versus design parameter W in FSS unit cell at 2.45 GHz.

Square patches are printed on to Rogers 5880 substrate of 0.788 mm thickness. Design of the patch is carried out in Ansoft HFSS ® with usage of floquet ports, which extends the slave-master boundary pairs to infinity. This presented structure shows a good reflection coefficient around the frequency of 2.45 GHz. Since the structure is symmetric along both of its dimensions, return and transmission characteristics are same for both TE and TM wave configurations. For this reason only a single (TE) wave configuration results will be presented. In figure 4.7, magnitude of reflection and transmission characteristics between 0.5GHz to 40 GHz are presented. In this design, conversion of wave configurations between each other, TE to TM or TM to TE, is not observed as it is not intended in the design after all. Higher order modes are non-propagative and thus are not concerned with the design.

Phases of reflection and transmission coefficients as a function of frequency are plotted in figure 4.8. As can be seen from figure 4.8, rapid phase changes occur at the frequencies where reflection characteristics are changing. This behaviour is consistent with the change of magnitude characteristics, since matching of the FSSs to propagation medium must occur with the change of phase as well. This behaviour is more eminent considering the general modeling of the FSS structure. FSS structures can be modelled with purely reactive lumped elements if the conduction losses are ignored.

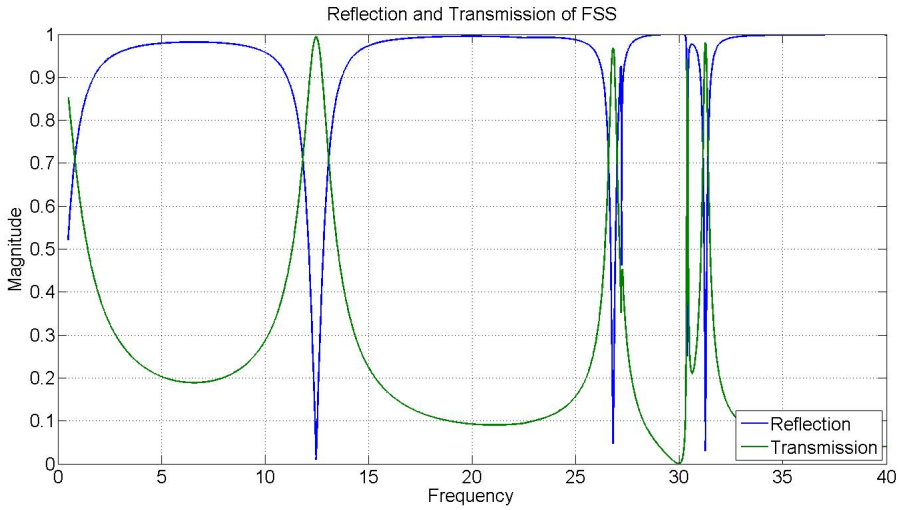

Figure 4.7: Magnitude of transmission and reflection characteristic of the designed unit cell.

This elements are associated with their structures along with the orientation of waves.

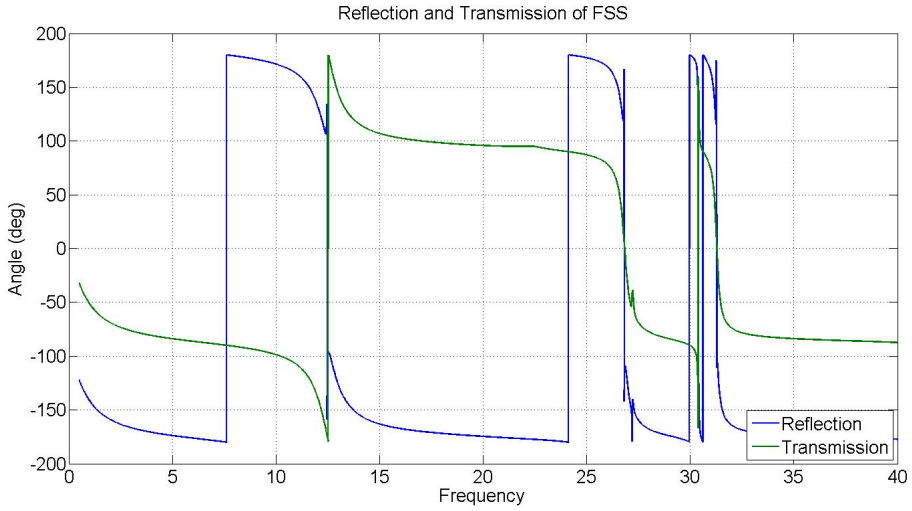

Figure 4.8: Phase of transmission and reflection characteristics of the designed FSS.

Since patch elements are used, a capacitive model is proposed as a capacitor and inductor in series that is replaced in the structure in a parallel manner between transmission lines. Proposed model and its representation in the medium can be seen in figure 4.9.

Before going any further into the design, it would be appropriate to associate the modelled geometrical structure to its lumped model. For a capacitive structure, as

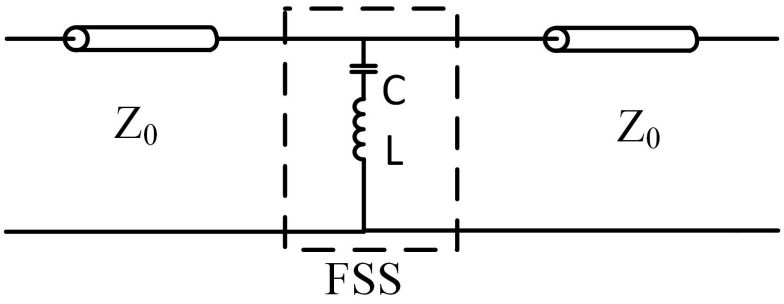

Figure 4.9: Modelling of a capacitive FSS.

proposed, a model that consists of a capacitor and a series inductor comes from the fact that electric field that is travelling transverse to this structure experiences an inductive behaviour due to the big patch conductor and a capacitive behaviour due to the gaps between neighbouring patches.

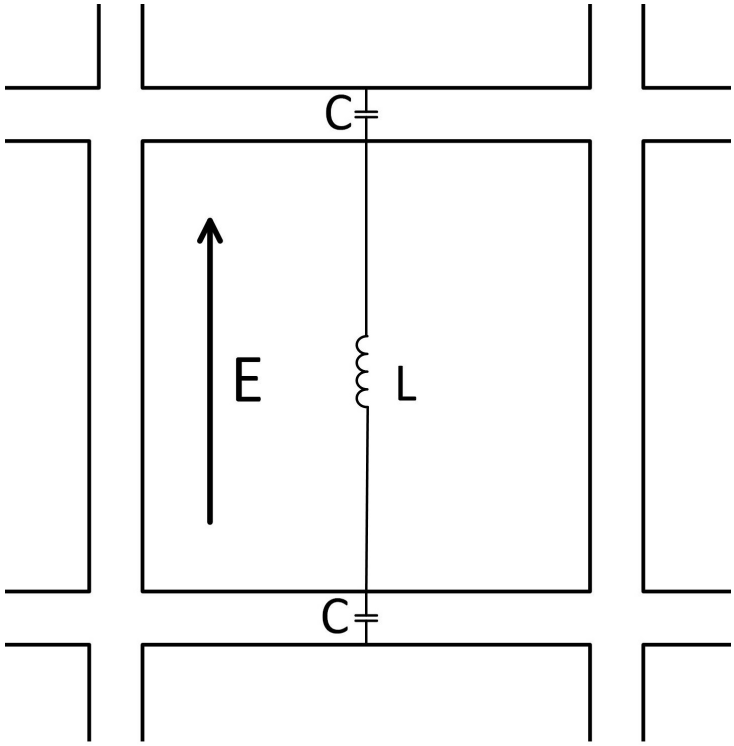

Figure 4.10: Relationship between FSS model and its geometry.

This representation stands for a single face of the structure. Magnitudes of transmission and reflection characteristics for this structure can be seen in figure 4.11. A quick comparison of figure 4.7 and 4.11 reveals that their frequencies allowing the transmission are different. A single layer FSS of same pattern yields its first transmission frequency around 10 GHz, while two layer designed structure exhibits first transmission at 12.5 GHz.

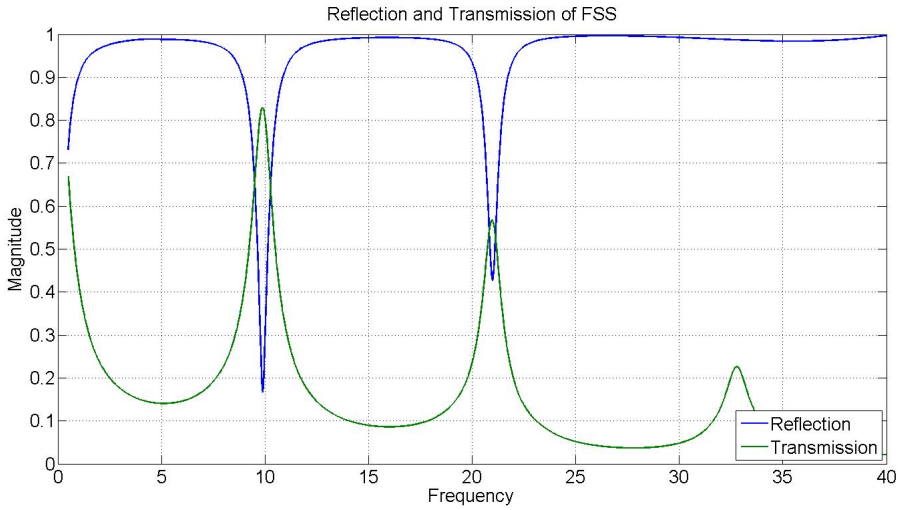

Figure 4.11: Reflection and transmission characteristics of a single face FSS structure.

In the point of view of a transverse equivalent network, this structure requires a modelling that is including both sides of FSS structure along with the effect of the dielectric between them, which affects the structure in terms of phase and can simply be modelled with a transmission line in the system.

Single layer structure is modelled with this model as it is proposed in the literature [58]. However, modelling of such structures with second order equations is not efficient, as it is described in literature. Such models are effective up to some frequency, however they fail to account for higher frequencies. For this reason a better fitting model is proposed and applied in this design. This model, as it is not outstandingly different from the basic one described, includes another L and C pair for better approximation. Best indicator for the success of such a model is comparison of input impedances obtained by lumped models and by full wave analysis method. This analysis is performed in the following way. S parameters for the structure is obtained via a HFSS® simulation with usage of floquet ports, master-slave boundaries and de-embedding of air regions. After this analysis, obtained parameters are transferred to a linear solver, which is AWR/MWO®. In this linear solver simulation, impedances of the structures are recreated with setting port impedances to 377 Ω and developing lumped models with same port parameters. Confirmation of such a method is being done with a given literature example [58]. After this point, lumped parameters are obtained by tuning the lumped elements for best fitting. There are other methods

for obtaining L and C values for given impedance values, however these methods, which include the solution of second order equations may become very unstable with respect to chosen trial points and fails to account for higher frequency impedances. This foretold extended model can be seen in figure 4.12 along with the simple model.

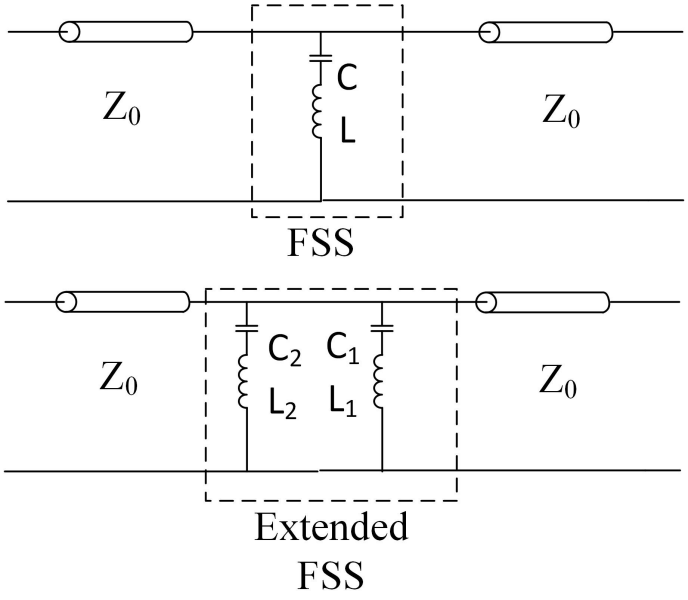

Figure 4.12: Extended FSS model.

S parameters of FSS structure which are extracted from HFSS are also placed in linear solver with same port impedances. Real and imaginary parts of input impedances of HFSS simulation and both models are shown in figure 4.14 and 4.13 respectively.

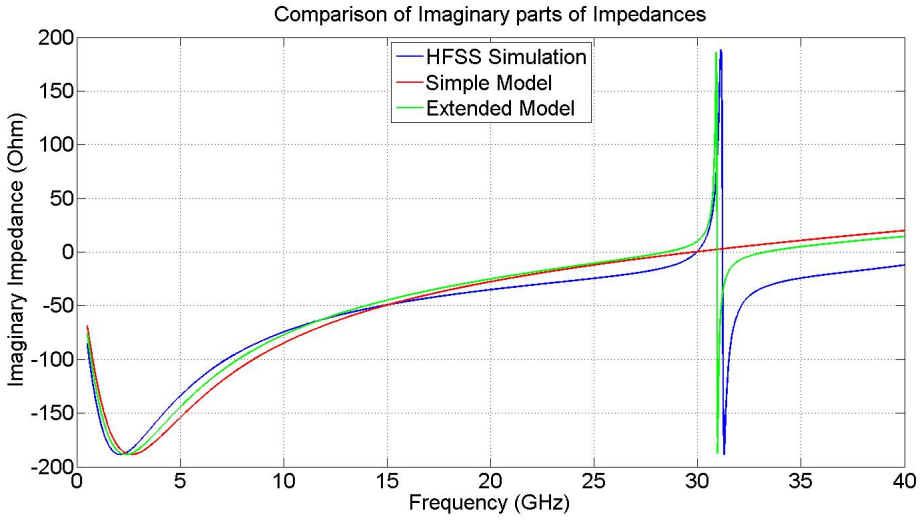

Figure 4.13: Comparison of imaginary parts of input impedance of FSS models and HFSS results.

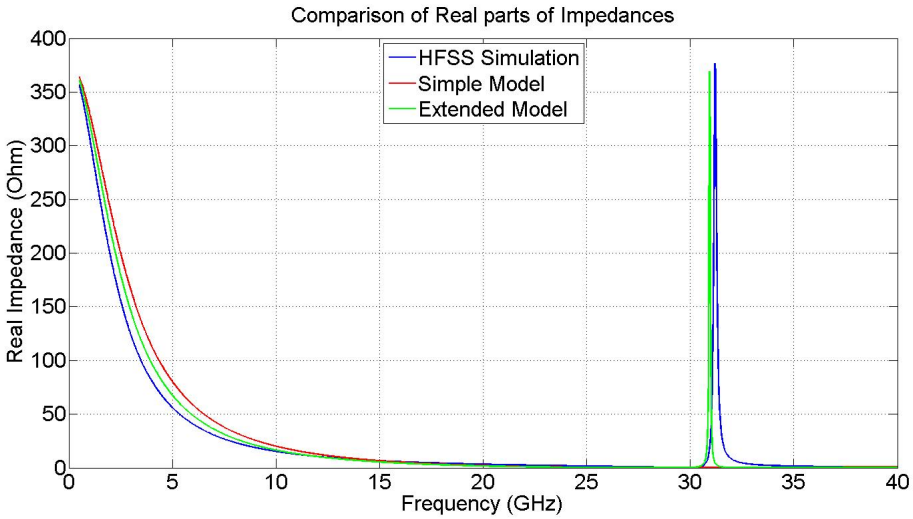

Figure 4.14: Comparison of real parts of input impedance of FSS models and HFSS results.

As can be seen from the figure 4.13, extended model is quite good at predicting the asymptotic nature of the impedance with its fourth order transfer equation. Figure 4.14 also shows the success of the model in real part of the input impedance. two inductance and capacitance values that are proposed for extended model are 0.312 nH, 0.301 nH and 0.1 pF, 0.0706 pF respectively. this values for simple model are 0.18 nH and 0.158 pF. With their own counterparts this values are logically comparable, to exemplify, for a patch FSS with dimensions of 7.5 mm of patch and 10 mm periodicity this values are, 0.729 nH 0.043232 fF [58] . This results are in correlation with the modeling of the structure since the distance between the patches are diminished, they are expected to show a greater capacitive value.

After the modelling single layer patch FSS, more complex model is also developed. This developed model consists of two single FSS layers that is split up by a section of electrical transmission line model which is actually a representation of dielectric layer that is separating and supporting two FSS layers. This model can be seen in figure 4.15.

In this proposed model, transmission line between two FSS structure models are included to stand for the phase term that is introduced by the supporting dielectric. This section is also modelled in HFSS and its characteristic impedance, as expected takes

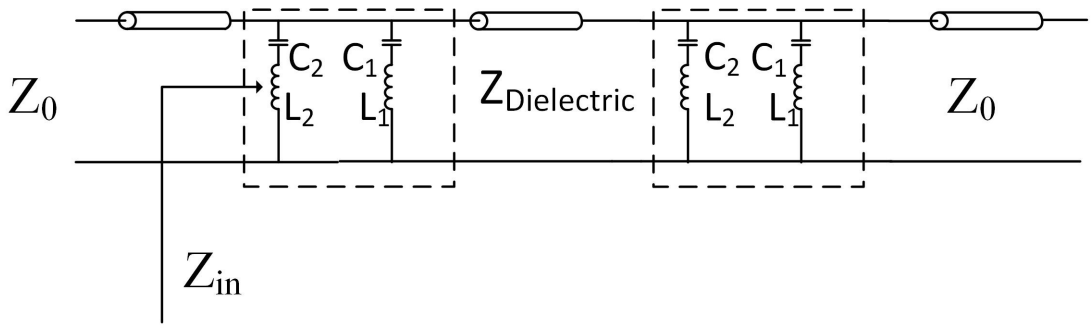

Figure 4.15: Lumped and distributed model of designed FSS structure.

the classical form of $\eta = \sqrt{\frac{\mu_0 \mu r}{\epsilon_0 \epsilon r}}$, which yields a characteristic impedance of 254 Ω with calculated electrical length in terms of degrees. This model is verified with linear solver.

This developed model also shows a good agreement with the simulation results from HFSS®.

Real and imaginary parts of input impedance of FSS as a whole is presented in figure 4.16. In figure 4.16 model and simulation shows a good agreement up to 25 GHz. However, after 25 GHz, simulation and model starts to differ from each other. This situation is expected since the models are reliable in a certain bandwidth. This situation is encountered and explained in literature as well [58].

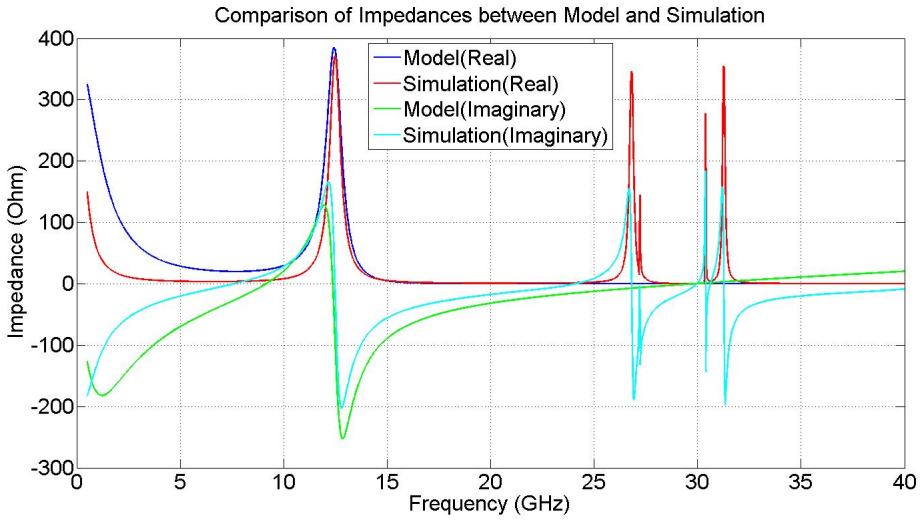

Figure 4.16: Comparison of real and imaginary parts of input impedance of FSS structure and lumped model.

Another property of the FSS structure is the transmission and reflection characteristics at different grazing angles. At the frequency of interest, 2.45 GHz, these characteristics are shown in figure 4.17. Since the structure is symmetric in both dimensions, only theta variation is presented.

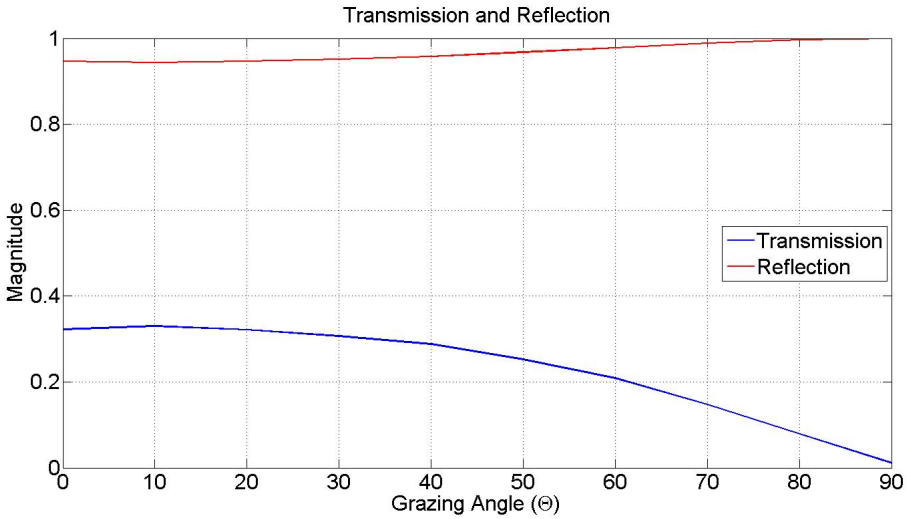

Figure 4.17: Transmission and reflection coefficients of FSS structure from different grazing angles.

4.2 Design and modelling of FSS Fabry-Pérot Cavity backed antenna

Fabry-Péreot cavity backed antenna consists of an FSS structure and a patch antenna. FSS structure is positioned at a certain height from the patch antenna. This FSS height is obtained with evaluation of equation 4.2. This evaluation yields an FSS height of 65.1 mm. Antenna is simulated in full wave solver HFSS®. HFSS® optimization, however yields an optimal height of 67.754 mm. This discrepancy is due to the assumption of infinite FSS and ground plane. Another assumption made by the equation is that the radiating source is a perfect hertzian dipole, radiating in only one phase term, however, for a real antenna radiation is not in perfect phase.

Dimensions of microstrip patch is also another concern regarding the matching of the structure. Since the FSS structure is in very close range of patch antenna, dimensions of patch antenna also optimized in design to yield a 2.45 GHz radiation. For a preliminary work another patch antenna is designed to operate at 2.45 GHz. This

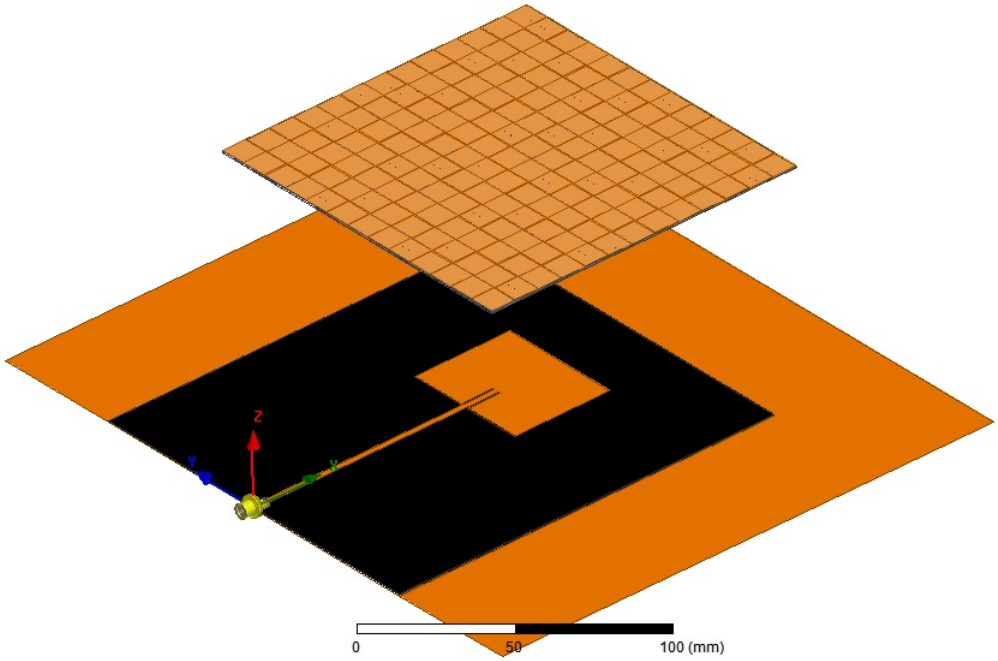

Figure 4.18: Representation of antenna in simulation environment.

patch antenna has length of 40.7 and width of 48.4 mm on Rogers® 5880, 0.788 mm substrate. In the design of FSS antenna, length and width of patch are found to be as 40.7 mm and 35.28 mm on the same substrate. Dimensions of patch antenna are modified to yield the maximum power transmission to free space. By changing the width of the antenna, if the transmission line model is taken in to account, characteristic impedance of the patch line is optimized to match the modified impedance seen from the edge of the antenna, which is due to the FSS structure.

Photographs of manufactured and tested antenna are presented in figures 4.19 and 4.20.

S parameters of the designed antenna is presented in figure 4.21 along with its simulation results. A 30 MHz shift in the centre frequency is observed. Designed antenna is a narrow bandwidth antenna since the employed radiating element is a narrow band patch. However, FSS Fabry-Pérot structure itself is also a narrowband antenna since FSS height is tuned for a certain wavelength. 10 dB bandwidth of the structure is calculated to be 26 MHz.

E and H plane measurements of the manufactured antenna are presented and com-

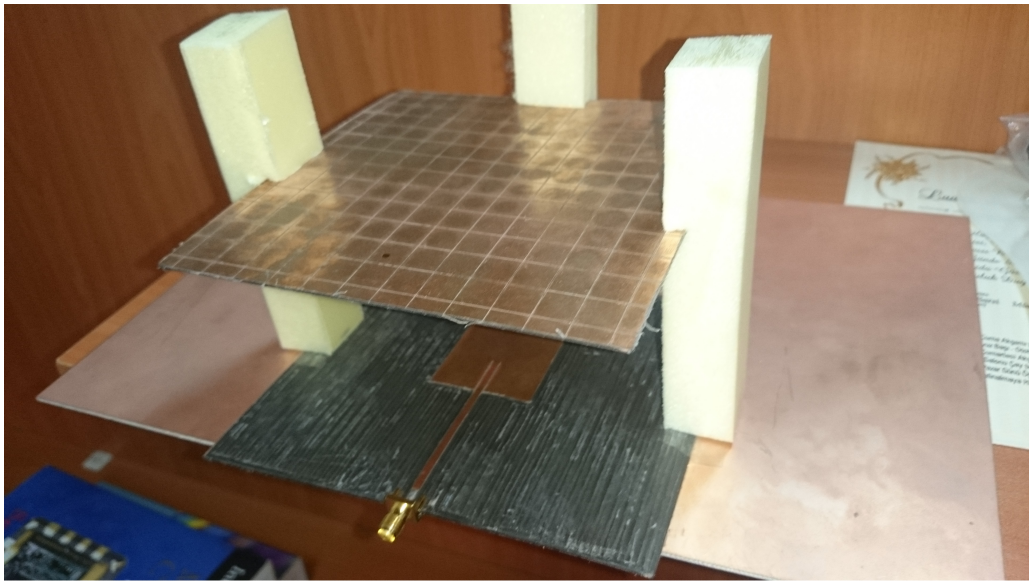

Figure 4.19: Picture of manufactured antenna.

Figure 4.20: Picture of manufactured antenna.

pared with simulation results in figure 4.22 and 4.23. Simulation results are in good agreement with the measurements. This developed antenna has a gain of 10.53 dBi, which is comparable to simulated gain of 12.04 dBi.

Simulated gain versus frequency of the structure is plotted in figure 4.24. 3 dB gain bandwidth of the structure is 50 MHz.

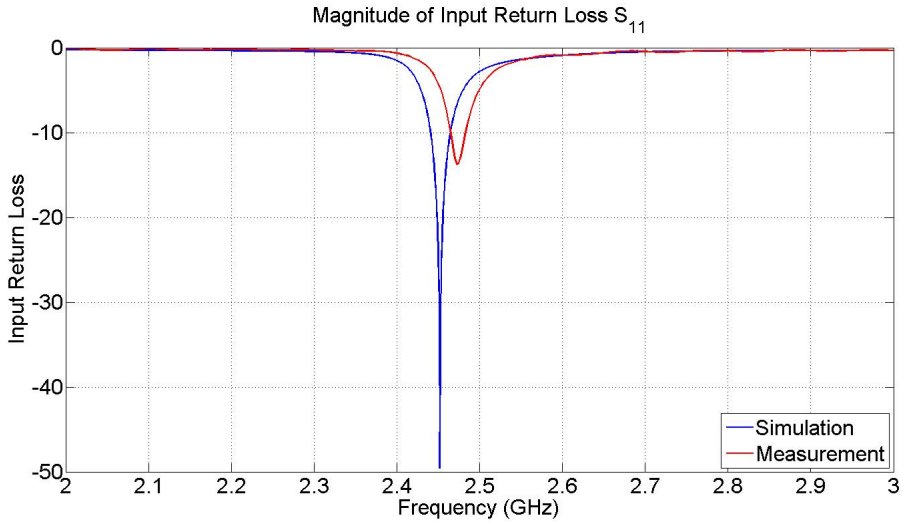

Figure 4.21: Simulation and measurement comparison of S parameters for designed FSS Fabry-Pérot antenna.

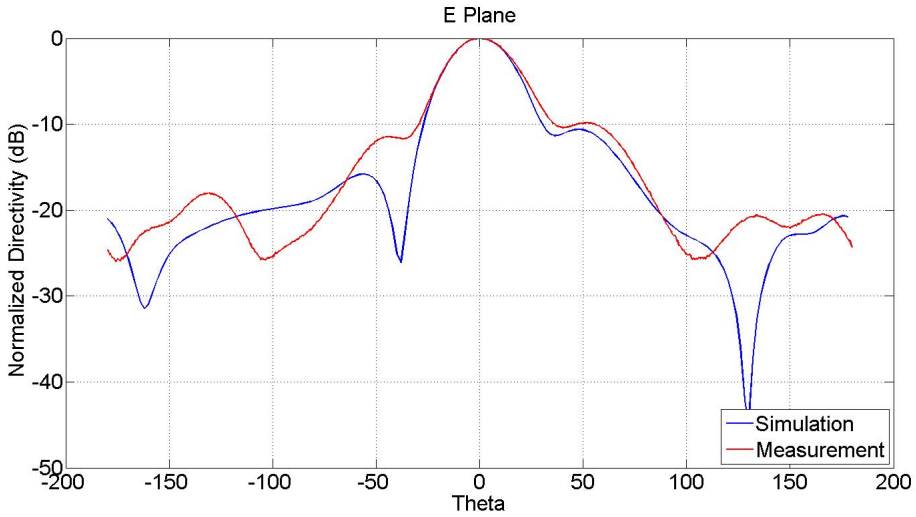

Figure 4.22: Simulation and measurement comparison of E plane radiation characteristic of the designed FSS Fabry-Pérot cavity backed antenna.

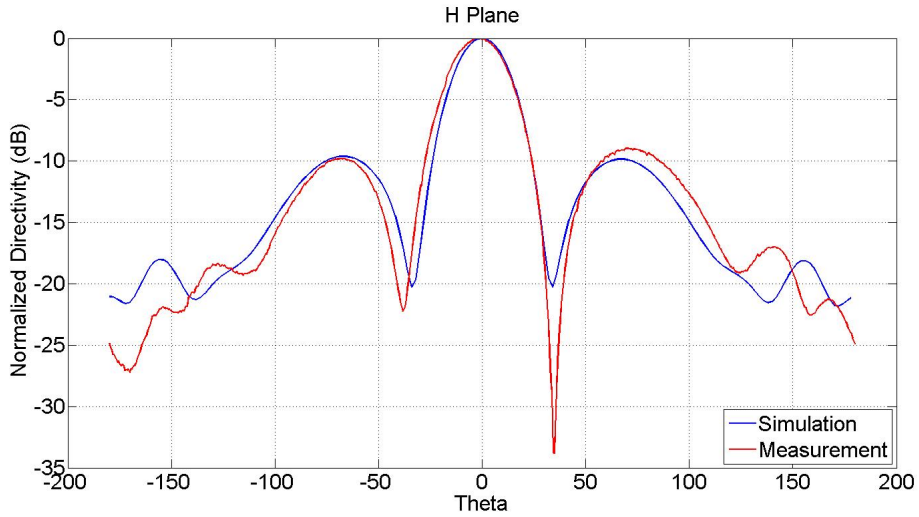

Figure 4.23: Simulation and measurement comparison of H plane radiation characteristic of the designed FSS Fabry-Pérot cavity backed antenna.

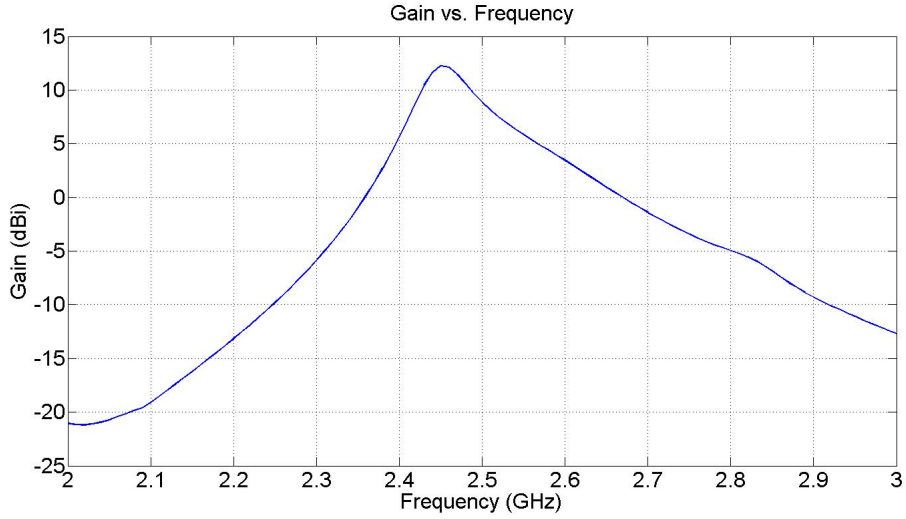

Figure 4.24: Simulation result for maximum gain and frequency relation.

CHAPTER 5

INTEGRATION OF RECTENNA

Designed antenna and microwave circuit are integrated to form a rectenna system. A signal generator is used as the source and standard gain horn antenna is used for the transmitting antenna. The distance between transmitting antenna and rectifier system is changed and output voltage of rectenna is recorded. Standard gain horn antenna and tested rectenna antennas are oriented to coincide with each other in the direction of main beam of each other. Depiction of test setup can be seen in figure 5.1. As can be observed from the figure 5.1, RF absorbers are used during the measurements to minimize undesirable reflections from the environment. Measurements are made with a multimeter in voltage measurement option. Measurement result is the voltage that is read from the multimeter versus the distance between the two antennas.

First, microwave rectifier is connected to the output of FSS superstrate Fabry-Pérot antenna. Measured output voltages which are plotted as a function of distance in figure 5.2 clearly show the decay that is due to the free space loss.

Figure 5.3 shows the total path loss in relationship with distance, calculated from Friis transmission equation . Gains of both transmitting and receiving antennas are included in the calculation. For further realization, losses of coax-to-planar and coax-to-coax adapters are also included in the calculation. Total loss that is due to the connectors and adapters are measured and found as 1.1 dB.

Considering gains of both antennas, path loss and cable loss, a theoretical value for input power of the microwave rectifier can be found. However, this value is not in good accordance with the measured values if the input power to the rectifier is calcu-

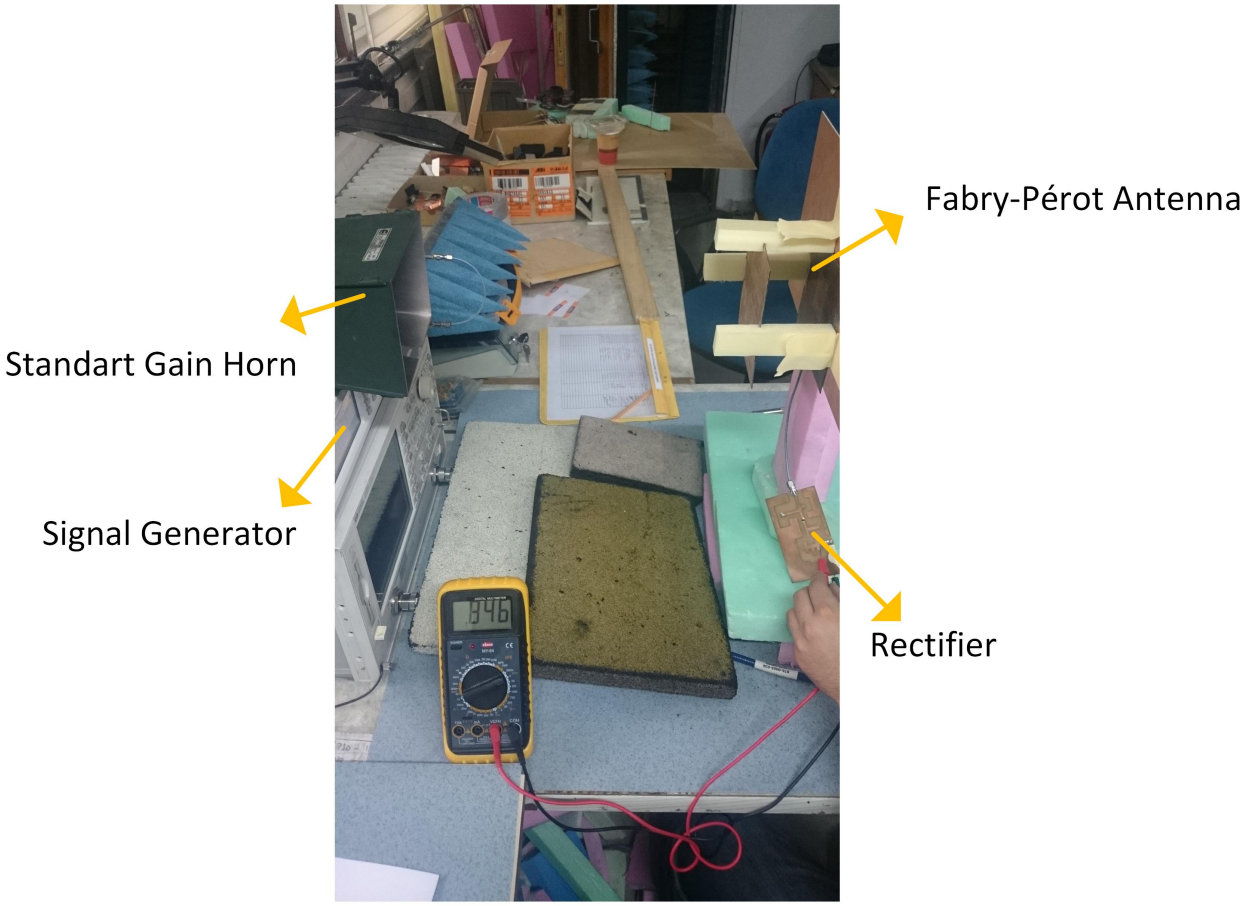

Figure 5.1: Measurement setup for power transmission in laboratory environment.

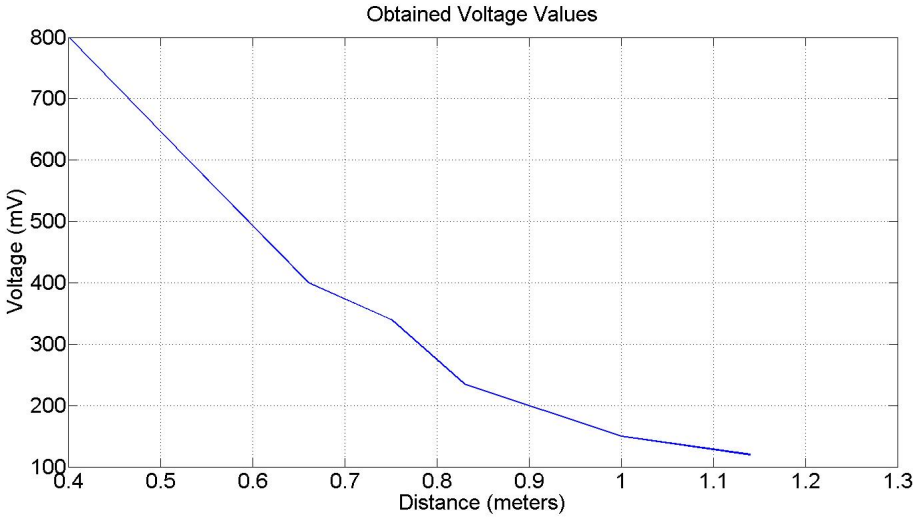

Figure 5.2: Measured voltages versus distance for Fabry-Pérot FSS antenna.

lated from the measured voltage values which were presented in 2.20. The difference between the calculated and measured values are plotted in figure 5.4

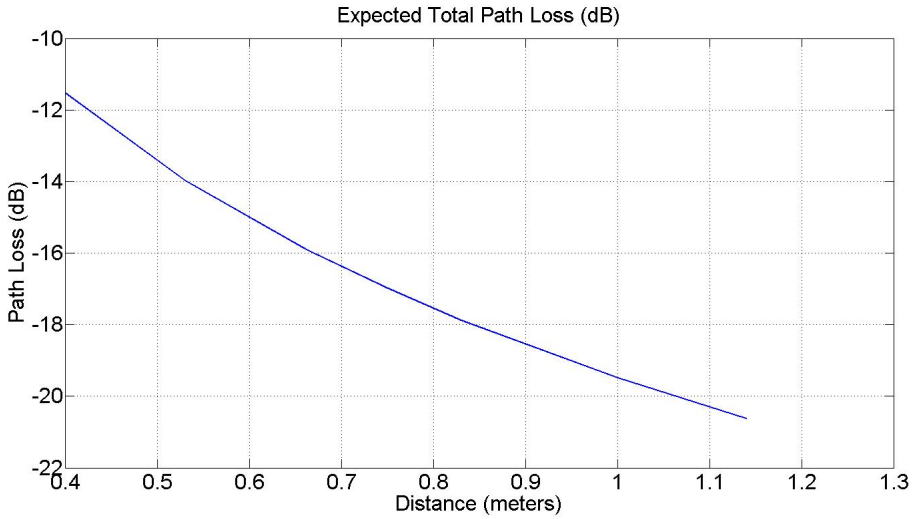

Figure 5.3: Total path loss versus distance in FSS Fabry-Pérot Measurement.

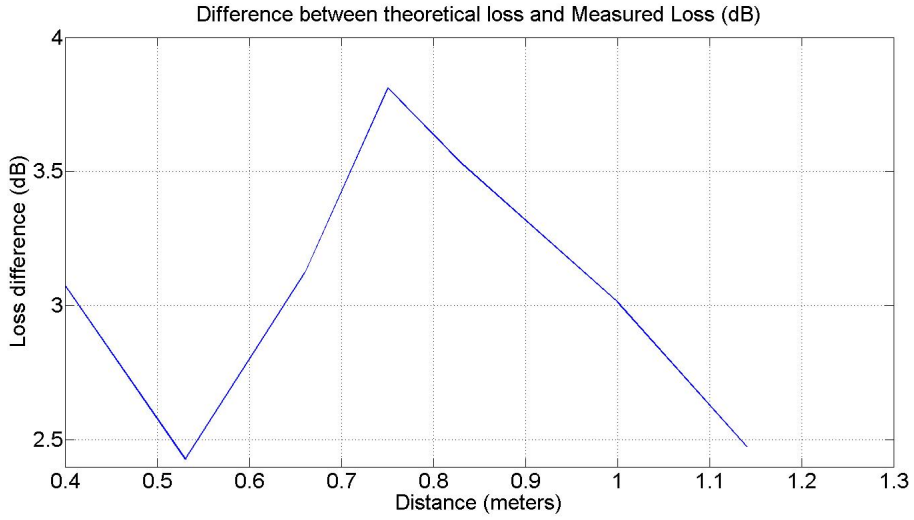

Figure 5.4: Difference between the theoretical path losses and measured loss values versus distance for Fabry-Pérot antenna measurement.

This difference of losses can be attributed to further losses of transmitting side, reflections from the environment and interaction of two antennas in transmission system. This presented loss difference is acceptable in nature. Another concern that is regarding the measurements is about the near field of the receiving antenna. If calculated, far zone of the receiving Fabry-Pérot antenna is about 2.15 meters. This value indicates that taken measurements may not be valid for a far field calculation.

Second test is performed by using SIWCB antenna. Measured output voltages are

presented in figure 5.5.

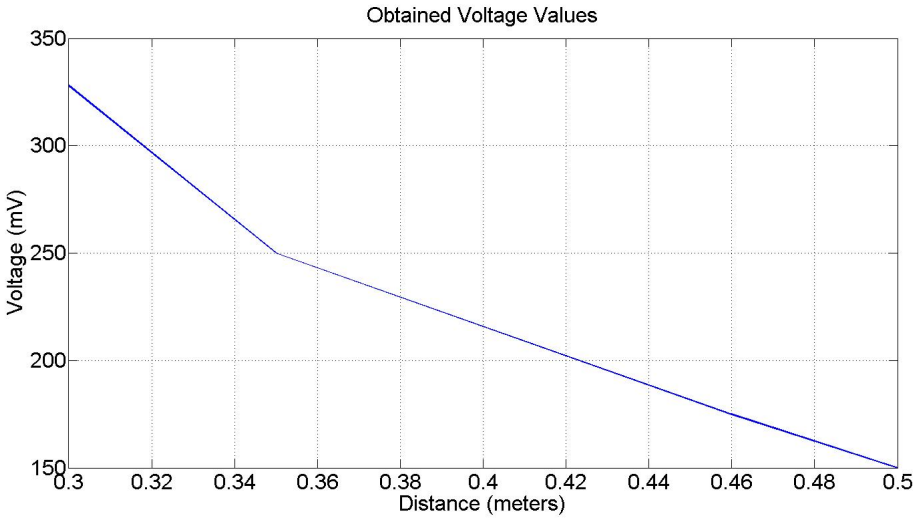

Figure 5.5: Measured voltages versus distance for SIWCB antenna.

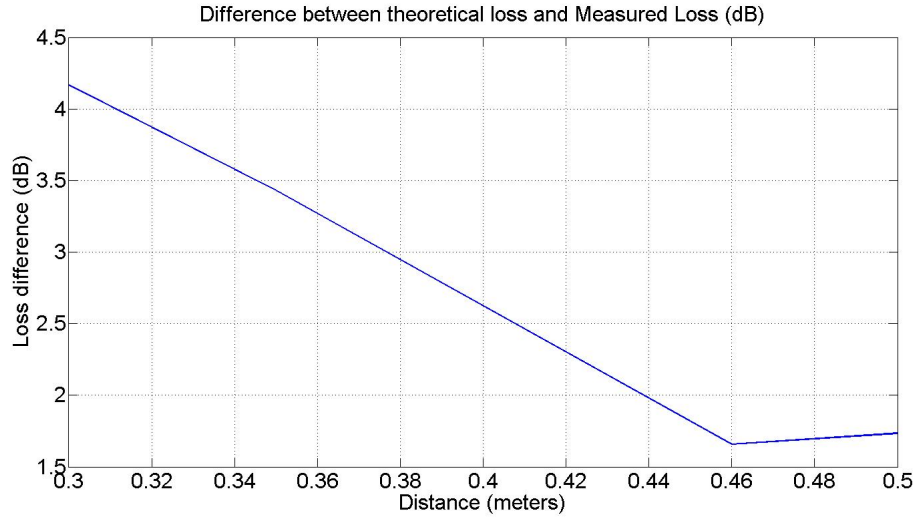

Figure 5.6: Difference between the theoretical path losses and measured loss values versus distance for SIWCB antenna measurement.

Maximum conversion efficiency of this rectenna system is measured as 0.8668% for Fabry-Pérot antenna with distance of 40 cm.

From the comparison of these two antennas, it is obvious that antenna gain plays an important role. Theoretical calculations support this conclusion alone.

CHAPTER 6

CONCLUSION AND FUTURE WORK

Objectives of this thesis work are accomplished by designing a functional rectenna system, along with two antennas, a SIW cavity backed antenna and a Fary-Pérot antenna and a microwave rectifier. All components are designed to operate at 2.45 GHz.

A microwave rectifier is designed based on distributed elements. Design details of this rectifier is also presented in Chapter 2 of this thesis work. Conversion efficiency of the rectifier is measured to be 56% where a harmonic balance simulation yields it as 59%. Measured efficiency values agree well with the ones obtained by simulation.

Substrate integrated waveguide cavity backed slot antenna is presented with all its design details in Chapter 3. Its stackability on surfaces, ease of feed and integration with microwave elements, low profile, light weight, high FTBR and efficiency can be listed as prominent features of this antenna design. Designed antenna has a gain of 2.9 dBi and 10dB bandwidth of 20MHz.

A Fabry-Pérot cavity backed antenna is also developed for the usage in rectenna system. Design details, manufacturing and testing of this antenna is presented in Chapter 4. An FSS structure is developed in this design for the purpose of using it in forming of cavity structure. Fabry-Pérot antenna outshines with its high directivity, however, as it is usually the case in antenna engineering, this high directivity of the antenna comes with the trade-off of size. However, FSSs can be used for a boost in the gain of an antenna where the antenna dimensions are limited in horizontal dimensions. Usage of FSS can be thought as a transformation of higher gain requirement of bigger

size of an antenna to vertical dimension. Designed antenna has a gain of 10.5 dB and 26 MHz 10 dB bandwidth.

Integrated rectenna is presented in chapter 5 of this thesis work with measurement values. It provides 0.8668% maximum transmission efficiency. Transferred power levels are in the order of miliWatts as consistent with the achieved values in the similar studies in literature.

In the light of this study, such rectenna systems can be suggested for powering up of remote sensor nodes [1] where usage of power lines are impossible or dangerous. Such applications may include human body embedded sensors, concrete-embedded pressure sensors and different hard-to-reach sensors. These applications can be extended to powering up of sleeping sensors for short periods of time, where the sensor is powered for only to respond to an interrogation, such as a passive transpoder of an aerial vehicle or a drone. These applications are possible with the enhancement of low power microcontroller units, where the system controller can be slept in low power mode for weeks or even months.

REFERENCES

[1] Tomar, Anuradha; Gupta, Sunil *Wireless power Transmission: Applications and Components* , International Journal of Engineering Research & Technology July 2012

[2] National Aeronics and Space Administration and U.S. Department of Energy *Satellite Power System (SPS) Concept Development and Evaluation Program Plan July 1977-August 1980* , Satellite Power System (SPS) Concept Development and Evaluation Program Plan July 1977-August 1980 & Technology February 1978

[3] R. M. Dickinson and W. C. Brown *Radiated microwave power transmission system efficiency measurements* , Jet Propulsion Lab., California Inst. Technol., Pasadena, CA, Tech. Memo. 33-727, Mar. 15, 1975

[4] Sasaki, S. *It's always sunny in space* , IEEE Spectrum Volume:51 , Issue: 5, May 2014

[5] W. C. Brown *The History of Power Transmission by Radio Waves* , IEEE Transactions on Microwave Theory and Techniques Volume:32 , Issue: 9, September 1984

[6] Naoki Shinohara and Hiroshi Matsumoto *Radiated microwave power transmission system efficiency measurements* , IEEE Transactions On Microwave Theory and Techniques, Vol. 46, No. 3, March 1998

[7] Wireless Power Consortium *Qi System Description Wireless Power Transfer Volume I: Low Power Part 1: Interface Definition* , Wireless Power Consortium, Version 1.1.2,June 2013

[8] Karalis, Aristeidis, Joannopoulos, J.D., Soljačić, Marin *Efficient wireless non-radiative mid-range energy transfer* , Annals of Physics 323 (1): 34–48 January 2008

[9] Thomas W. R. East *A Self-steering Array for the SHARP Microwave-Powered Aircraft* , IEEE Transactions on Antennas and Propagation, Vol. 40, No. 12, December 1992

[10] W. C. Brown *The Technology and Application of Free-Space Power Transmission by Microwave Beam* , Proceedings of the IEEE, Vol. 62, No. 1, January 1974

[11] Olgun, U., Chi-Chih Chen , Volakis, J.L. *Investigation of Rectenna Array Configurations for Enhanced RF Power Harvesting* , Antennas and Wireless Propagation Letters, IEEE (Volume:10), 2011

[12] Triet Le, Karti Mayaram and Terri Fiez *Efficient Far-Field Radio Frequency Energy Harvesting for Passively Powered Sensor Networks* , Journal Of Solid-State Circuits, IEEE, 2008

[13] Nintanavongsa, P., Muncuk, U., Lewis, D.R., Chowdhury, K.R. *Design Optimization and Implementation for RF Energy Harvesting Circuits* , Emerging and Selected Topics in Circuits and Systems, IEEE Journal on (Volume:2 , Issue: 1) RFID Virtual Journal, IEEE, 2012

[14] Fangyi Xie ,Guo-Min Yang, Wen Geyi *Optimal Design of an Antenna Array for Energy Harvesting* , Antennas and Wireless Propagation Letters, IEEE (Volume:12), 2013

[15] T. Sakamoto, Y. Ushijima, E. Nishiyama, I. Toyoda, M. Aikawa *Differential Mode Rectenna Array* , Antennas and Propagation Society International Symposium (APSURSI) July, 2012

[16] T. Sakamoto, Y. Ushijima, E. Nishiyama, I. Toyoda, M. Aikawa *5.8-GHz Series/Parallel Connected Rectenna Array Using Expandable Differential Rectenna Units* , IEEE Transactions On Antennas and Propagation, Vol. 61, No. 9, September 2013

[17] Jui-Hung Chou, Ding-Bing Lin, Kuo-Lin Weng, Hsueh-Jyh Li *All Polarization Receiving Rectenna With Harmonic Rejection Property for Wireless Power Transmission* , Antennas and Propagation, IEEE Transactions on (Volume:62 , Issue: 10), 2014

[18] McSpadden, J.O., Yoo, T. ; Kai Chang *Theoretical and Experimental Investigation of a Rectenna Element for Microwave Power Transmission* , Microwave Theory and Techniques, IEEE Transactions on (Volume:40 , Issue: 12), 1992

[19] Zbitou, J., Latrach, M., Toutain, Serge *Hybrid Rectenna and Monolithic Integrated Zero-Bias Microwave Rectifier* , Microwave Theory and Techniques, IEEE Transactions on (Volume:54 , Issue: 1), 2006

[20] Franciscatto, B.R., Freitas, V., Duchamp, J.-M., Defay, C. *A Different Approach to a Highly Efficient Wireless Energy Harvesting Device for Low-Power Application* , Microwave & Optoelectronics Conference (IMOC), 2013 SBMO/IEEE MTT-S International, 2013

[21] Jeffrey A. Jargon and Donald C. DeGroot. *Frequency-Domain Models for Nonlinear Microwave Devices Based on Large-Signal Measurements* , Journal of Research of the National Institute of Standards and Technology, Volume 109, Number 4, July-August 2004

[22] Steer, M.B., Khan, P.J. *Large Signal Analysis of Nonlinear Microwave Systems* , Microwave Symposium Digest, 1984 IEEE MTT-S International, 1984

[23] Majewski, M.L., Rose, R.W., Scott, J.R. *Modeling and Characterization of Microstrip-to-Coaxial Transitions* , Microwave Theory and Techniques, IEEE Transactions on (Volume:29 , Issue: 8), 1981

[24] Eric Holzman *Essentials of RF and Microwave Grounding, Chapter 4: Transmission Line Transitions pp 86-115* , Artech House Microwave Library, ISBN-13: 000-1580539416.

[25] *S01-SJEDM-11BS02, dimension specifications of connector* ,

[26] Avago Technologies *Avago Technologies, HSMS282x diodes datasheet* ,

[27] Avago Tchnologies *Avago Tchnologies, Linear Models for Diode Surface Mount Packages, Application Note 1124* ,

[28] Aik Yean Tang ,Drakinskiy, V., Yhland, K., Stenarson, J. *Analytical Extraction of a Schottky Diode Model From Broadband -Parameters* , Microwave Theory and Techniques, IEEE Transactions on (Volume:61 , Issue: 5), 2013

[29] Nimo, A., Albesa, J., Reindl, L.M. *Investigating the Effects of Parasitic Components on Wireless RF Energy Harvesting* , Multi-Conference on Systems, Signals & Devices (SSD), 2014 11th International, 2014

[30] McSpadden, J.O., Lu Fan, Kai Chang *Design and Experiments of a High-Conversion-Efficiency 5.8-GHz Rectenna* , Microwave Theory and Techniques, IEEE Transactions on (Volume:46 , Issue: 12), 1998

[31] Jiapin Guo, Xinen Zhu *An Improved Analytical Model for RF-DC Conversion Efficiency in Microwave Rectifiers* , Microwave Symposium Digest (MTT), 2012 IEEE MTT-S International, 2012

[32] Yoo, T.-W., Kai Chang *Theoretical and Experimental Development of 10 and 35 GHz Rectennas* , Microwave Theory and Techniques, IEEE Transactions on (Volume:40 , Issue: 6), 1992

[33] Feng Xu and Ke Wu *Guided-Wave and Leakage Characteristics of Substrate Integrated Waveguide* , IEEE Transactions on Microwave Theory and Techniques, vol. 53, No. 1, January 2005

[34] Daniels R.C., Heath R.W. *60 GHz wireless communications: emerging requirements and design recommendations* , EURASIP Journal on Wireless Communications and Networking, vol. 2007, 2007

[35] S.K. Yong, C.-C. Chong *An overview of multigigabit wireless through millimeter wave technology: Potentials and technical challenges* , Vehicular Technology Magazine, IEEE (Volume:2 , Issue: 3)

[36] Cojocaru, R.I., Moldovan, E., Boukari, B., Affes, S. *A new 77 GHz automotive phase coded CW multi-port radar sensor architecture* , Radar Conference, 2008. EuRAD 2008. European

[37] Yujiri, L., Shoucri, M., Moffa, P. *Passive millimeter wave imaging* , Microwave Magazine, IEEE (Volume:4 , Issue: 3)

[38] M. Bozzi1, A. Georgiadis, K. Wu *Review of substrate-integrated waveguide circuits and antennas* , IET Microwaves, Antennas & Propagation, December 2010

[39] Guo Qing Luo, Zhi Fang Hu, Lin Xi Dong, and Ling Ling Sun *Planar Slot Antenna Backed by Substrate Integrated Waveguide Cavity* , IEEE Antennas and Wireless Propagation Letters, Vol. 7, 2008

[40] Guo Qing Luo, Zhi Fang Hu, Yaping Liang, Li Yang Yu, and Ling Ling Sun *Development of Low Profile Cavity Backed Crossed Slot Antennas for Planar Integration* , IEEE Transaction on Antennas and Propagation, Vol. 57, No. 10, October 2009

[41] Guo Qing Luo, Zhi Fang Hu, Wen Jun Li, Xiao Hong Zhang, Ling Ling Sun, and Jian Feng Zheng *Bandwidth-Enhanced Low-Profile Cavity-Backed Slot Antenna by Using Hybrid SIW Cavity Modes* , IEEE Transactions on Antennas and Propagation, Vol. 60, No. 4, April 2012

[42] Onofrio Losito, Luciano Mescia, Michele A. Chiapperino, Tiziana Castellano, Giuseppe Venanzoni, Davide Mencarelli, Giacomo Angeloni, Pasquale Carta, Emanuele Michele Starace, Francesco Prudenzano *X-Band SIW Cavity-Backed Patch Antenna for Radar Applications* , IEEE Proceedings of the 43rd European Microwave Conference, 2013

[43] M. Laribi, M.Nedil, N. Kandil and D. Hammou, K. Sellal *SIW-Horn Antenna Gain Controllable at 60 GHz* , IEEE Antennas and Propagation Society International Symposium (APSURSI), 2014

[44] Li Yan, Wei Hong, Guang Hua, Chen, Jixin *Simulation and experiment on SIW slot array antennas* , Microwave and Wireless Components Letters, IEEE (Volume:14 , Issue: 9)

[45] Constantine A. Balanis *Antenna Theory - Third Edition* , John Wiley & Sons, Inc., Hoboken, New Jersey

[46] Constantine A. Balanis *Advanced Engineering Electromagnetic - Second Edition* , John Wiley & Sons, Inc., Hoboken, New Jersey

[47] Constantine A. Balanis *Waveguide Modes Vla an Integral Equation Leading to a Linear Matrix Eigenvalue Problem* , IEEE Transactions on Microwave Theory and Techniques, Vol. MTT-32, NO. 11, 1984

[48] A. Kumar, H.D. Hristov *Microwave Cavity Antennas* , Arctech House, Inc., Norwood, MA 02062, 089006-334-6

[49] A.P. Feresidis and J.C. Vardaxoglou *High gain planar antenna using optimised partially reflective surfaces* , IEE Proc-Microwave. Antennas and Propaq., Vol. 148, No. 6, December 2001

[50] Alexandros P. Feresidis, George Goussetis, Shenhong Wang, and John (Yiannis) C. Vardaxoglou *Artificial Magnetic Conductor Surfaces and Their Application to Low-Profile High-Gain Planar Antennas* , IEEE Transactions on Antennas and Propagation, Vol. 53, No. 1, January 2005

[51] Alireza Foroozesh and Lotfollah Shafai *Investigation Into the Effects of the Patch-Type FSS Superstrate on the High-Gain Cavity Resonance Antenna Design* , IEEE Transactions on Antennas and Propagation, Vol. 58, No. 2, February 2010

[52] Shih-Chia Chiu and Shih-Yuan Chen *Circularly Polarized Resonant Cavity Antenna Using Single-Layer Double-Sided FSS Superstrate* , Antennas and Propagation Society International Symposium (APSURSI), 2012 IEEE

[53] Jia Di Wang, Ling Ji, Zhi Ning Chen, Weidong Chen *Efficiency Enhancement of Integrated Fabry-Pérot Cavity Antenna* , 2012 IEEE Asia-Pacific Conference on Antennas and Propagation, 2012, Singapore

[54] Alister Hosseini, Filippo Capolino, Franco De Flaviis *Gain Enhancement of a V-band Antenna using a Fabry-Pérot Cavity with a Self-sustained All-metal Cap with FSS* , IEEE Transactions on Antennas and Propagation 2014

[55] Michael Mirbach, Wolfgang Menzel *A High Gain Planar Antenna With Improved Bandwidth Using a Fabry-Pérot Resonator* , Antennas and Propagation (EuCAP), 2010 Proceedings of the Fourth European Conference on

[56] Tianxia Zhao, David R. Jackson, Jeffery T. Williams, and Arthur A. Oliner *General Formulas for 2-D Leaky-Wave Antennas* , IEEE Transactions on Antennas and Propagation, Vol. 53, No. 11, November 2005

[57] Xuan Hui Wu, Ahmed A. Kishk, and Allen W. Glisson *General Formulas for 2-D Leaky-Wave Antennas* , IEEE Transactions on Antennas and Propagation, Vol. 54, No. 10, October 2006

[58] Filippo Costa, Agostino Monorchio, and Giuliano Manara *Efficient Analysis of Frequency-Selective Surfaces by a Simple Equivalent-Circuit Model* , IEEE Antennas and Propagation Magazine,Vol. 54, No. 4, August 2012

APPENDIX A

MODELING OF COAX-TO-PLANAR TRANSITION

For SMA connectors, linear models are available [23], and many other point regarding the Edge-Mounted transitions are well studied [24]. A simple lossless model for an Edge-Mounted SMA connector can be seen in figure A.1.

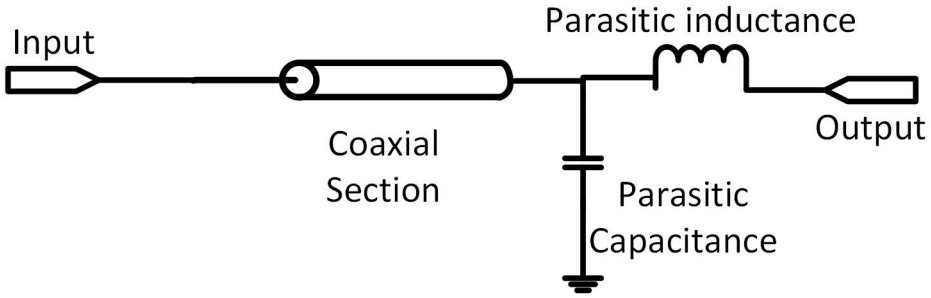

Figure A.1: A simple lossless model for an Edge-Mounted SMA connector.

In this model, a physical loss coaxial transmission line is used for modeling the phase delay that is introduced by the coaxial transmission part of the circuit. Inductance L and capacitance C can be associated with the classical modeling of a planar lossless transmission line. L stands for a length of conductor that is introducing inductance and capacitance stands for the capacitive effect that are between extending ground arms of the connector and extending signal arm. A visual representation can be seen in figure A.2. It should be noted that in the design of SMA coax-to-planar connector, C and L values are deliberately created by the designer of the connector to create a balanced transition between the coaxial line and microstrip line. However this values are measured here to represent any unbalanced distribution that is possibly caused by soldering of the lines and other physical imperfections in the integration of connector with the planar circuit.

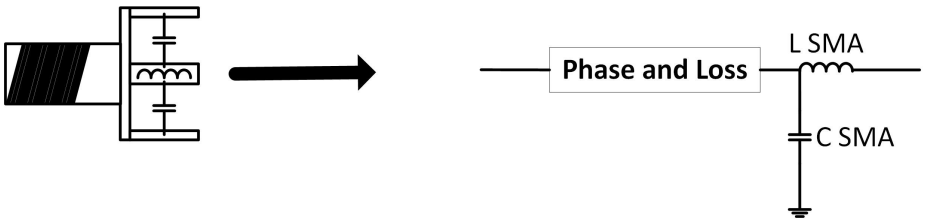

Figure A.2: A visual representation of Edge-Mounted SMA connector for extraction of parasitic contents.

For measurement purposes a microstrip transmission line that is ending with an open circuit is build and measured. The following figure A.3 presents a comparison of the measured and tuned model of SMA connector open circuit test setup. Figure A.1 contains sample points from 1 GHz to 5 GHz. The model is tuned for showing a good comparison around 2 GHz to 3 GHz which covers the centre frequency of the circuit. The datasheet of the connector can be viewed for further dimension specification [25].

A structure solver model for connector test circuit is also developed and presented in figure A.4. The results for the analysis can be seen in figure A.5. HFSS® V15.1 is used for simulation of the structure.

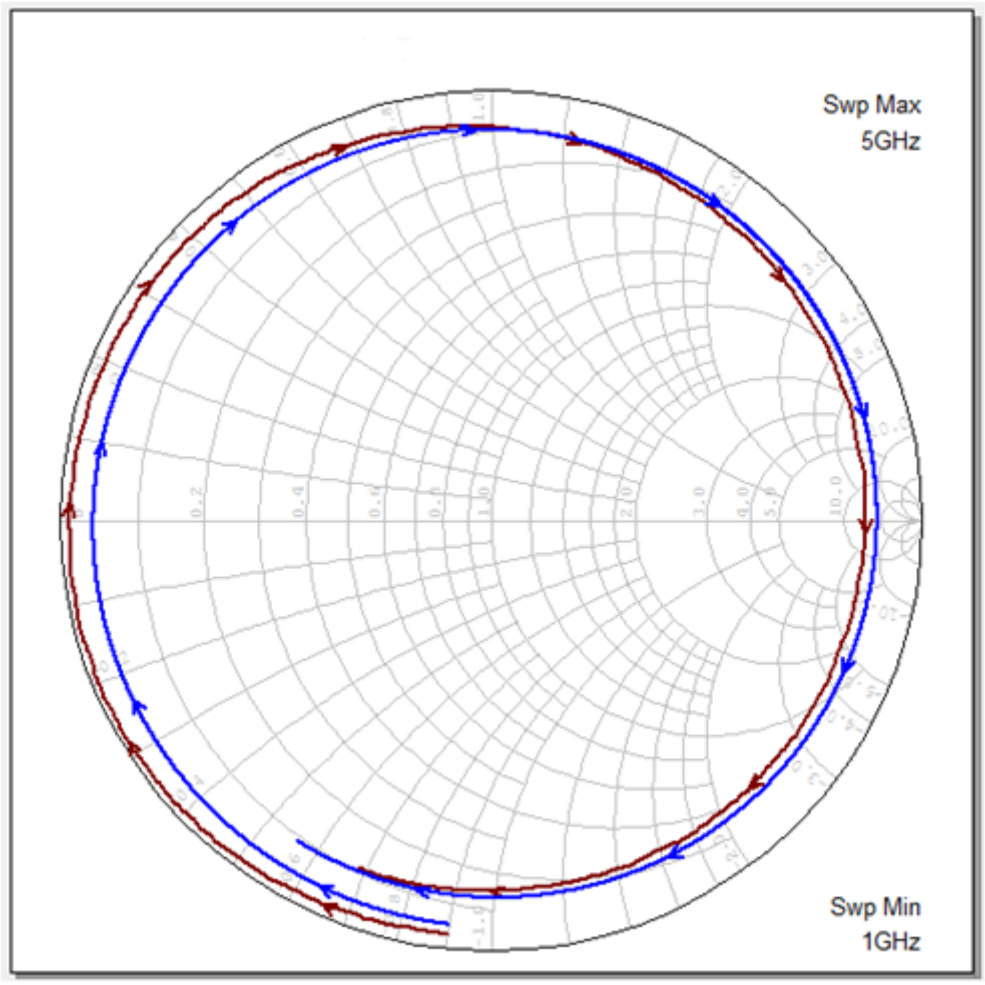

Figure A.3: A comparison of the measured and tuned model of SMA connector open circuit test setup, setup is from 1 GHz to 5 GHz.

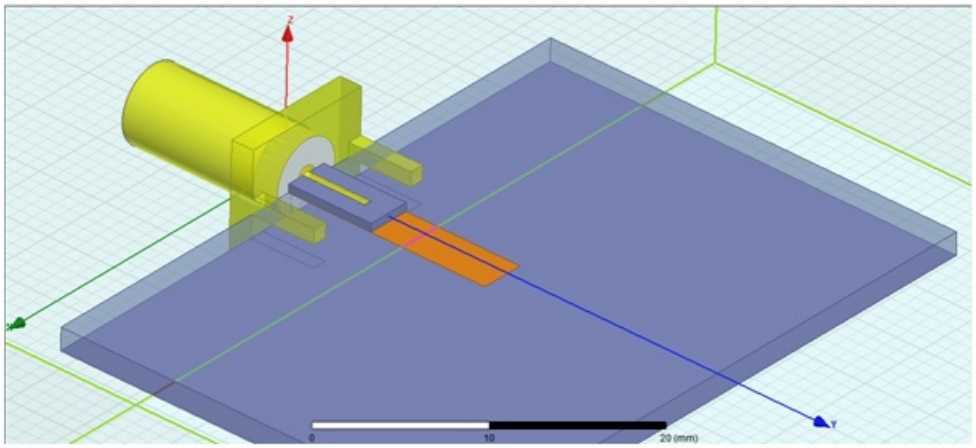

Figure A.4: Model for connector test circuit.

In Figure A.5 it can be seen that the connector simulation is in good agreement with measured values around the centre frequency of 2.45 GHz. In Figure A.6 and A.7 measured and simulated values are presented in a wider range.

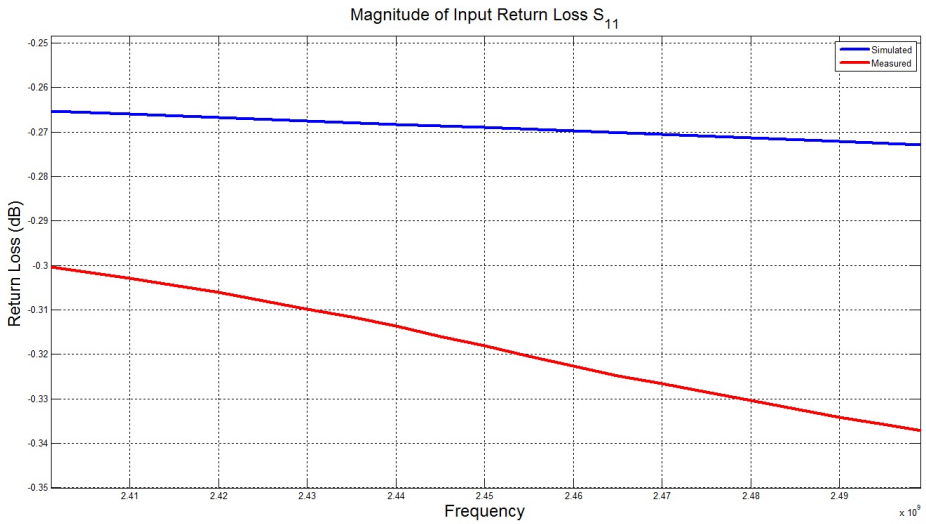

Figure A.5: S_{11} Magnitude comparison of simulated and measured values, blue line shows simulation, red line shows measurement.

From figures A.6 and A.7 connector measurement is observed to be diverging from simulation results. This behaviour is also observable in circuit model of the SMA connector. This drift of measurement is more evident in magnitude rather than in phase, which gives the clue that frequency dependent loss mechanisms are prominent in higher frequencies. If properties of SMA connector is taken into account, which is designed for usage up to 10 GHz at most, this loss is acceptable. This loss mechanisms are actually related to grounding connections of the extending ground arms of connector. This phenomena is explained and studied in [24].

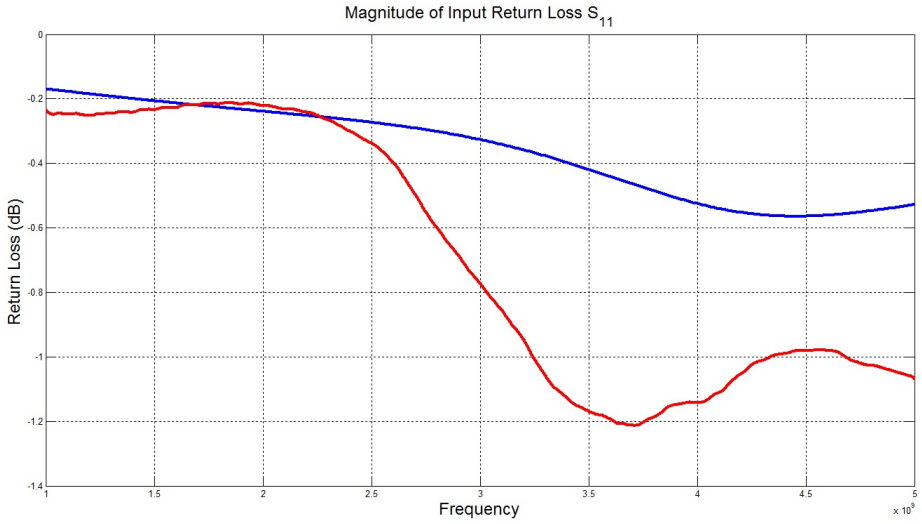

Figure A.6: Magnitude of Input Return Loss S_{11}, blue line shows simulation, red line shows measurement.

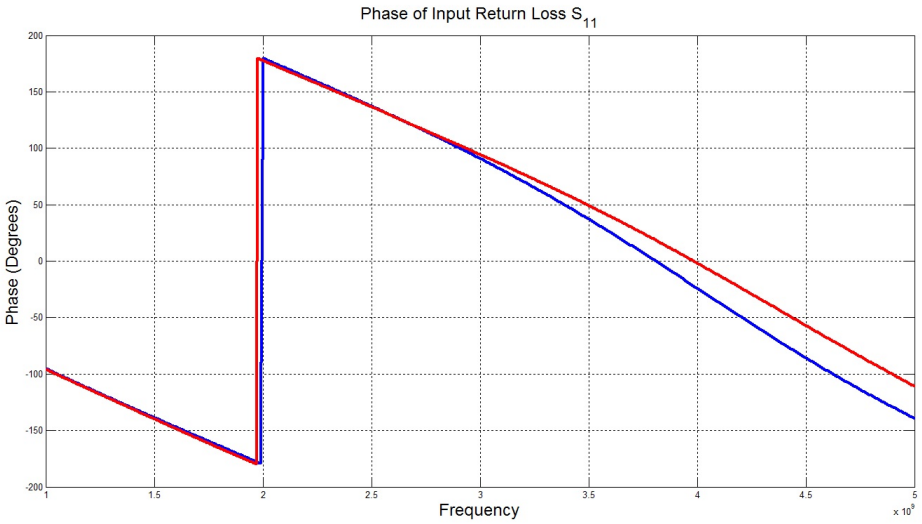

Figure A.7: Phase of Input Return Loss S_{11}, blue line shows simulation, red line shows measurement.

Picture of manufactured testing circuit can be seen in figure A.8.

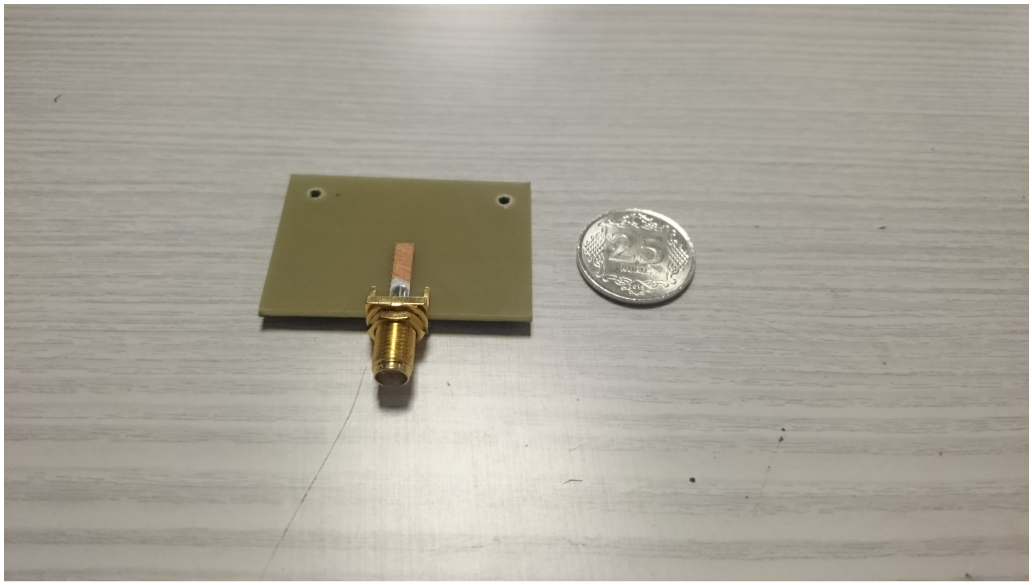

Figure A.8: Picture of manufactured testing circuit.